CPT-based Axial Static Capacity Approaches to Evaluate Pile Driveability in Sand

Putri Suciaty Gandina

TU Delft

CPT-based Axial Static Capacity Approaches to Evaluate Pile Driveability in Sand

By

Putri Suciaty Gandina

in partial fulfilment of the requirements for the degree of

Master of Science
in Civil Engineering

at the Delft University of Technology.
to be defended publicly on Friday 10th of August 2018 at 10:00 AM.

Thesis committee

Prof. Dr. Kenneth G. Gavin,	TU Delft
Dr. Luke J. Prendergast,	TU Delft
Dr. Federico Pisano,	TU Delft
Dr. Bas van Dijk,	Fugro
Dr. Phil Vardon,	TU Delft

TU Delft

Preface

This thesis is final task in fulfilment of the requirement for master's degree in Civil Engineering with specialisation in Geo-Engineering at Delft University of Technology (TU-Delft). I would like to use this opportunity to acknowledge some people for their contribution in this thesis.

First of all, praise be to Allah SWT, Most Gracious, so that I can finish my study.

I would like to thank my supervisor and former chairman, Prof. Kenneth G. Gavin. Big thanks for the opportunity to do a thesis related with pile foundation. Thank you for all of his advice, technical support and guidance during my thesis phases.

Many thanks for my daily supervisor Dr.Luke J.Prendergast. He has been there every moment when I need advice. Luke kept me calm when I was too worried about doing something wrong in the analysis. He patiently checked my work and gives me feedback during writing thesis report. Thank you for always being nice, without his guidance this thesis would not be achieved.

Dr.Federico Pisano as my chairman. I would like to thank you for his commitment. Thanks for immediately respond my e-mail and give a feedback during the meeting. Thank you for his support during my timeline deadline, without his support I would not finish my study on time.

Dr.Bas van Dijk as my committee members. I would like to thank you for his commitment and dedication to come to the meeting despite his busy schedule. Thanks for immediately respond my e-mail and give technical suggestion during the meeting.

Dr.Phil Vardon as my committee member. Thank you for his commitment to join my committee member. I cannot finish my study on time without his support during public defence.

Thank you to my family for their endless support throughout my entire phases in my life. My mother who always pray for me. My sister, who always patiently listening to my random story. I would like to thank Rafil Fikriyan for his love and kindly support. Thanks to all my friends who always be there through up and down in my thesis weird mood. They always provide me with comfort. Lastly, I would like to thank LPDP scholarship which gives me financial support during my study in the Netherlands.

Putri Suciaty Gandina
Delft, August 2018

Abstract

The demand for offshore wind farm installation is increasing in recent years as the concern in using sustainable energy source is rising. One of the primary steps in constructing offshore wind farm is the pile installation which is a high-risk activity due to the expensive offshore installation vessels requirement. Any factor which can result in delaying the pile installation process will lead to financial losses. Therefore, a comprehensive driveability analysis using an efficient pile model is favourable. From the driveability model, the suitable pile equipment can be selected consider the underlying soil condition. The selected equipment must be capable of installing pile into the target depth without overstressing the pile within the design time.

An essential component in driveability model is to estimate the static resistance to driving (SRD). The SRD in analogues with axial static pile capacity approaches. These approaches use the Cone Penetration Test (CPT) data to determine the axial pile capacity. Factors such as the friction fatigue effect, stress equalisation and soil plugging are related and affect axial pile capacity. These factors are integrated into driveability analysis in this study to provide a more reliable result when using CPT-based approaches to calculate static axial capacity.

Pile installation data records from Blessington, Ireland are used as a part of the axial static load test programme. Pile load tests have been performed on open-ended steel piles with a diameter of 0.34m. The site condition consists of glacial deposit dense sand. From this database, the performance of driveability models by using the available and modified CPT-based approaches (e.g., the UWA-05, ICP-05, and Fugro-05) are assessed in this study. The modified model considers the friction fatigue effect, the pile ageing effect, the soil plugging condition, the pile tip mobilisation and the base residual stresses while the SRD is calculated by using the available CPT-based approaches.

The recent CPT-based axial static capacity methods are investigated to see if they can be used as a reliable method to determine static resistance to driving (SRD) profiles. The SRD profiles are comparable to the axial static capacity approach which account for the pile ageing effect, the soil tip displacement, and residual stresses during driving. The pile ageing effect that is incorporated in the model as installation resistance is set for the time equals to zero, unlike with the static capacity load test which is derived after a certain time after end installation. The total resistance that is recorded for open-ended small diameter piles is calculated to model the pile tip mobilisation which is associated with the base resistance. The residual base stresses are modelled for each hammer blow during driving. The wave equation analysis uses a combination of the SRD profiles and dynamic soil components, pile properties and installation equipment resulting in total resistance as the blow count prediction.

This study provides information on how to model driveability analysis from the recent CPT-based axial static capacity approaches. The models one modified to include related factors that affected pile installation process. The performance of predicted blow counts result from unmodified and modified CPT-based methods are appraised and compared to the recorded blow count as a model verification. The UWA-05 modified model can be considered as an appropriate model to estimate pile driveability from CPT-based axial static capacity approach.

Contents

List of Figures

List of Tables

List of Symbols and Abbreviations

a	Parameter in ICP-05 Method for incorporate open-ended piles in tension
A_b	Base area
A_r	Area ratio
$A_{r,eff}$	Effective Area Ratio
b	Parameter in ICP-05 Method for incorporate compression or tension load tests
D	External pile diameter
D_{50}	Soil particle diameter at which 50% of the mass of soil sample is smaller
D_i	Internal pile diameter
D_r	Relative density of the soil
e	Void ratio
E_{beq}	Young's modulus
E_o	Small strain elastic stiffness of the soil
F_{time}	Time factor for shaft friction calculation
G_o	Shear modulus of the soil
h	Distance above pile tip level
Δh_{plug}	Change in plugging length
L	Pile penetration length below ground level
ΔL_{pile}	Change in pile penetration length
P_{ref}	Reference atmospheric stress
q_{ann}	Unit bare resistance at pile annulus
q_b	Unit base resistance
$q_{b0.1}$	Unit base resistance when 0.1 pile diameter mobilise
$q_{b,n\%(z)}$	Additional step wise unit base resistance at z
$q_{b,res}$	Base residual stresses
q_c	Cone tip resistance
$q_{c,avg}$	Average cone tip resistance
q_n	Net cone resistance
q_t	Total cone resistance
Q_b	Axial base resistance
Q_s	Axial shaft resistance
$\sum Q_{s,L}$	Cumulative shaft resistance at the pile tip depth
$\sum Q_{s,L-1}$	Cumulative shaft resistance at the previous depth increment
Q_t	Total axial capacity
R	Pile outer radius
R_i	Inner pile radius
R^*	Equivalent pile radius
t	Time after driving
t_w	Pile wall thickness
T	Time
u_o	Pore-water pressure
V_s	Shear wave velocity
Δy	Radial displacement of interface zone during dilation
z	Element depth

α	Adhesion factor
δ_f	Constant volume interface friction angle
π	Pi, mathematical constant = 0.314
σ'_3	Effective confining stress (triaxial test)
σ_{vo}	Total vertical overburden pressure
σ'_{rc}	Radial effective stress after installation and stress equalisation
σ'_{rf}	Radial effective stress at failure
$\Delta\sigma'_{rd}$	Increase in radial stress due to dilation at the soil-structure interface during loading
τ_f	Shaft friction at failure
$\tau_{f,in}$	Internal shaft friction
$\tau_{f,neg}$	Negative shaft friction
$\Delta\tau_{f,avg}$	Average shaft friction
ν	Poisson's ratio

API	American Petroleum Institute
bgl	Below ground level
CoV	Coefficient of Variation
CPT	Cone Penetration Test
FFR	Final Filling Ratio
GRLWEAP	GRL's Wave Equation Analysis of Pile Driving
IAC	Intact Ageing Curve
ICP	Imperial College Pile
IFR	Incremental Filling Ratio
NGI	Norwegian Geotechnical Institute
SRD	Static Resistance to Driving
UWA	University of Western Australia

1 Introduction

Pile driving is a high-risk activity, especially in the offshore environment. Inefficient driveability can cause delay and material damage that may lead to financial overspending. Selected equipment must be capable of installing the pile at the target depth within the given time-frame without overstressing the pile. Therefore, a comprehensive driveability analysis is essential to any offshore project. Driveability must consider all aspects, such as soil condition and soil-structure interaction, driving equipment performance and pile specifications such as the geometry and material properties.

Any driveability study requires calculation of Static Resistance to Driving (SRD). SRD is analogous to the axial capacity of a pile and represents the cumulative increase in shaft capacity associated with further pile penetration and encompasses a base resistance that is associated with each driving increment. The SRD is a measure of the expected resistant of the pile to driving and develops during pile installation. Schneider and Harmon (2010) claim that SRD is similar to pile static axial capacity except for the resistance often differs due to consolidation, stress equalisations, and ageing (capacity increases over time).

The total resistance of a pile driving is commonly presented in terms of the blow count required to drive the pile or as resistance curves. Typically, the number of blows that it takes the hammer to drive the pile to a certain depth (per 0.25m usually) and the soil resistance at the time of driving are measures used to appraise the difficulty associated with a given pile driving. A combination of SRD and associated dynamic components is the input required to conduct a total resistance of a pile driving. Wave equation analysis is essential to incorporate the dynamic component increase due to inertia and the viscous rate effects. The obligatory inputs for wave equation analysis are the SRD, the dynamic components that are represented by damping and a quake values, the pile and the hammer properties. Analysis of this solve the wave equation that simulates the responses of a pile from each hammer blow.

Cone Penetration Test (CPT) is commonly used in construction projects in Europe where almost every project has a minimum of one single complete CPT. There are various CPT-based methods to determine the axial static capacity of piles. These load capacity calculation methods are derived from pile load tests that are usually conducted between 10 and 30 days after pile driving. Past studies have indicated that static pile capacity may increase over time after pile driving (Jardine *et al.*, 2006; Gavin *et al.*, 2013; Karlsrud *et al.*, 2014; Kirwan, 2014; Gavin *et al.*, 2015). That study suggests that pile resistance during installation will be lower than the available model calculation. A time factor should be applied to determine the driveability from the available CPT-based static axial capacity methods.

During pile driving, shear resistance reduction occurs as the distance from the pile to the tip increases. This phenomenon is known as friction fatigue. Schneider and Harmon (2010) suggest calculating the pseudo average shaft friction to accommodate changes in the shape of shear resistance distribution during pile driving.

The pile penetration per blow during driving is less than the failure criteria of base capacity from the ICP-05, Fugro-05 and UWA-05 model which suggests a pile tip displacement of 0.1 of the pile diameter. A reduction factor is required to consider the actual pile tip displacement during driving. On the other hand, the residual load on the pile base may have been significantly miss-represented which could lead to considerable error in UWA base resistance method (Xu, 2007). Ignoring residual loads can lead to an underestimating of the base resistance in a compression load test which can cause significant errors when correlating base resistance with cone resistance (White and Bolton, 2005). This residual stress study suggests stress may be higher at the pile toe. Therefore, taking an additional residual base will be reasonable to develop a proper model.

The purpose of this research thesis is to develop an efficient model for driveability analysis using CPT-based axial static capacity methods. Moreover, several parameters will be examined to determine which factors influence pile driveability. For this purpose, the analysis will use Blessington database (see Section 3.1). The Blessington project consists of 7 steel open-ended full-scale test pile at Blessington, Ireland. The pile penetration length is 7m with a diameter of 0.34m. The soil profile at this location form of a very dense, fine sand deposit. The groundwater located at 13m below the ground level.

1.1 Research Question

The objective of the research is to gain knowledge on the performance of CPT-based axial static capacity approaches to evaluate pile driveability in the sand. Therefore, the research question can be listed into work as follows:

1. How to calculate axial static capacity using available CPT-based methods?
2. How to develop an efficient model for the driveability analysis using the CPT-based axial capacity methods?
3. What parameters primarily affect pile driveability analysis?

1.2 Approach to Research

To be able to answer above mention research question, this thesis will consist of several phases:

1. A literature review that consists available method to conduct driveability analysis. Several CPT-based methods commonly used for the axial static capacity analysis in sand such as the UWA-05, ICP-05, and Fugro-05.
2. Collecting data available from site location to perform driveability analysis. Required data consist of soil data, pile properties and hammer properties. Soil data will be needed to calculation soil model using the available CPT-based method. Perform driveability data will depend upon wave equation analysis which requires all these data. Wave equation analysis will be implemented by using driveability analysis software, GRLWEAP.
3. Modifying model to determine an efficient driveability model that will be validated with the actual blow counts data. To be able to make an efficient prediction, modification

needed with considering several parameters in driveability analysis. The result of modified method will be validated by comparison with recorded blow counts in the field.

4. Sensitivity analysis varying the primary parameters of driveability analysis. It is essential to perform sensitivity analysis to quantify the change in the primary parameters affecting driveability analysis results.
5. The application of driveability model will be applied in pile driven in different soil conditions. The CPT-based axial static capacity in clay layers is also assessed. Later, this model will be validated with recorded blow count data which is available from the site.

1.3 Limitations

There are several limitations that confine all result and conclusion in this study:

1. Methods chosen are only the CPT-based approaches for axial static capacity calculation.
2. The driving stresses and installation time is disregarded in this study.
3. Organic soil that presents in the soil profile will be recognised as clay layer.
4. An external environmental condition such as wave at the offshore pile will be ignored.
5. The weight of the driving system (all components between the hammer and pile top) are excluded in performing wave equation analysis.

2 Pile Driveability

A pile is a structural foundation made of steel, concrete, timber or composite that is used to transfer load from the superstructure to the soil layer and to improve the bearing capacity, density or stiffness of the soil without directly carrying the load. Figure 2.1 shows some of typical conditions where the use of a pile foundation is possibly being required to ensure structural safety.

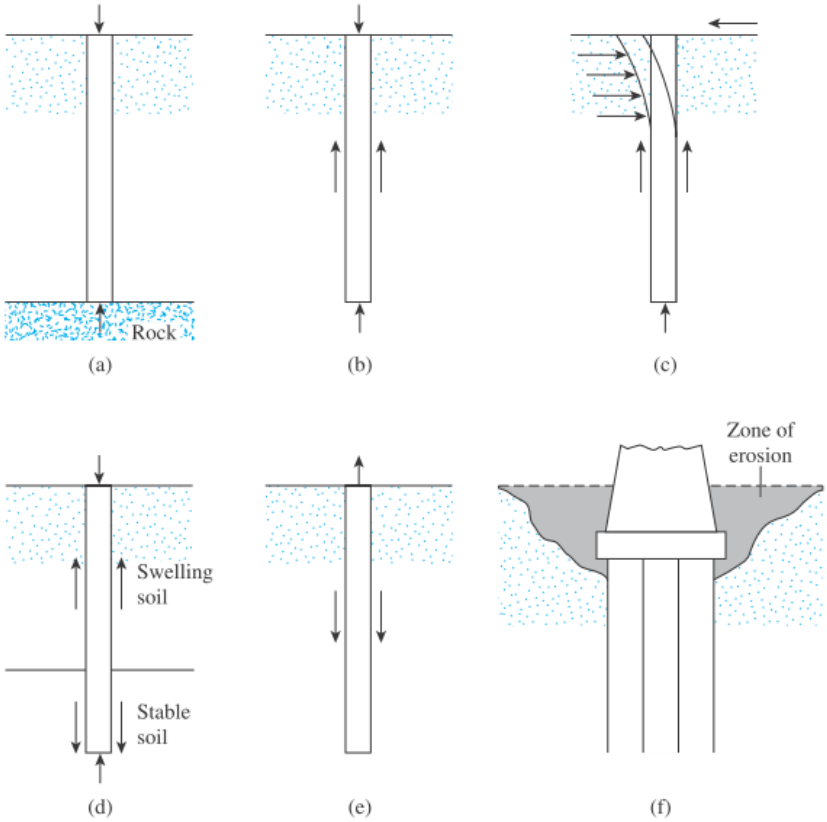

Figure 2.1 Conditions that required a pile foundation (Das, 2011)
(a) transfer load to stronger soil or bedrock, (b) transfer load to soil gradually with frictional resistance at the soil-pile interface, (c) pile subjected to lateral loading, (d) transfer to the stable soil below the expansive and collapsible soil, (e) resist the uplifting forces for foundation below the water table, (f) prevent the loss of bearing capacity due to erosion at the ground surface.

Piles can be classified by their load transfer mechanism, installation method and geometry. The load transfer mechanism can differentiate the piles into point bearing, friction, and compaction piles. A point bearing pile is one where the ultimate pile capacity depends on the capacity of underlying soil or rock as shown in Figure 2.1a. If the ultimate pile capacity depends on the pile skin (shaft) friction, the pile is called a friction pile which is shown in Figure 2.1b. A compaction pile is the one that is driven into the granular soil to achieve soil surface compaction. The lengths of compaction piles are determined by the soil density before and after compaction and the required depth of compaction.

There are several terms used to describe the various elements in the analysis of piles as shown in Figure 2.2. The pile cap is the connection between superstructure and the pile. The upper part of the pile or the end of the pile cap is called the pile head or the pile top. The bottom end of the pile is known as the pile toe, the pile tip or the pile base. The pile skin or the pile shaft is a term for the pile segment between the pile head and the pile tip.

Piles have various shapes and cross-sections as shown in Figure 2.3. The pile base can be cylindrical or conical with smooth or tapered shape. The pile base can be equipped with a pile shoe which can enlarge the pile diameter which increases pile base resistance to prevent pile damage during hard driving. Circular and square shapes are the most common cross-sections adopted for piles. Other examples of cross-sections include octagonal, hexagonal, triangular, H-shaped, and hollow (Fang, 1991).

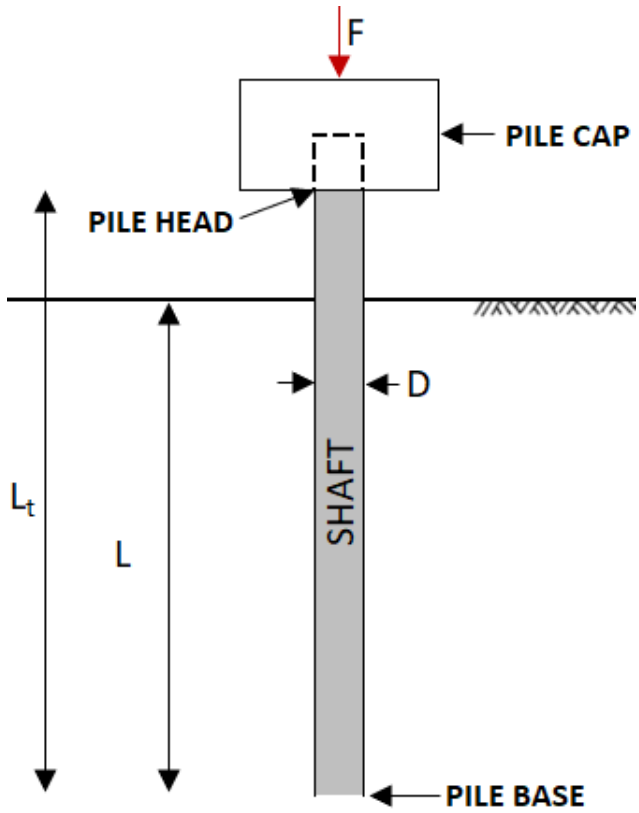

Figure 2.2 Term of the pile structures

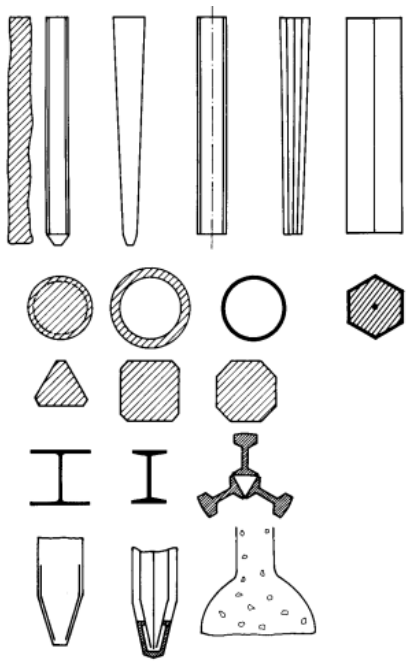

Figure 2.3 Various shapes and cross-sections of the pile (Kezdi, 1975 and Fang, 1991)

2.1 Installation of piles into the soil

Piles are classified according to the installation method, as driven, bored or cast-in-situ, and screw piles. The installation method influences the pile behaviour under load and the state of

stress in the surrounding soil (Poulos and Davis, 1984). Pile driving process causes soil rearrangement, in loose sand driving will advantages rather than pile boring due to increase in relative density.

Based on the nature of the soil placement during pile installation, the piles can be divided into displacement piles and non-displacement piles. Displacement piles are those whereby the installation process causes soil densification that leads to stress changes in the soil. Driven piles or jacking piles are an example of displacement piles. Bored piles which give very little change in the state of stress in the surrounding soil are called non-displacement piles.

Piles are driven into the ground using hammers. Pile driving hammer can be classified as diesel hammer or internal combustion hammer, external combustion hammer, and vibratory hammer as shown in Figure 2.4. According to working principles, the external combustion hammers are classified as steam hammer, air hammer, hydraulic hammer, and drop hammer. Drop hammer as shown in Figure 2.4a which the oldest type of hammer is lifted with hoist and rope and allow to drop from a certain height. Drop hammer has a slow rate of blows hence hydraulic hammer developed with adjustable ram fall height and various energy settings during the downstroke. Vibratory hammer as shown in Figure 2.4b consists of pairs counter-rotating weights (oscillator) that cancel the presence of horizontal forces resultant and generate centrifugal force. A clamp is used to transfer centrifugal force from oscillator into vertical forces which drive the pile.

The diesel hammer as shown in Figure 2.4c consists of the ram, anvil block, and fuel-injection system. The ram is released with gravity and fuel is squirt at the top of the anvil. The ram drops compress the air-fuel mixture which causes the heated air combusts after a short delay. This combustion process is delayed due to the time required for fuel mix with the heated air to ignite. The combustion pushes the pile downward into the soil and raises the ram. The ram will ascends to a certain stroke height and begin a new cycle. Almost all hammers impact the pile head, but certain external combustion hammers can be driven at the pile tip or in the pile shaft (Pile Dynamics Inc., 2010a).

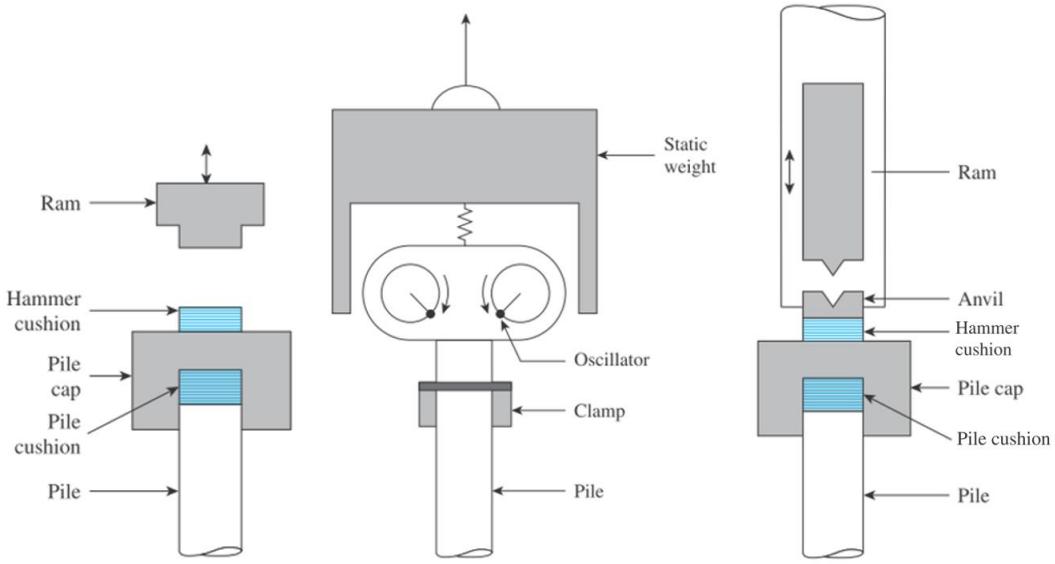

(a) Drop hammer (b) Vibratory hammer (c) Diesel hammer

Figure 2.4 Type of pile driving hammers (modified after Das, 2011)

During the pile driving process, a pile cap is attached to the pile head, and a pile cushion may be used in between the pile head and the pile cap. The hammer drops on the hammer cushion that is placed on the pile cap. The cushion function is to reduce the impact-force and distribute the force.

2.2 Static Resistance to Driving

Soil resistance during driving is a combination of static and dynamic components. The static resistance to driving (SRD) is a static component of the soil resistance during driving which is analogues with static axial capacity. The SRD has shaft friction which changes with each driving increment. Unlike static capacity that only has single base resistance, the SRD profile has base resistance for each driving increment. The difference between the static capacity and the SRD is due to time effect or ageing, consolidation, stress equalisation, and definition of soil failure in static load tests (Schneider and Harmon, 2010).

The same as the axial static capacity, plugging condition of the pile tip during each driving increment which represents by IFR will affect base resistance in the SRD. In fully coring condition (IFR=1), the unit end bearing is occurred on the pile annulus (q_{ann}), and the pile shaft friction is occurred both internal ($\tau_{f,in}$) and external (τ_f) along the shaft surface area. Alm and Hamre (2001) and Schneider and Harmon (2010) suggest to reduce unit friction to 50% and apply on both inside and outside of the pile wall which is the same as applying full external shaft friction without internal shaft friction. The static axial capacity calculation is addressed further in Section 2.4.

The shaft resistance distribution associated with each pile penetration is altered due to the friction fatigue effect. The axial static capacity method (i.e. UWA-05, ICP-05, and Fugro-05) is difficult for estimating the change in shaft friction distribution during pile driving. Therefore, an appropriate technique is introduced to account for the change of the shaft friction distribution. The parameters influence prediction bearing graph and blow counts from SRD which have a maximum to minimum effect are a fraction of resistance from Q_b and Q_s, pile penetration depth, and shape of shaft friction distribution (Alm and Hamre, 2001). The shape of the shaft friction has a minimum effect, so Schneider and Harmon (2010) suggest to calculate the pseudo average shaft friction ($\Delta\tau_{f,avg}$) using change in shaft capacity between two successive depth increment follows :

$$\Delta\tau_{f,avg} = \frac{\sum Q_{S,L} - \sum Q_{S,L-1}}{\pi D\, \Delta L} \qquad \text{Equation 2.1}$$

Where $\sum Q_{S,L}$ is the cumulative shaft resistance at the pile tip depth, $\sum Q_{S,L\text{-}1}$ is the cumulative shaft resistance at the previous depth increment, ΔL is the depth increment, D is the pile diameter. Friction fatigue cause $\Delta\tau_{f,avg}$ is less than τ_f near the pile tip and possible to have negative value due to decreasing soil strength profile in the soil and small values of ΔL. The detail explanation about friction fatigue is addressed in Section 2.4.1.

2.3 The Dynamic Approach

The dynamics components that increase soil resistance during driving are due to inertial and viscous rate effects. Soil dynamics components are accounted in wave equation analysis use GRLWEAP program by Pile Dynamics Inc. (2010b). This program will solves the one-dimensional wave equation theory as proposed by Smith (1960) based on mass discretisation with pile-soil interaction simplification as

$$\frac{\partial u^2}{\partial t^2} = c^2 \frac{\partial u^2}{\partial x^2} \qquad \text{Equation 2.2}$$

Where *c* is a velocity of propagation of longitudinal strain wave along the rod (hammer, driving system and pile) = $\sqrt{E/\rho}$, *x* is a direction of the longitudinal axis of the pile, *u* is a displacement of pile cross section in the *x* direction, *t* is time, *E* is the elastic modulus and *ρ* is the mass density.

GRL's Wave Equation Analysis of Pile Driving (GRLWEAP) is a computer program which simulates motions and forces along the pile when driven by hammer (Pile Dynamics Inc., 2010a). The program predicts the blow counts from SRD inputs and soil dynamics components by varying hammer and pile properties. Hammer type, hammer stroke height, hammer efficiency, driving systems such as cushion and helmet are hammer properties inputs that needed to do wave equation analysis. Furthermore, wave equation analysis also can give analysis output as installation stresses along the pile and driving time to install the pile.

Soil damping and quake are soil dynamic components to incorporate inertia and viscous effect. Lowery *et al.* (1968) conduct a triaxial test in sand and shows that damping value varied from 0.16 to 0.65 s/m and increase as effective confining stress (σ'_3) and sand density increases (void ratio e decreases). The soil damping depends on soil type and independent of the total soil resistance and pile size properties. Smith (1960) recommend taking toe damping larger than shaft or skin damping. Smith shaft and base damping of 0.25 and 0.5 s/m respectively use for the UWA-05 method in sandy soil (Schneider and Harmon, 2010). The other calculation method (ICP-05 and Fugro-05) will use a GRLWEAP recommendation for shaft and base damping of 0.16 and 0.5 s/m in sandy soil.

The load-deformation relationship during pile driving is defined by a static resistance and a quake value for each spring shown in Figure 2.5. The quake value represents a maximum elastic pile displacement before yield. The journal that is written by Lowery *et al.* (1968) state difficulty in determining the quake value for the various type of soil condition. In the absence of the quake value, it is recommended to use 2.5mm for both shaft and base quake value.

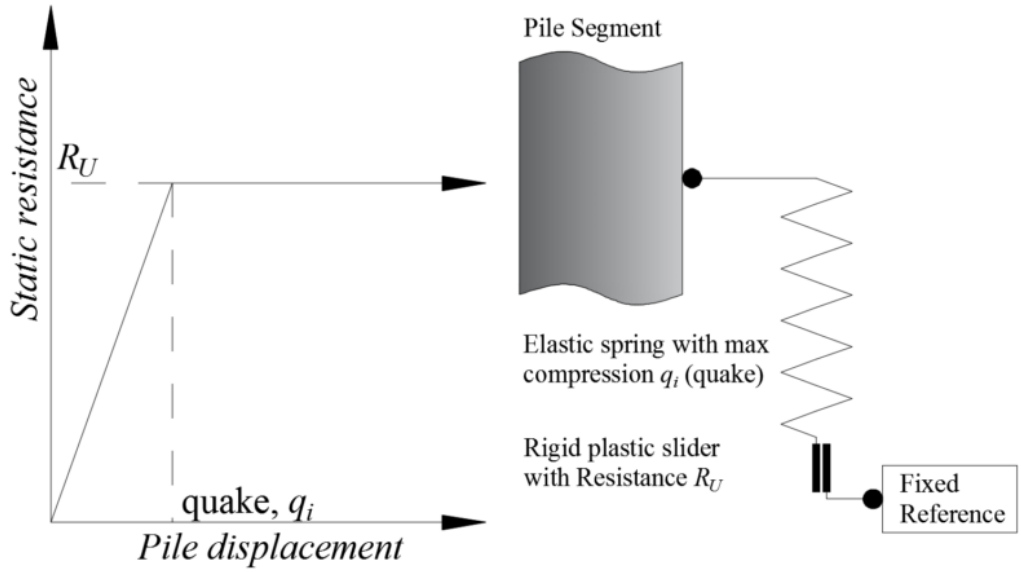

Figure 2.5 The quake definition (Byrne *et al.*, 2018)

2.4 The CPT-based Static Capacity Methods

The most common site investigation method, especially in Europe, is the Cone Penetration Test (CPT). Site investigation must be undertaken to determine the strength parameters of the soil. The correlation between cone tip resistance (q_c) value to calculate shaft friction and base resistance has been developed over the years. This development due to addressing a various aspect of design piled foundation such as friction fatigue and plugging effect at pile capacity.

The latest methods which used the q_c value as a primary input parameter in the sand are Imperial College (ICP-05) by Jardine *et al.* (2005), University of Western Australia (UWA-05) by B.M. Lehane (2005), and Fugro-05 by Kolk *et al.* (2005). This recent CPT-based approach considers friction fatigue and plugging effect on a pile. Other methods that are broadly used to calculate the axial static capacity of a pile in the sand such as Norwegian Geotechnical Institute (NGI-05) and American Petroleum Institute (API-00) will not be considered in this study. The NGI-05 use pile capacity direct to the sand relative density (D_r) and API-00 is a non-CPT based method.

Various traditional SRD approaches have been proposed by Toolan and Fox (1977), Stevens *et al.* (1982), and Alm and Hamre (2001). In sand, Toolan and Fox (1977) proposed the unit base resistance and the unit skin friction determined as a weighted average and a fraction of q_c respectively. The q_c value in base resistance calculated over a number of pile diameter above and below the pile tip. Stevens *et al.* (1982) propose determining both the unit base and skin resistance by limiting for plugged and coring conditions. Alm and Hamre (2001) developed a model-based CPT approach with back-calculated driveability studies which incorporate the friction fatigue effect. These traditional driveability approaches to calculate

SRD will not assess future in this study, as the development of this method more reliable for the pile with a large diameter.

The ultimate capacity is the summation of the shaft and base resistance as written in the following

$$Q_t = Q_s + Q_b = P \int \tau_f \, dz + A_b \, q_b \qquad \text{Equation 2.3}$$

Where: Q_s is the total shaft capacity, Q_b is the total base capacity, P is a perimeter of the pile ($P=\pi D$ for a circular pile and $P= 4B$ for square pile), τ_f is the local shaft friction at failure along the shaft of a pile, z is the embedded shaft length, A_b is a base area ($A_b = \frac{\pi D^2}{4}$ for a circular pile, and $A_b = B^2$ for square pile), q_b is the base resistance assumes a displacement of 0.1D as failure criteria (at a pile head for ICP-05, at a pile tip for UWA-05 and Fugro-05), and D is the pile outer diameter.

2.4.1 Shaft Friction

The shaft friction develops following a Coulomb failure criterion as proposed by Jardine *et al.* (2005) and Lehane *et al*. (2005) as shown below

$$\tau_f = \sigma'_{rf} \tan \delta_f = (\sigma'_{rc} + \Delta\sigma'_{rd}) \tan \delta_f \qquad \text{Equation 2.4}$$

Where σ'_{rf} is a radial effective stress at failure, δ_f is a constant volume interface friction angle, σ'_{rc} is a radial effective stress after installation and equalisation, and $\Delta\sigma'_{rd}$ is a change in radial stress due to dilation at the soil-structure interface during loading.

The increase in radial stress due to loading stress path relates to lateral expansion or dilation ($\Delta\sigma'_{rd}$) at the soil-structure interface during loading can be modelled using the cavity expansion theory (Lehane, 1992). The change in radial stress is a function of soil shear stiffness normalised by the pile diameter and radial expansion which is influenced by a pile shaft roughness (Δy). Pile shaft roughness depends on the material in the shear zone. The roughness of concrete piles is higher than steel piles (0.01-0.02mm). The dilation or shear zone thickness is approximately ten times the mean size of the soil (D_{50}). In a full-scale pile test which has a D/D_{50} between 1000-8000, the magnitude of $\Delta\sigma'_{rd}$ is negligible. However, in a laboratory test with D/D_{50} less than 1000, $\Delta\sigma'_{rd}$ will have a significant contribution (Lehane, 1992). Morphology or particle shape affects $\Delta\sigma'_{rd}$, an angular particle has greater dilation than a more rounded particle (Santamarina and Cho, 2004).

The radial effective stress after installation and equalisation (σ'_{rc}) is a function of cone resistance and relates to the friction fatigue effect. The friction fatigue phenomenon refers to the behaviour of soil shear resistance reduction as a vertical distance from the pile tip to a specific soil horizon increases. This phenomenon leads to high stress close to the pile tip and contraction of the shear zone along the pile shaft with each installation cycle (Kirwan, 2014). Chow (1996) listed the possible cause reduction in radial effective stress as shown in Figure 2.6 as (a) the free surface effect which can affect up to 20D in clay and less in sand, (b) the lateral movement during driving can cause whip or gapping until 4D below the soil surface,

(c) the geometry of the steady flow system around pile tip which can cause high stress during installation, and (d) the cyclic loading imposed on the pile shaft by the driving process.

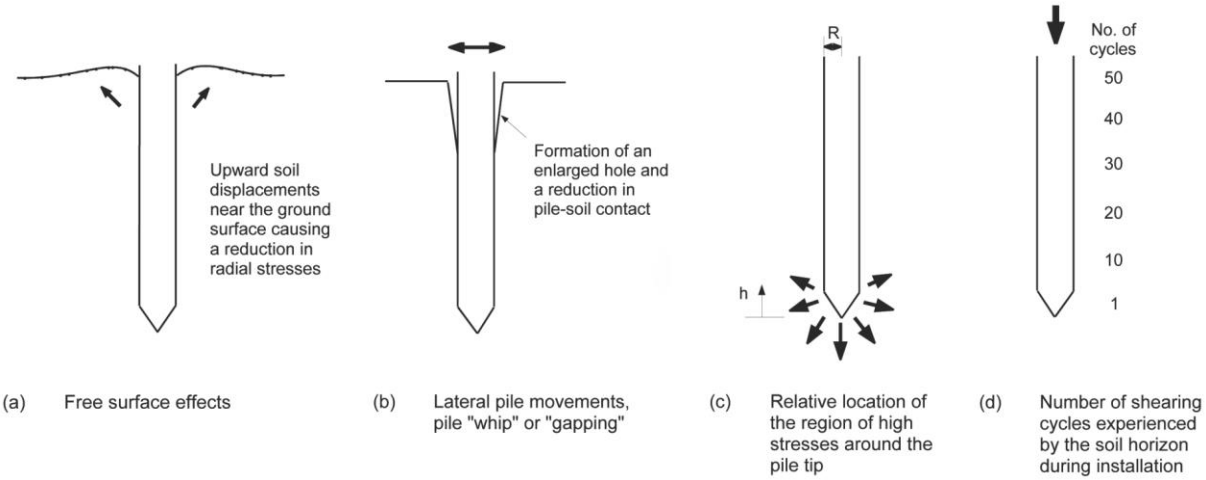

Figure 2.6 Possible sources of friction fatigue (Jardine and Chow, 2007)

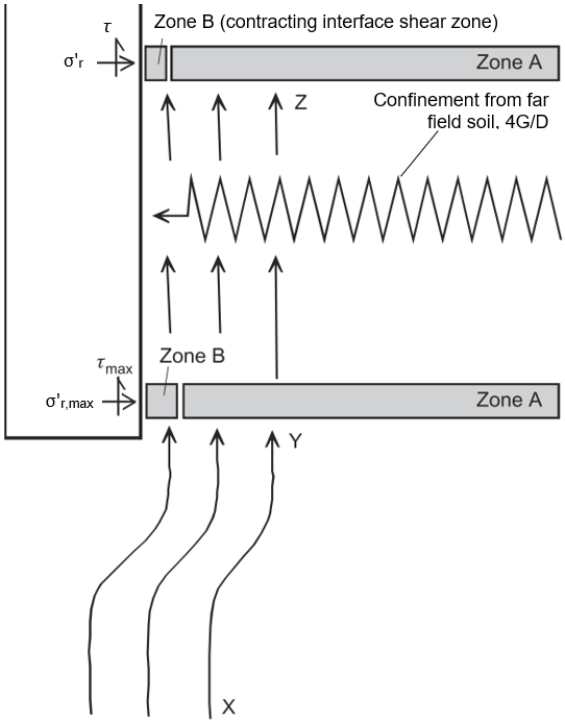

Figure 2.7 Kinematics of friction fatigue close to the pile tip
(modified after White and Bolton, 2004; Kirwan, 2014)

White and Bolton (2004) explain kinematics of friction fatigue close to the pile tip as shown in Figure 2.7. Soil compressed laterally along streamline XY creates high radial stresses. The soil continues along streamline YZ causing the interface zone immediately adjoining the pile to contract with continued shearing at the pile-soil interface or at zone B. The contraction of the interface zone causes unloading of the far field soil or zone A. The far field is a stiff over-

consolidated soil due to pile installation. As a stiff soil unloading response, a small contraction of the interface zone causes significant radial stress reduction applied by the far field on the pile shaft. As the relative depth to pile tip (h) increases, the interface zone contracts and the spring unloads, thus reducing the shaft friction on the pile.

The friction fatigue effect is represented in ICP-05, and Fugro-05 method by the relative depth to pile tip (h) normalised by an equivalent radius of the pile (R^*). Gavin and Lehane (2007) state that the local shaft friction was affected by the degree of plugging during installation as defined by Incremental Filling Ratio (IFR). White and Bolton (2005) show that profiles of radial stress along the pile shaft can be differentiated by an effective area ratio ($A_{r,eff}$) which is a measure of the soil displacement during installation determined by the IFR. Xu (2007) state to avoid term h/R^*, the shaft friction UWA-05 method uses h/D and $A_{r,eff}$ to incorporate friction fatigue and soil displacement in the specific soil horizon during pile installation. Summaries shaft friction calculation method in sand shows in Table 2.1.

2.4.2 Base Resistance

The ultimate base stress is defined as the unit base resistance developed at a pile displacement equating to 10% of the pile diameter ($q_{b0.1}$). The base resistance calculation is a function of average cone resistance ($q_{c,avg}$) which depends on the method of pile installation, the surface scale effect, and the pile end conditions (closed and open-ended). The degree of soil displacement during installation has a significant effect on pile response to static loading (Gavin and Lehane, 2007). The base resistance stress for an unplugged open-ended pile acts in the annular area, whereas the plugged pile will have bearing capacity in the full area of the pile.

During pile driving, the soil plug condition inside the pile affects the behaviour of dynamic driving resistance and static bearing capacity. White and Bolton (2005) illustrated the schematics streamline of soil flow and profiles of radial stress in closed-ended piles, fully coring or unplugged open-ended piles and partially plugged open-ended piles as shown in Figure 2.8. In the fully plugged condition, soil displaces roughly equal to the solid pile volume which causes an increase in the radial and base stress thus resulting in higher driving resistance and static capacity (Xu, 2007). In an unplugged condition which usually occurs for a large diameter pile, the soil displacement is approximately the same as the pile volume causing lower radial and base stress.

Table 2.1 The CPT-based design method for shaft friction calculation of driven piles in sand (modified after Xu, 2007)

Methods	Design Equations
Fugro-05	$\tau_f = 0.08\, q_c \left(\frac{\sigma'_{v0}}{p_{ref}}\right)^{0.05} \left(\frac{h}{R^*}\right)^{-0.9}$ $compression\ loading\ \ for\ \left(\frac{h}{R^*}\right) \geq 4$ $\tau_f = 0.08\, q_c \left(\frac{\sigma'_{v0}}{p_{ref}}\right)^{0.05} (4)^{-0.9} \left(\frac{h}{4R^*}\right)$ $compression\ loading\ for\ \left(\frac{h}{R^*}\right) < 4$ $\tau_f = 0.045\, q_c \left(\frac{\sigma'_{v0}}{p_{ref}}\right)^{0.15} \left[max\left(\frac{h}{R^*}, 4\right)\right]^{-0.85}$ $tension\ loading$
ICP-05	$\tau_f = a\left(0.029\, b\, q_c \left(\frac{\Delta\sigma'_{v0}}{p_{ref}}\right)^{0.13} \left[max\left(\frac{h}{R^*}, 8\right)\right]^{-0.38} + \Delta\sigma'_{rd}\right) tan\ \delta_f$ a = 0.9 for open-ended piles in tension and 1.0 in all other cases b = 0.8 for piles in tension and 1.0 for piles in compression
UWA-05	$\tau_f = \frac{f_t}{f_c}\left(0.03\, b\, q_c\, {A_{r,eff}}^{0.3} \left[max\left(\frac{h}{D}, 2\right)\right]^{-0.5} + \Delta\sigma'_{rd}\right) tan\ \delta_f$ $\frac{f_t}{f_c}$ (ratio of tension to compression capacity) = 1 for compression and 0.75 for tension $A_{r,eff}$ (effective area ratio) $= 1 - IFR\ (D_i/D)^2$ IFR (Incremental Filling Ratio, the incremental increase in soil plug length over the pile penetration depth) $= \Delta h_{plug}/\Delta L_{pile}$
Notes	τ_f is the local ultimate shaft friction q_c is the cone tip resistance σ'_{v0} is the effective vertical soil stress at specific depth z δ_f is the constant volume interface friction angle h (relative depth to pile tip) = pile tip elevation – specific depth z p_{ref} (reference atmospheric stress) = 100 kPa R^* (equivalent radius) $= (R^2/{R_i}^2)^{0.5}$ where R_i is the pile internal radius R^* *is* a radius equivalent to a circular pile with the same end area (for non-circular pile) $\Delta\sigma'_{rd}$ (change in radial stress during pile loading) $= (4G_0/D)\,\Delta y$ G_0 (shear modulus) $= q_c 185\, {q_{c1N}}^{-0.7}$ where $q_{c1N} = \left(q_c/P_{ref}\right)/\left(\sigma'_{v0}/P_{ref}\right)^{0.5}$ D is the pile outer diameter Δy (radial displacement during pile loading) = 0.02mm

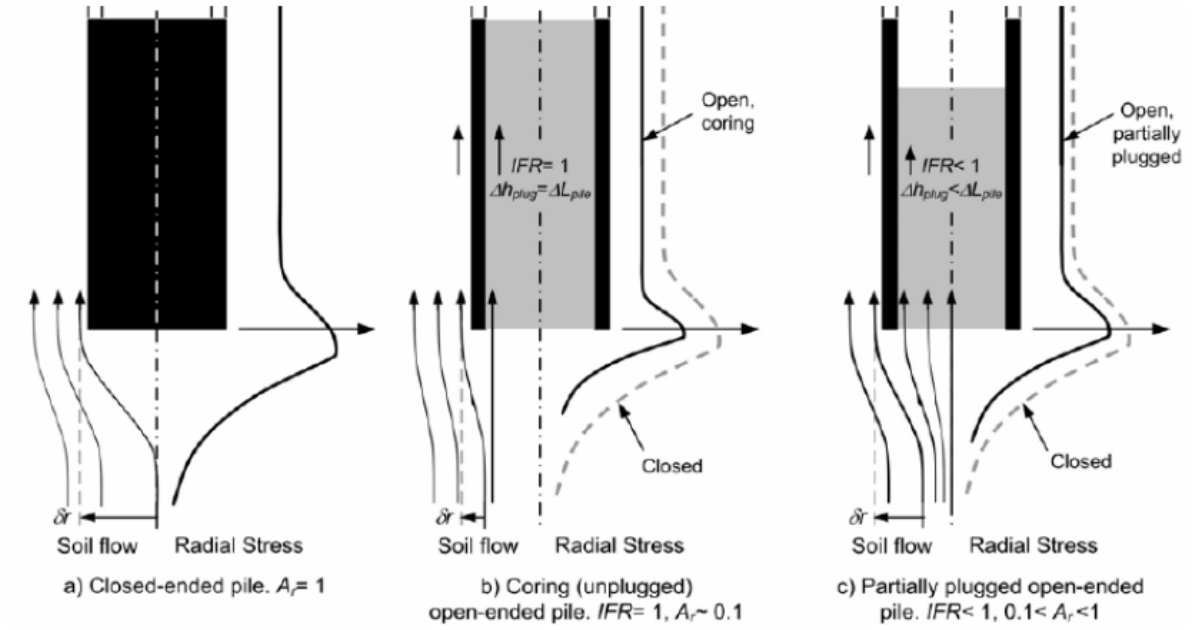

Figure 2.8 Soil flow and profiles of radial stress; δr is radial displacement of soil element at pile wall (White and Bolton, 2005)

The Incremental Filling Ratio (IFR=$\Delta h_{plug}/\Delta L_{pile}$) is zero when there is no soil plug movement inside the pile, between zero and one when the pile is partially plugged and one when the pile is fully coring. The base condition when installing a large diameter of an open-ended pile in the uniform soil is likely fully coring or unplugged (IFR=1). The soil will tend to be plugged or move along with the pile increment (0<IFR<1) under slow loading condition such as a static load test.

The UWA-05 approach that is proposed by Lehane, Schneider and Xu (2005) including the effect of partial plugging during installation on base resistance mobilised at the base displacement of 10% of the pile diameter. The UWA-05 takes the final filling ratio (FFR) as IFR at the final stage of installation to calculate base resistance. The other methods such as ICP-05 and Fugro-05 neglect partially-plugging condition in base resistance calculation. The Fugro-05 also calculate base resistance at pile tip displacement of 10% diameter of the pile whereas ICP-05 takes pile head displacement for 10% of the pile diameter. Both Fugro-05 and ICP-05 will take base resistance as fully coring or fully plugged. The CPT-based calculation methods to compute unit base resistance in sand are summarised in Table 2.2.

During pile installation process, the driving force will push the pile until exceeding the ultimate pile capacity resulting pile move forward into the ground. When removing driving force at the pile top (zero pile load) the base resistance (Q_b) will equal with downward shaft resistance ($Q_{s,neg}$), and the pile tends to move backwards or rebound. At zero pile loading, unit base residual and downward skin friction refers as a base residual stresses ($q_{b,res}$) and negative skin friction ($\tau_{f,neg}$) respectively.

Table 2.2 The CPT-based design method for unit base resistance calculation of driven piles in sand (modified after Xu, 2007)

Methods		Base Condition	Design Equation
Sand	Fugro-05	Close & open	$\frac{q_{b0.1}}{q_{c,avg}} = 8.5\left(\frac{P_{ref}}{q_{c,avg}}\right)^{0.5} {A_r}^{0.25}$
	ICP-05	Close	$\frac{q_{b0.1}}{q_{c,avg}} = maximum\left[1 - 0.5\, log\left(\frac{D}{D_{CPT}}\right), 0.3\right]$
		Open	If $D_i \geq 2.0\,(D_r - 0.3)$ or $D_i \geq 0.083\,\frac{q_{c,avg}}{P_{ref}}\,D_{CPT}$ pile is unplugged $\frac{q_{b0.1}}{q_{c,avg}} = A_r$ if not, pile is plugged $\frac{q_{b0.1}}{q_{c,avg}} = maximum\left[0.5 - 0.25\, log\left(\frac{D}{D_{CPT}}\right), 0.15, A_r\right]$
		Non-circular	$\frac{q_{b0.1}}{q_{c,avg}} = 0.7$
	UWA-05	Close & open	$\frac{q_{b0.1}}{q_{c,avg}} = 0.15 + 0.45\, A_{r,eff}$
Notes			D is the pile outer diameter D_i is the pile inner diameter D_{CPT} (conus diameter) = 0.036 m A_r (area ratio) $= 1 - (D_i/D)^2$ $A_{r,eff}$ (effective area ratio) $= 1 - FFR\,(D_i/D)^2$ FFR (final filling ratio) = IFR $\left(= \Delta h_{plug}/\Delta L_{pile}\right)$ average over the last $3D_i$ of the pile penetration $q_{c,avg} = q_c$ average $\pm 1.5D$ over pile tip level for Fugro-05 and ICP-05 $q_{c,avg} = q_c$ average using the Dutch averaging technique for the UWA-05*) D_r (nominal relative density) $= 0.4\, ln\left[\left(q_{c,tip}/22\right)/\left(P_{ref}/\sigma'_{v0}\right)^{0.5}\right]$ *) $q_{c,avg} = q_c$ average ± $\pm 1.5D$ for UWA-05 as SRD input

3 Modelling Process

This chapter discusses all aspects to consider when developing driveability analysis models. These aspects are the time effect, soil displacement during driving and base residual loads after each driving increment. Furthermore, this chapter presents the inputs data from Blessington site which are required to perform driveability analysis such as soil parameters, hammer specification, and pile properties including material and geometry. This chapter also presents recorded blow counts and measured incremental filling ratio (IFR). These data are essential to verify blow count predictions from this study.

Figure 3.1 shows a flow chart of driveability analysis in this study. The soil data and pile properties will be needed to calculate shaft and base resistance with axial static capacity methods (i.e., UWA-05, ICP-05 and Fugro-05). The calculated base resistance is inputted directly to the SRD profile, while the shaft resistance must be calculated with the pseudo average skin friction before inputted in the SRD profile. The wave equation analysis is performed with a combination of soil data in the form of the SRD and dynamics soil component (i.e., quake and damping), pile, and hammer properties. The total resistance (blow counts) is resulted from the wave equation analysis. The first modification into the model integrates the base resistance-displacement to the base resistance and add the time factor to the shaft resistance. More modification is applied by including the base residual stresses to the base resistance in the SRD profile.

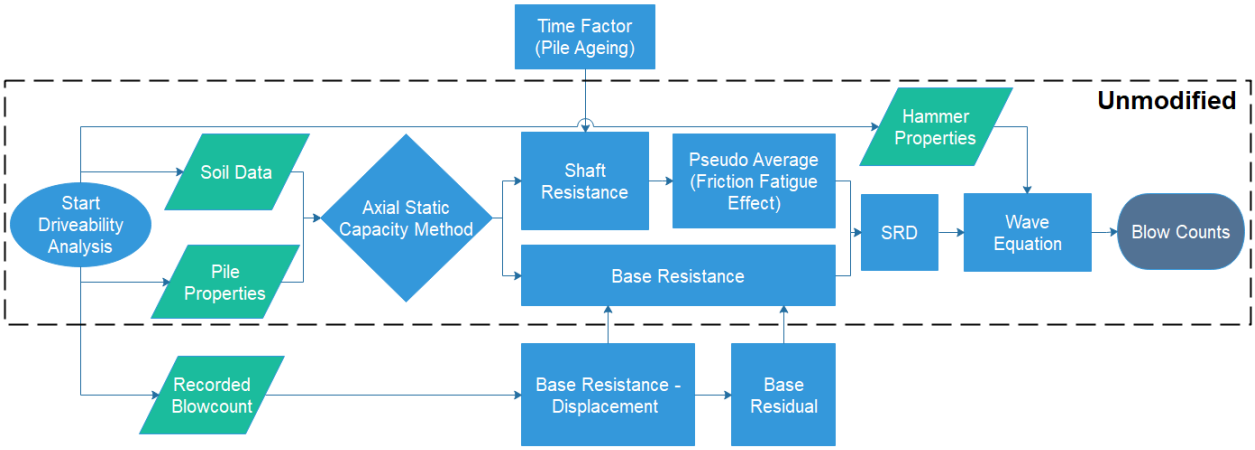

Figure 3.1 Flow chart driveability analysis

3.1 Database Assessment

The project consists of 7 steel open-ended full-scale test piles at Blessington, southwest of Dublin, Ireland. Soil properties and ground conditions at the Blessington site have been used in the various experiments as reported in Gavin and Lehane (2007), Gavin *et al*. (2013), Prendergast *et al.* (2013), and Kirwan (2014). The soil profile at this site consists of very dense sand in the heavily over-consolidated state due to glacial deposit history and previous significant overburden pressure. The groundwater table is approximately 13m below ground level (bgl). The in-situ water content relatively uniform at 10-12% above the water table. Blessington pile tests are conducted above the water table where pore pressure dissipates almost immediately. This test does not compromise the comparability of the site to offshore deposits where the soil is fully saturated as pile capacities are determined by effective stresses (Gavin *et al.*, 2013).

The sand relative density ranges between 90% and 100%. The particle size (D_{50}) was varied between 0.1mm and 0.15mm based on particle size distribution analysis from samples located between 0.7-2m bgl. From the grain size analysis, the soil is well-graded angular sand with 5-10% fines content (percentage of clay or silt particle). The sand has a unit weight of 20 kN/m^3. The constant volume friction angle from ring shear test, the triaxial test is 36˚ and 37˚. Particle morphology (particle size, angularity and roundness) have been correlated to the constant volume friction angle. Kirwan (2014) link particle morphology (particle size, angularity and roundness) at Blessington site with the constant volume friction angle give results of 30˚ and 32˚.

A total of 10 CPTs was conducted at the site. Cone tip resistance (q_c) profile shows at Figure 3.2a indicate that q_c ranging from 10 MPa at 2m bgl to 20 MPa at 7m bgl. The shear wave velocity (V_s) shows at Figure 3.2b obtained in the field using the multi-channel analysis of surface wave (MASW) method. The soil shear modulus (G_o) profiles are derived from V_s are shown in Figure 3.2c. This G_o profiles has a comparable ratio with G_o/q_c of 6 as suggested in Prendergast *et al.* (2013) which is applicable for unknown V_s value. The assumption of Poisson's ratio (ν) equal to 0.1 is used at very small strain levels. The peak friction correlated with the CPT q_c value and based triaxial test give similar result range from 54˚ near ground surface to 42˚ at 7m bgl.

At Blessington site, seven open-ended piles named S1-S7 were driven into the ground. The total pile length of 8.76m were driven up to 7m bgl except for pile S7 which driven until 6.5m bgl. All piles are steel piles with Young's modulus value of 2x10^{11} N/m^2 and have identical geometry with an external diameter (D) of 0.34m, internal diameter (D_i) of 0.312m, and wall thickness (t_w) of 0.014m. Blessington pile tests can be considered as a representative of typical offshore piles geometries with the diameter to wall thickness D/t_w ratio of 24.3 and length to diameter L/D ratio S1-S6 and S7 of 20.6 and 19.1, respectively (Kirwan, 2014). Offshore piles have D/t_w ratio between 15 and 45 (Jardine and Chow, 2007), and a diameter between 0.66m and 2.13m which are paired with pile penetration between 26m and 87m bgl (Overy and Sayer, 2007).

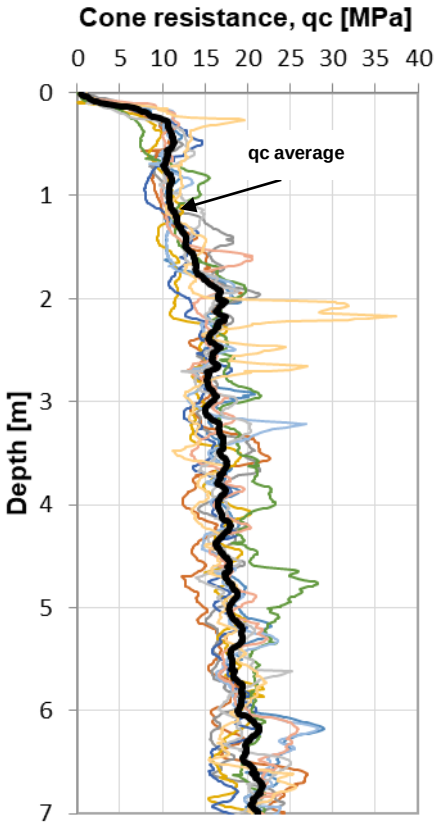

(a) Cone tip resistance, q_c

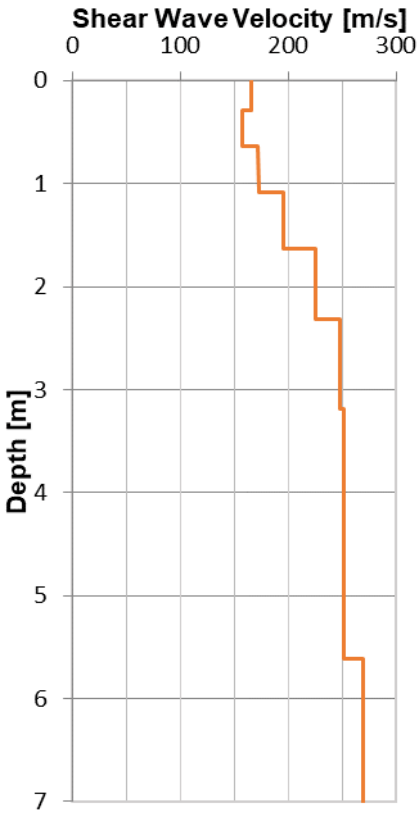

(b) Shear wave velocity, V_s

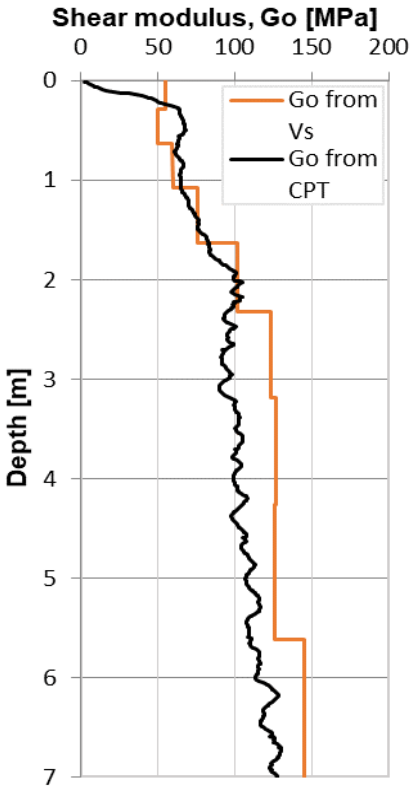

(c) Shear modulus, G_o

Figure 3.2 Soil properties at Blessington

Blow count records at Blessington for all piles are plotted in Figure 3.3a. All piles tend to increase in blow counts with depth. Blow count recorded shows that pile S4 has low blow counts compared to S2, S3 and S5. Pile S6 gives highest blow count result compare to the other piles. The blow counts recorded are not directly comparable since the piles had different hammers and stroke heights except for piles S2-S5. Table 3.1 shows hammer properties at Blessington pile tests. Pile S1-S5 and S6-S7 were driven using 4000kg Junttan PM16 and 5000kg Junttan PM20 respectively as a piling hammer. Piles S1 and pile S2-S5 were driven with the same constant stroke height of 0.4m and 0.3m accordingly. Pile S6 had combine stroke height from 0.2m for the first four meter and 0.35m for the rest installation. Pile S7 had stroke height varies along the pine penetration, begin with 0.2m until 0.3m in 0.025m increment stroke height.

Table 3.1 Hammer properties at Blessington

Pile Name	Penetration length [m]	Hammer	Cushion	Stroke height [m]
S1	7	4000kg Junttan PM16	None	0.4
S2	7	4000kg Junttan PM16	None	0.3
S3	7	4000kg Junttan PM16	None	0.3
S4	7	4000kg Junttan PM16	None	0.3
S5	7	4000kg Junttan PM16	None	0.3
S6	7	5000kg Junttan PM20	50mm ash timber	0.2 (0-4m) & 0.35 (4-7m)
S7	6.5	5000kg Junttan PM20	50mm ash timber	0.2 - 0.3m (increment 0.025m)

Figure 3.3b shows Incremental Filling Ratio (IFR) measure during pile installation. All piles developed a similar IFR profile. Pile S1, S2, S3 and S5 were nearly fully coring or unplugged (IFR=1) over the first meter of the pile penetration and becoming partially plugged (IFR=0.4) at the end of driving with 2.45m final plug depth. Pile S4 has less plugging during installation indicate with IFR profile with IFR=0.75 at the end of driving with 2.26m final plug depth. IFR measurement from S6 is not considered as reliable due to significant scatter at 2m final penetration with 2.56m final plug depth. Pile S7 experience more plugging which is indicated by deeper final plug depth (3.3m) and lower IFR at the end of driving. The calculation of pile capacity UWA method requires IFR that will be taken from S1, S2, S3, S5 as representative IFR value.

Pile S6 has the highest blow counts despite there being no significant difference in cone tip resistance (q_c) value near this pile location compared to the other piles. This condition could be resulted because pile S6 has lower stroke height for the first 2m than the other piles even though It has higher hammer energy. Another possibility is due to pile S6 has a slightly higher final plug depth which gives higher resistance as a consequence pile driving becomes more difficult. As noted from Kirwan (2014) pile S6 was driven 1-year after S1-S5, the distance between S6 pile is 6.4D which larger than 6D as the minimum recommendation distance to avoid pile group effect noted in Yang (2006).

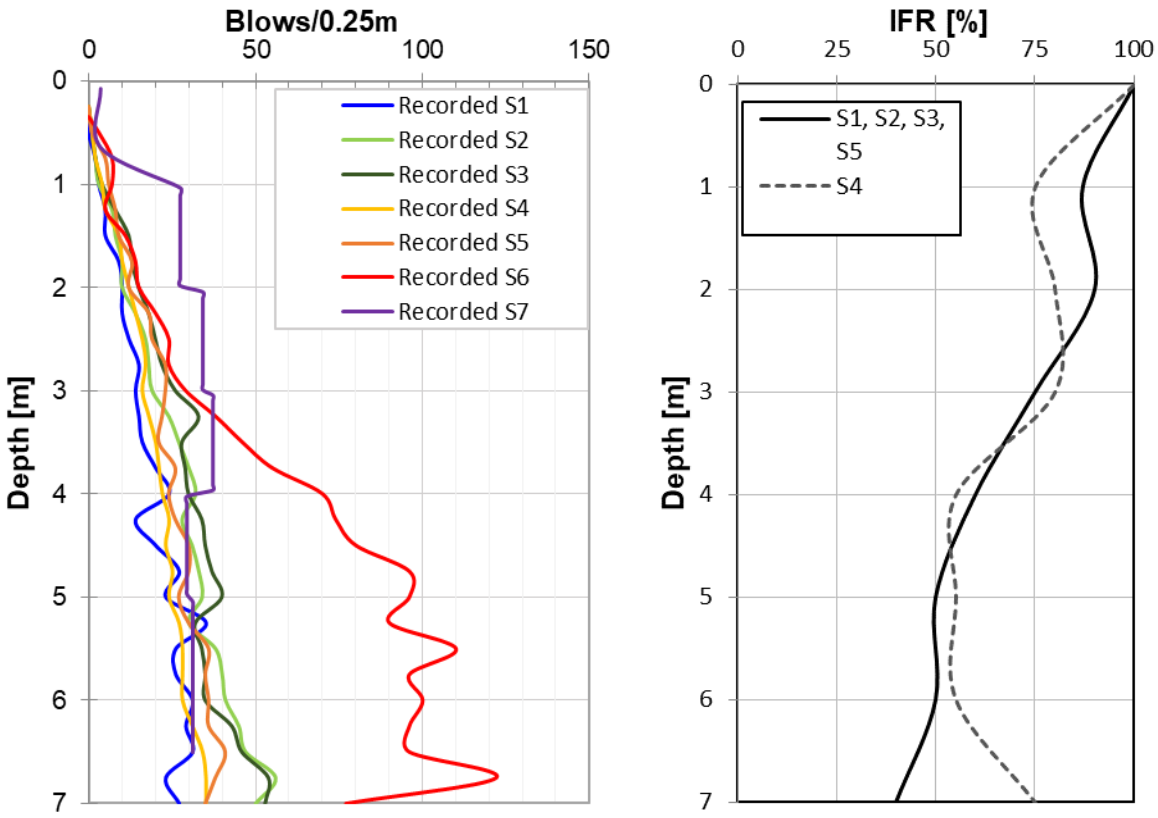

(a) Incremental blow counts (b) IFR

Figure 3.3 Measurement during driving

3.2 Time Effect

There are various CPT-based methods to determine the axial static capacity of piles such as the UWA-05, ICP-05, and Fugro-05. These methods to calculate the axial capacity are derived empirically from a pile load test between 10 and 30 days after pile installation. Various studies indicate axial static capacity increase with time (Jardine *et al.*, 2006; Gavin *et al.*, 2013; Karlsrud *et al.*, 2014; Gavin *et al.*, 2015). These studies suggest that pile resistance during installation will be lower than the available model calculation. A time factor should be applied to determine the driveability from the available CPT-based static axial capacity methods.

Jardine *et al.*, (2006) observe the ageing effect in the dense sand by determining Intact Ageing Curves (IAC) which indicate a reduction in capacity to 0.7 times for 1-day shaft capacity. Lehane *et al.* (2017) collected recent pile ageing database including field test at Dunkirk (Jardine *et al.*, 2006), Blessington (Gavin *et al.*, 2013), and Larvik (Karlsrud *et al.*, 2014) to determine an equation that represents continuous time factor in shaft friction calculated as

$$F_{time} = \frac{1}{\exp(-0.1\ t^{0.68})+0.45} + d_{offset} \qquad \text{Equation 3.1}$$

Where t is the pile age in days and d_{offset} is the vertical offset that best fits the data points. The observation that includes the five of the design methods (NGI-05, ICP-05, UWA-05, API-00, and Fugro-05) gives median ageing periods for piles database derived at a time equal to 14

days and d_{offset} equal to zero. This time factor can be applied to define shaft friction during driving with a time equal to zero. Based on this calculation, the time factor of 0.69 is applied for shaft friction SRD calculation.

Time effect results from the changes in the total stress and pore pressure due to soil displacement during the pile driving (Schneider and Harmon, 2010). The pile ageing observation at Blessington is controlled by a combination of creep and interface roughness. Creep leads to an increase in the radial effective stress equalisation and enhanced dilation while the increase in the interface roughness actuates large mobilised pile capacities (Gavin *et al.*, 2013).

3.3 Base Resistance-Displacement

Laboratory and field test indicated the degree of soil displacement during driving affect the pile response during static loading (Paik *et al.*, 2003). The unit base resistance definition proposed by the CPT-based axial capacity methods such as UWA-05, ICP-05, and Fugro-05 are assumed pile displacement of 0.1*D* (outer pile diameter). During pile installation, pile experiences less displacement than 0.1*D*. Besides that, fully coring pile or unplugged pile (IFR=1) will experience less displacement than close-ended piles. As mentioned in Section 2.4.2, the UWA-05 method is the only method that considers partially plugging condition which is represented by the Final Filling Ratio (FFR) value. This means that there is a possibility for integrating actual displacement with the UWA-05 method to produce base resistance model that resemble actual driving process.

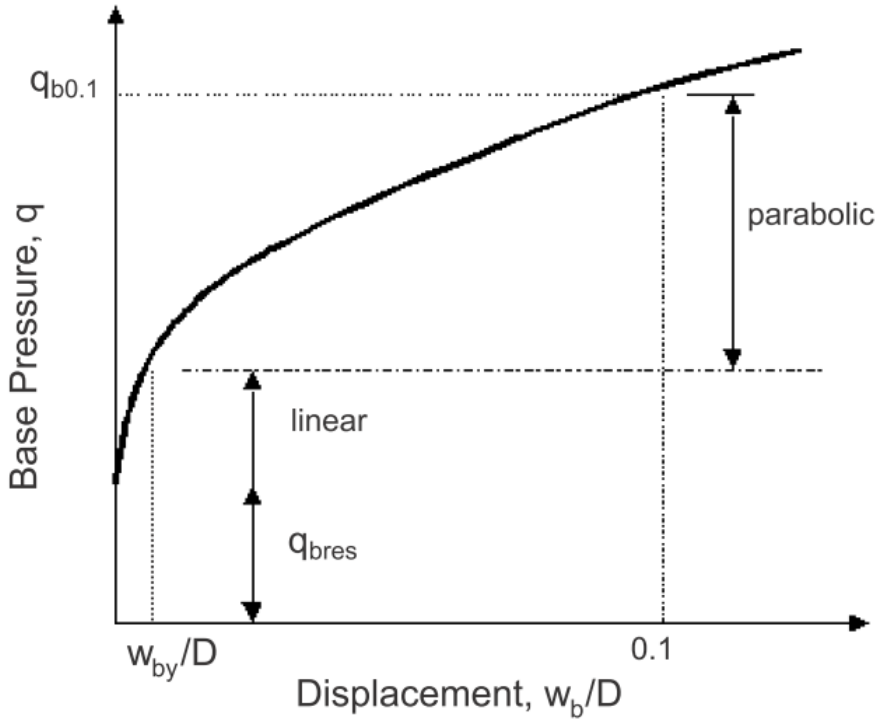

Figure 3.4 Base resistance-settlement model (Gavin and Lehane, 2007)

Byrne *et al.* (2018) propose the implementation of the three-stage base resistance-displacement model (Gavin and Lehane, 2007) to estimate the base resistance mobilise during each hammer impact. Figure 3.4 shows the idealised base resistance-displacement model that is consisted of the unit base resistance (q_b) versus the pile tip displacement (w_b) normalised by pile diameter (D). The ratio of w_b/D is calculated for every depth from the actual blow counts that is recorded. The base stiffness formulation at the three-stage $q_b - w_b$ relationship based on (Gavin and Lehane, 2007). In the first stage, no pile tip movement occurs until the residual base stresses ($q_{b,res}$) is exceeded.

In the second stage, the relationship between q_b and w_b/D is linear until the strain level (w_{by}) of 0.015D (Byrne *et al.*, 2018). The strain level is controlled by stress history at the pile base. The magnitude of strain level depends on equivalent Young's modulus (E_{beq}) which comparable with a very small strain elastic stiffness (E_o) at the in-situ stress level. The expression for the shear modulus (G_o) correlation with the E_o and the linear stage of the curve are represented by following

$$E_0 = 2G_o(1 + \nu) \quad \text{Equation 3.2}$$

$$q_b = \left[k_1 \left(\frac{w_b}{D}\right)\right] + q_{b,res} \quad \text{Equation 3.3}$$

$$k_1 = \left(\frac{4}{\pi}\right)\left[\frac{E_0}{1-\nu^2}\right] \quad \text{Equation 3.4}$$

Where E_o is a small strain elastic stiffness, G_o is the shear modulus, ν is the Poisson's ratio, w_b is the pile tip displacement, D is the outer pile diameter, and $q_{b,res}$ is the residual base resistance.

The last stage, the non-linear part where $w_{by}/D < w_b/D < 0.10$ is approximately parabolic, but in this research, it will be simplified by another linear part. In this stage, the level of prestress that occurs in the sand at the pile tip causes the significant strain degradation in base resistance increase. The maximum base resistance from UWA occurs when displacement 0.1D.

$$q_b = k_2\left[\left(\frac{w_b}{D}\right) - 0.015\right] + 0.015k_1 \quad \text{Equation 3.5}$$

$$k_2 = \frac{y_2 - y_1}{x_2 - x_1} = \frac{q_{b01,UWA} - 0.015\ k_1}{0.085} \quad \text{Equation 3.6}$$

Where w_b is the tip displacement, D is the outer pile diameter, (x_1 ; y_1) = (0.015 ; 0.015 k_1), (x_2 ; y_2) = (0.1 ; $q_{b01,UWA}$), and $q_{b01,UWA}$ is the unit base resistance from UWA-05 method.

3.4 Residual Base Effect

During driving, the pile will experience compression due to the hammer blow and tension due to zero pile loading. The hammer blow results in the driving force will push the pile forward into the ground. At zero pile loading, tension force occurs at the pile will tend to move

backwards or rebound. In this condition, the residual base stress ($q_{b,res}$) at the pile base area will equate with negative skin friction ($\tau_{f,neg}$) along the pile shaft. Figure 3.5 illustrate the development of residual base stress during the pile driving.

Paik *et al.* (2003) state that the presence of residual base stresses did not affect the ultimate bearing capacity during the axial static load test due to the summation of residual shaft and base for the pile will equal to zero. However, the $q_{b,res}$ must be acknowledged when considering the pile driveability analysis due to the proportion of base and shaft resistance. Except in ultimate bearing capacity calculation, ignoring residual load will overestimate the shaft resistance and underestimate the base resistance.

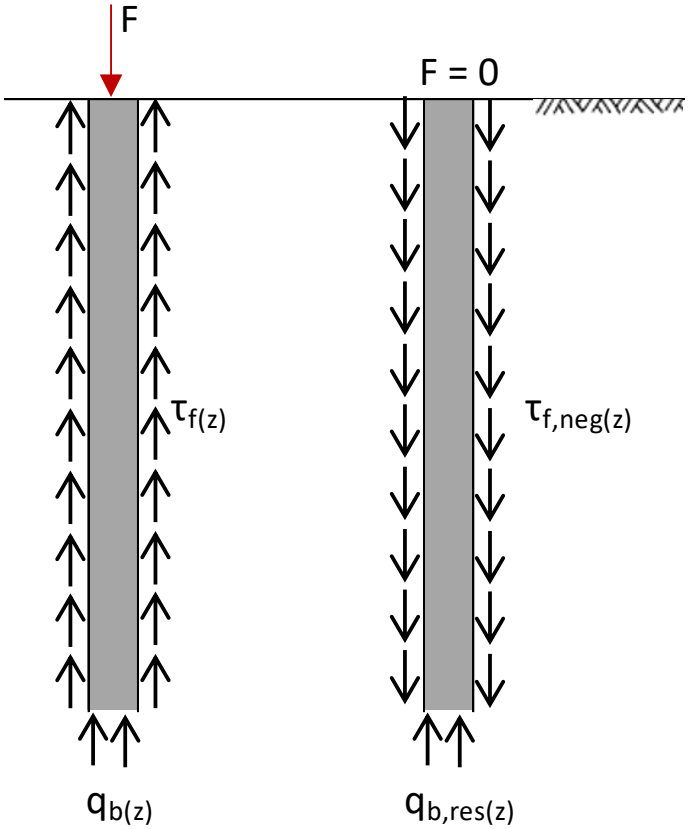

(a) Pile in compression (b) Residual stresses at zero pile loading

Figure 3.5 The development of residual base stress during pile driving

Alawneh and Husein Malkawi (2000) propose a method to estimate the post-driving base residual stresses as a function of the pile penetration length, pile diameter, pile area, shear modulus and pile Young's modulus. This method gives residual stresses that range between 0 and 4000 kPa which represent the stiff-short pile in the loose sand and the flexible-long pile in the dense sand, respectively. Paik *et al.* (2003) measure the residual stress at Pigeon River site with 0.356m diameter closed and open-ended piles that give a similar result between 11-14% of q_c.

The estimation of the residual base stress method is highly empirical. Pile with the same installation method in a similar soil condition will have a similar residual load. There is no method which is reliable to estimate the magnitude of the residual base stresses without future

adjustment based on site soil condition. This research will assess the sensitivity analysis incorporate the residual base stresses ($q_{b,res}$) for every UWA-05 unit base resistance. The residual base stress is range between 1% and 10% of the q_c value as recommend in Byrne *et al.* (2018).

The base resistance assessment estimates the residual base stress that incorporates the time effect and degree of the pile tip displacement. Firstly, the sensitivity analysis of an additional unit base resistance at every penetration depth is calculated as follows.

$$q_{b,n\%(z)} = \{1\,;2\,;5\,;8\,;10\}\,\%\;\; q_c \qquad \text{Equation 3.7}$$

Where q_c is the cone tip resistance, n is an additional number, and z is the element depth. The second and third steps are essential to convert stresses to load due to equilibrium occurs when the negative shaft resistance ($Q_{s,neg}$) equals to the base resistance (Q_b). The second step is the calculation of the base resistance from additional stepwise the unit base resistance along the pile base area.

$$Q_{b,n\%(z)} = q_{b,n\%(z)}\;\; A_b \qquad \text{Equation 3.8}$$

Where $q_{b,n\%(z)}$ is an additional $n\%$ of unit base resistance at depth-z, and A_b is the pile base area. Thirdly, the negative shaft resistance calculation at every pile depth following skin friction UWA-05 method ($\tau_{f,UWA(z)}$) for the pile in tension are incorporated with the time effect.

$$Q_{s,neg(z)} = 0.75\, F_{time}\, \tau_{f,UWA(z)}\, A_{s(z)} \qquad \text{Equation 3.9}$$

Where F_{time} is a time factor, $\tau_{f,UWA(z)}$ is average skin friction at z using the UWA-05 method, and $A_{s(z)}$ is pile shaft area until depth-z. The additional base residual in the pile must be smaller than the negative shaft resistance. Last step is base residual stress calculation.

$$q_{b,res(z)} = \frac{minimum\,(\,Q_{b,n\%(z)}\,;\;Q_{s,neg(z)}\,)}{A_b} \qquad \text{Equation 3.10}$$

Where $Q_{b,n\%(z)}$ is the base resistance from additional unit base resistance at z, and $Q_{s,neg(z)}$ is the negative shaft resistance.

4 Analysis & Results

The database of full-scale test piles at Blessington site is used as the primary input for the SRD calculation which integrates several modification factors such as displacement during driving, pile ageing effect, and residual base stresses. The SRD modified will be input for wave analysis to result in blow counts. This chapter shows the result of various model CPT-based axial static capacity as applied in driveability analyses. This chapter presents modelling result piles S1-S2 Blessington site as representative piles. The other Blessington piles result analysis are summaries in the Appendix B.

4.1 Base Resistance-Displacement Curve

This section investigates the base resistance-displacement curves based on a simplified three-stage base resistance-displacement (Gavin and Lehane, 2007) that is mentioned in Section 3.3. During the pile driving, the pile experiences lower tip displacement than the failure criteria of 0.1 of the pile diameter (D) as suggested on the UWA-05, ICP-05 and Fugro-05 approaches. This base resistance (q_b) – displacement (w_b) modification incorporates the actual pile tip displacement (w_b) for each hammer blow to estimate the actual mobilised end resistances. The initial pile displacement is linear until a yield strain assumes of 0.015 of pile diameter (D). Next stage is a non-linear parabolic stage while in this study will be simplified by another linear model between 0.015D until 0.1D. The actual displacements for each hammer blows are back-calculated from blow counts recorded at Blessington piles. Then, each displacement is normalised by the pile diameter. The residual base stress assumes to be zero. The base resistance calculated using the UWA-05 approach which accommodates partial plugging condition at pile tip.

Figure 4.1 shows the base resistance-displacement curve at various depth. In the first linear part, at w_b/D < 0.015, the q_b - w_b/D curves are increased mirroring soil elastic stiffness (E_o) value which increases along the pile depth. The base resistance value from the UWA-05 approach ($q_{b01,UWA}$) is used as a limit when w_b greater than the failure criteria of 0.1 of pile diameter (D). The pile tip displacement normalises by the pile diameter (w_b/D) during the pile driving are shown in the red dot. Almost all w_b/D occur at the second linear stage between 0.015 and 0.1. The w_b/D are decreased as the blow counts increased at deeper pile penetration. The w_b during driving less than failure criteria of 0.1D except for the first meter when the pile is fully coring (IFR=1).

Figure 4.1a shows the base resistance - displacement curves for pile S1 at various depth. It can be observed that at 0.5m, q_b - w_b/D equal to zero correspond to zero recorded blow count at this depth. Zero blow count can be an indication of self-weight penetration occurrence at 0.5m depth. Although pile self-weight calculation indicates no self-weight penetration in Blessington site, ignoring equipment weight can be the reason zero blow count record occurs at a depth near the surface. At 1-1.5m depth, w_b value is higher than 0.1D due to back-

calculated from small blow count recorded. Figure 4.1b shows pile S2 base resistance-displacement curves at various depth. Pile displacement (w_b) pile S2 is smaller than S1 due to recorded blow count pile S2 higher than S1 as shown in Figure 3.3a. Regardless of different hammer properties and recorded blow counts, all piles in Blessington have a similar trend. Piles tend to have smaller displacement as the pile penetration increases.

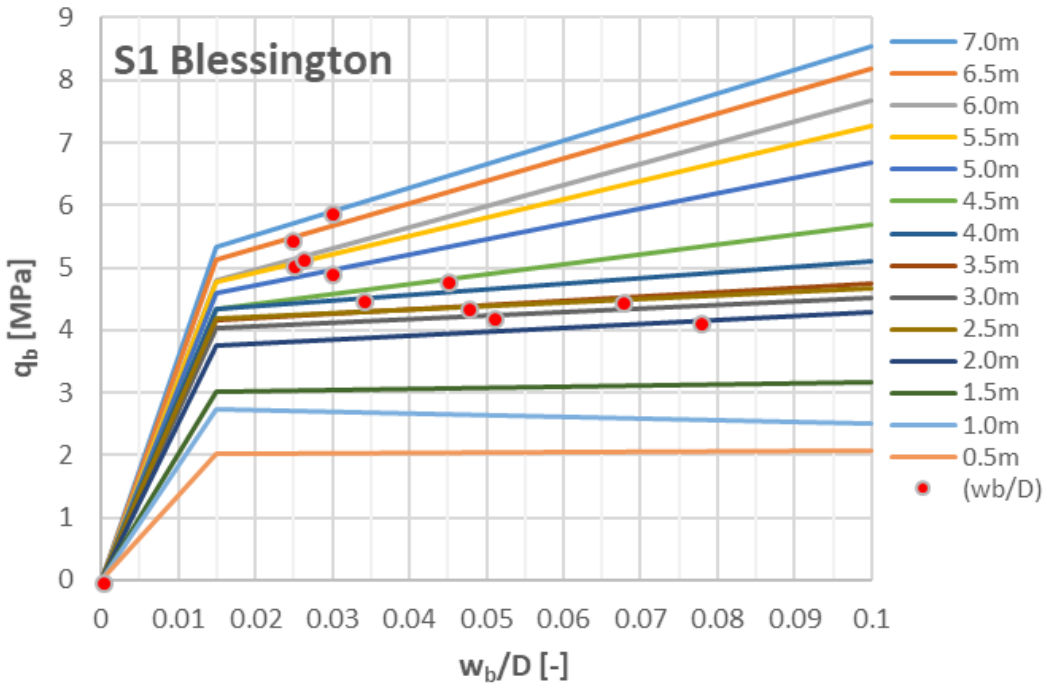

(a) Pile S1

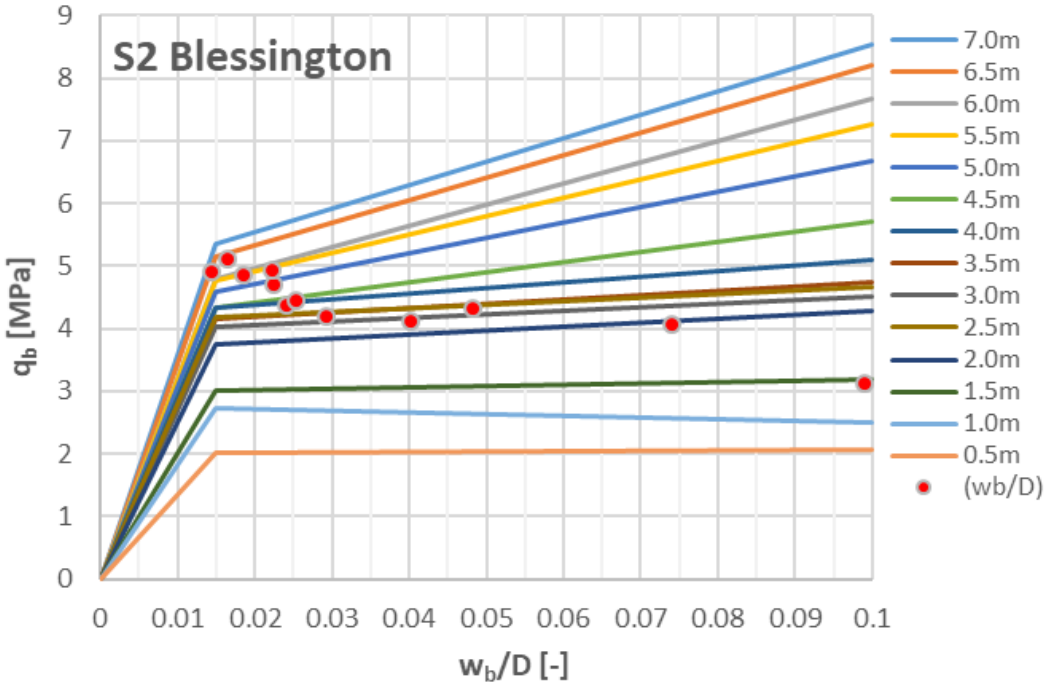

(b) Pile S2

Figure 4.1 Base resistance-displacement curves at various depth

4.2 Static Capacity Approach Comparison

The model is conducted to perform driveability based on CPT-based axial static capacity and depicted in the previous flowchart, Figure 3.1. The model is divided into two categories, the unmodified and modified. Both models are based on the CPT-based axial static capacity approach proposed by UWA-05, ICP-05, Fugro-05 (Lehane *et al.*, 2005; Jardine *et al.*, 2005; Kolk *et al.*, 2005). The shaft resistance and unit base resistance compose SRD profile that are derived from axial static calculation approaches. Every model computes the skin friction average that incorporates friction fatigue based on pseudo-average calculation as mention in Equation 2.1. The ICP-05 and Fugro-05 method are modelled with plugged and unplugged conditions since the unit base resistance calculation are not able to integrate partially-plugging condition. Later, the SRD profiles are derived for all methods. Then, the wave equation is performed to predict blows/0.25m. In this comparison, there are a total of 10 model which are consisted of the unmodified and modified with base-displacement are applied using the UWA-05, ICP-05, Fugro-05 in plugged and unplugged condition.

The unmodified model is the original model proposed by the UWA-05, ICP-05, Fugro-05 for calculating the axial static capacity without any modification factor to estimate driveability. The predicted blow counts at Blessington for pile S1 and S2 are shown in Figure 4.2a and Figure 4.2b respectively. The result shows the comparison of the driveability analysis from all model and the actual blow counts. Pile S1 as shown in Figure 4.2a has smaller blow counts estimation along the pile compared to pile S2 as shown in Figure 4.2b. However, the prediction trend for every CPT-based axial static capacity method is similar for piles S1 and S2 in Blessington.

The relatively reasonable estimation with a slight of underprediction and overprediction are given when applying the unmodified model to Fugro-05 in unplugged and ICP-05 in plugged respectively. However, both unmodified model of UWA-05 and Fugro-05 in plugged condition give poor prediction with overestimate increase along the pile depth. On the other hand, the unmodified model for both S1 and S2 with SRD that are derived from the ICP-05 approach in unplugged condition provide under-estimate blow counts prediction. Despite all the unmodified models assume the base resistance at failure criterion of 0.1D and derived several days after the end of the installation, the blow count profile result still describes the soil layer along the pile. Therefore, the modification models to the axial static capacity approaches will be applied to give a better prediction that represent actual driving resistance.

The modified models are the UWA-05, ICP-05, and Fugro-05 static capacity approaches with some consideration for modification that integrates pile ageing effects and the base-displacement model to estimate driveability. The static axial approaches are derived several days after the installation which obtains time-dependent increases in axial capacity. For this reason, pile ageing effect is essential to consider when using the static capacity approach to estimate pile driveability. The pile ageing applied with a time factor following Equation 3.1 which show a reduction value of 0.69 will be applied to skin friction from all unmodified model along shaft area.

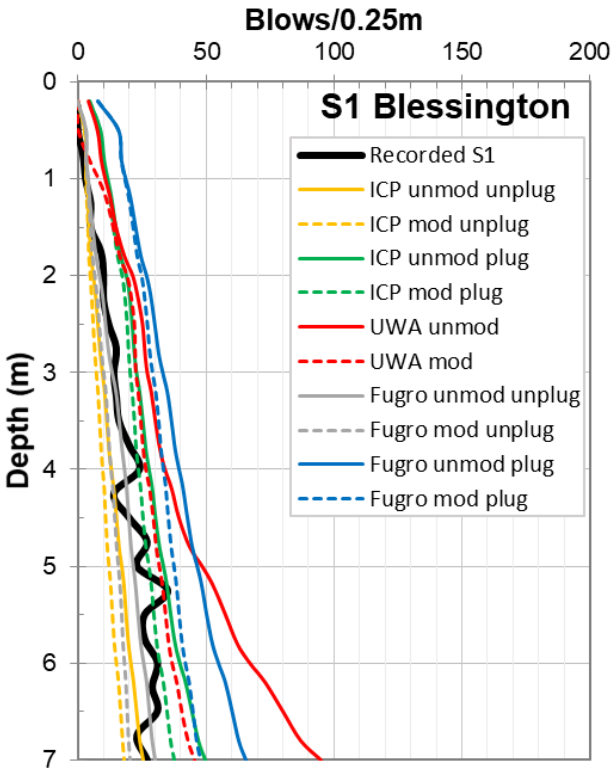

(a) Pile S1

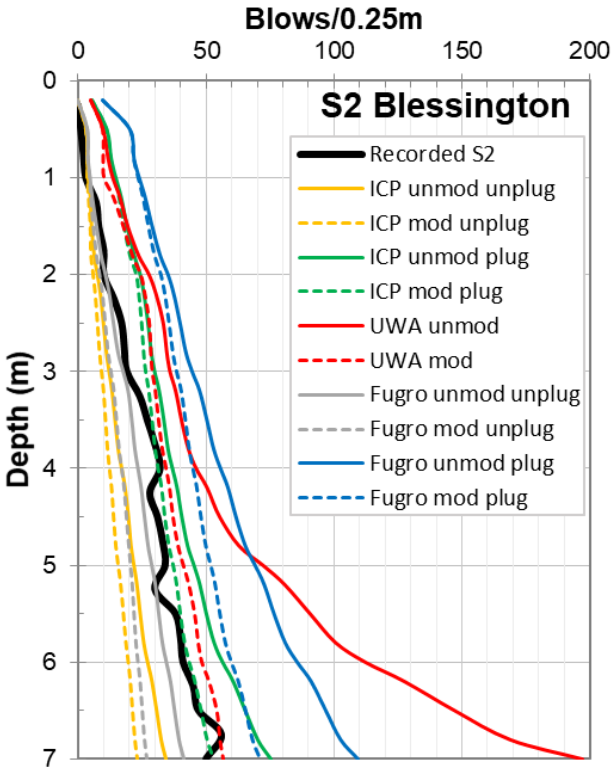

(b) Pile S2

Figure 4.2 Recorded and predicted blow counts comparison with CPT-based axial static capacity approach

The unit base resistance of UWA-05 which incorporate partial plugging will be modified further based on base-displacement as mentioned in Section 3.3. The calculation of pile tip displacement per blow during driving is essential due to suggest base resistance failure criteria assume at 0.1 of pile tip displacement which less during driving. Therefore, a reduction factor is required to consider the actual pile tip displacement during driving. The result of the base-displacement modification is presented in Figure 4.1. The unit base resistance in the modified model assumes no residual base stress ($q_{b,res}$) occurs in a pile. The modified ICP-05 and Fugro-05 only consider ageing effect with reducing shaft friction during driving while unit base resistance remains the same as the unmodified model.

As presented in Figure 4.2, the modification factors provide the UWA-05 with a better prediction than the unmodified model. The UWA modified prediction shows in the red dashed line, give a good prediction without underpredict the recorded blow counts. The ICP modified in a plugged condition which shows in green dashed line present reasonable estimation with slight over-prediction in the upper layer and slight under-prediction in several locations along the pile depth. The blue dash line shows the Fugro modified in a plugged condition, estimate overpredict blows/0.25m at upper layer but improve the prediction as the penetration depth increases. The modified model of the ICP and Fugro in unplugged condition under-predict the blow counts required to drive the pile.

4.3 Residual Base Modification

The base resistance for the SRD input with the UWA modified is modified further to account for the residual base stresses that occur after each hammer blow during the pile installation. The residual base stress that is previously neglected in the base resistance-displacement will be determined. The base residual stress will be varying of stepwise {1%, 2%, 5%, 8%, 10%} of cone tip resistance (q_c) as mention in Section 3.4. This sensitivity analysis with additional base resistance load ($Q_{b,n\%(z)}$) must not exceed the negative shaft resistance ($Q_{s,neg(z)}$) available at that specific pile depth penetration. Therefore, the base resistance stress from the sensitivity analysis must be converted to the base resistance load before comparing to the negative shaft resistance. The negative shaft resistance calculation incorporates the time factor of 0.69 due to ageing and tension factor of 0.75 as recommended by UWA-05. The minimum value between $Q_{b,n\%(z)}$ and $Q_{s,neg(z)}$ is the value of residual stresses which is added to base resistance SRD profile as input for wave equation analysis.

The result from the modified UWA base resistance SRD with different residual base stresses at piles S1 and S2 are shown in Figure 4.3a and Figure 4.3b respectively. Both piles S1 and S2 have a similar trend when adding stepwise 1%q_c, 2%q_c, 5%q_c, 8%q_c, and 10%q_c to q_b. Initially, the base resistance SRD versus depth has an independent curve. Then, more q_c percentage is added as residual base stress ($q_{b,res}$) until exceeding negative skin friction along the pile shaft area. In the case of negative shaft resistance is exceeded, the base residual will follow the previous additional value. For instance, at the first 2m in Figure 4.3 shows adding 10% q_c as $q_{b,res}$ will exceed the negative skin friction value, as a consequence, the curve intersects with 8% q_c at this depth. Despite the base resistance SRD for piles S1 and S2 have

a similar trend when adding base resistance stresses, pile S1 has higher base resistance SRD profile than pile S2.

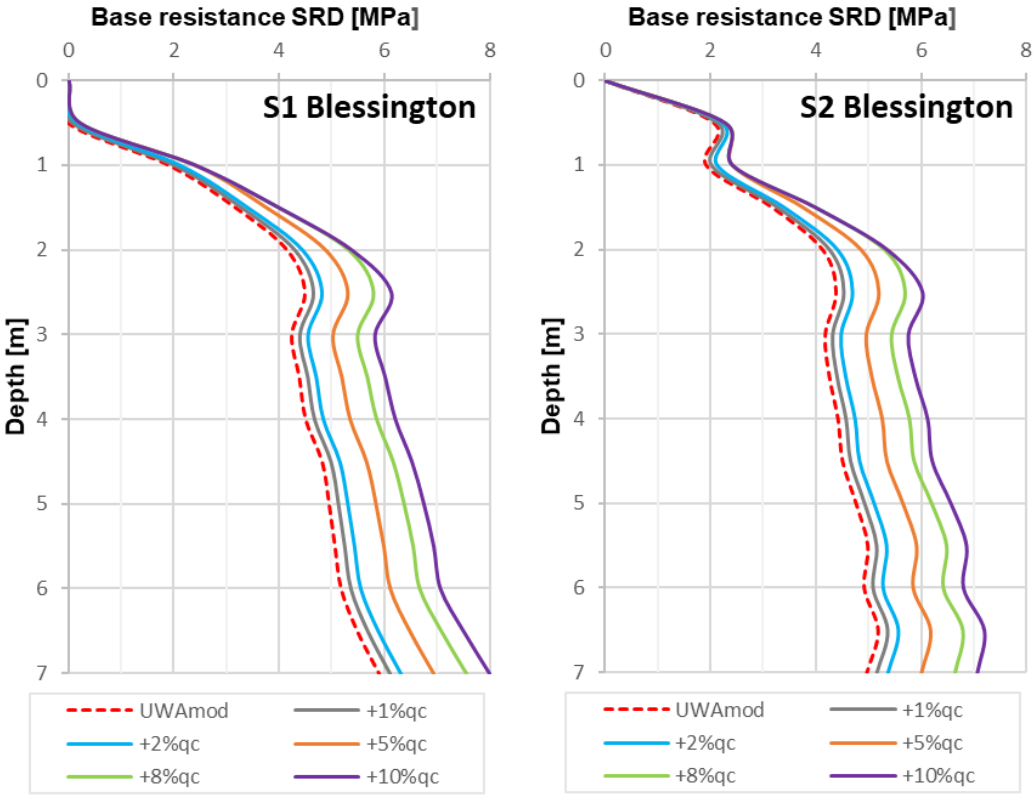

(a) Pile S1 (b) Pile S2

Figure 4.3 UWA unit base resistance with varying residual base stresses added

Figure 4.4a and Figure 4.4b illustrate the blow count prediction when residual base stresses are incorporated at pile S1 and pile S2 respectively. These figures also present the recorded blow counts as a reference for the comparison to blow count prediction. Reversely with base resistance SRD profile as shown in Figure 4.3, pile S2 has a higher blow counts prediction compare to pile S1 as shown in Figure 4.4. This is due to pile S1 has higher hammer stroke than pile S1.

Figure 4.4 highlights that the UWA modified without additional base residual stresses is closest to the actual blow counts profile along the pile length. However, without additional base residual stresses, pile S1 and S2 still have underpredicted at 5.25m and 6.25m respectively. Adding the residual base stresses lead to higher prediction at piles S1-S2. The reasonable blow count estimation without underprediction is provided by adding 5% q_c and 2% q_c at pile S1 and S2 accordingly.

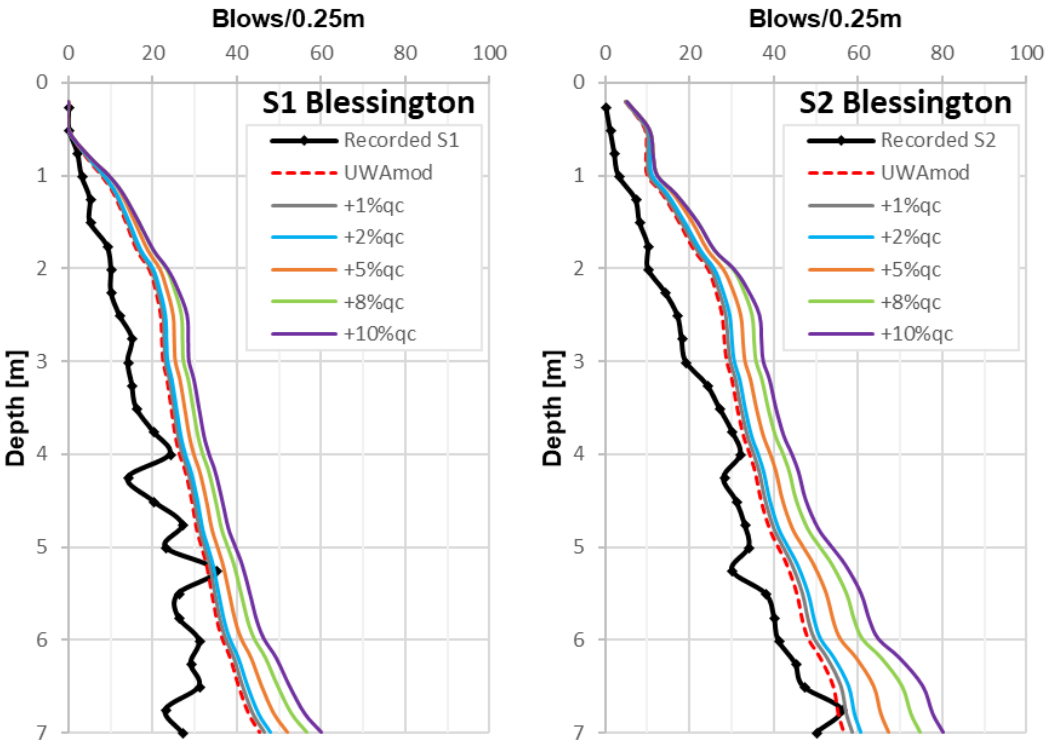

(a) Pile S1 (b) Pile S2

Figure 4.4 Recorded and predicted blow count with residual base stresses added

5 Parameter Study

This chapter examines parameters that influence the pile driveability analysis. For this purpose, the analysis focusses on pile S2 as a representative pile using the UWA-05 unmodified model. A parameter study is conducted in the form of sensitivity analysis to ascertain the influence of various factors. The pile geometries, pile penetration depth, and hammer manufacturer are assumed unchanging. The Coefficient of Variation (CoV) is adopted to represent the ratio of change in each parameter compared to the reference UWA-05 unmodified model.

Figure 5.1 shows the total blow count change for different study parameters. It shows that the dynamic soil parameters (i.e., skin quake, toe quake, skin damping and toe damping) and the total blow count give the positive linear relationship. The total blow counts get higher as the soil dynamic parameters increase. On the other hand, the stroke height and the total blow count have a negative non-linear relationship. The negative relationship also provides when changing the hammer efficiency. Total blow count has a smaller decrease with higher the stroke height and the hammer efficiency. Influence parameters from the most to the less sensitive is the hammer efficiency, stroke height, quake, and damping value.

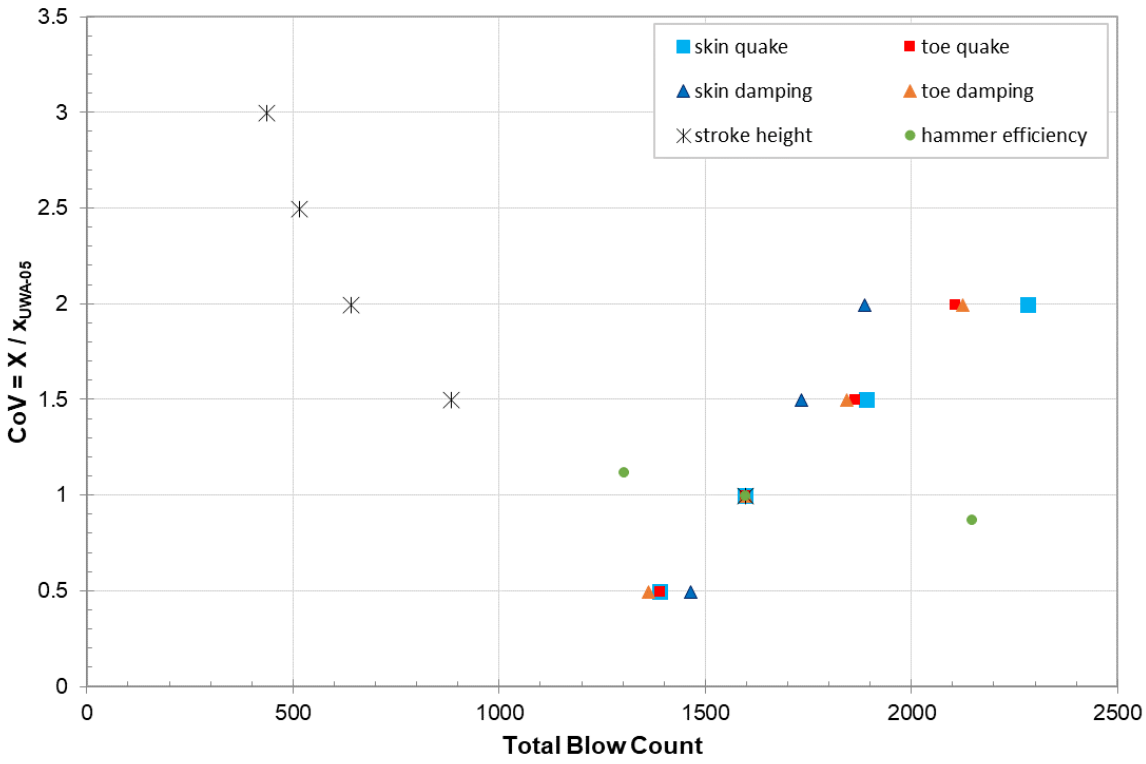

Figure 5.1 Parameters analysis compare to the UWA-05 method

5.1. Damping

Damping value influences the driveability analysis as shown in the blow count result. The damping value depends solely on the soil type. Damping value in the sand layer suggested by the UWA-05 method is 0.25s/m and 0.5s/m respectively for skin and toe. Figure 5.2 shows that the sensitivity analysis with changing the toe damping give greater blows than changing the skin damping. The effect of changing the damping parameter is not constant along the pile but increase as the pile depth increases. At the pile base, an increase of 50% of the skin and toe damping provide increased blows of 1.1 and 1.2 respectively. Generally, the blow counts and damping value are positively correlated. The blow counts are increased with increased damping value. Soil damping in the wave equation analysis represents the energy loss within the soil in the pile-soil interface during the pile driving process. Hence, higher damping value means more energy lost and more blow count required for pile driving.

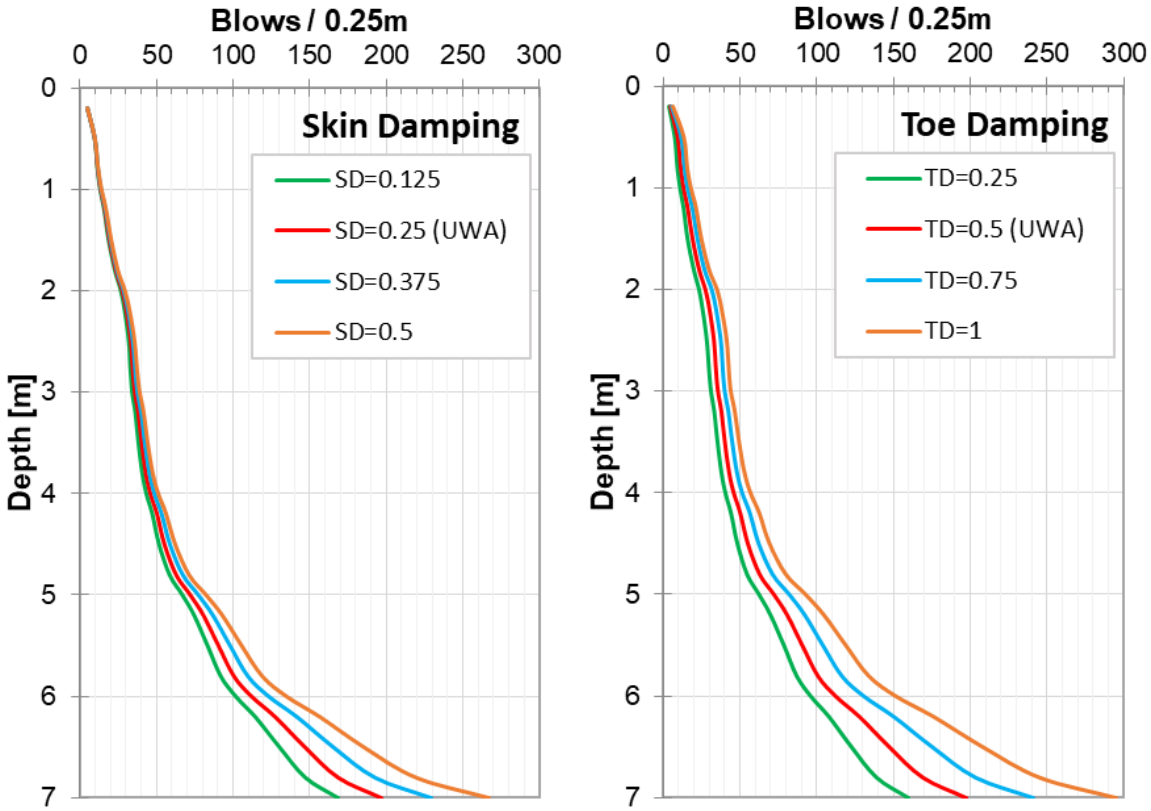

(a) Skin damping (b) Toe damping

Figure 5.2 Effect of damping

5.2. Quake

Quake is the maximum displacement to achieve yield. Increasing the quake value causes extension of the soil elastic displacement range before yield and decreases the soil stiffness. The quake value suggested by the UWA-05 method is 2.5mm both for the skin and toe. The blow count result is influenced by the quake value as shown in Figure 5.3. The toe quake has less influence on the result blow count than the skin quake. The blow count increase due to

the quake value is developed along the pile penetration depth. At 7m depth, 50% increase in the quake value give increase blows/0.25m of 1.4 and 1.3 for changing the skin and toe quake accordingly. The quake value in wave equation analysis input does not represent pile displacement rather than marking the yield displacement point in the soil resistance-pile displacement curve (Figure 2.5). Changing the quake value will move the yield displacement point and enlarge the linear relationship of soil resistance-pile displacement. Thus, higher quake causes more blow count is required to install the pile. The effect of changing the quake value similar to the damping, the blow counts are increased with increased quake value. Although, the blow count increases due to the quake value slightly higher than the blow count increase due to the damping value.

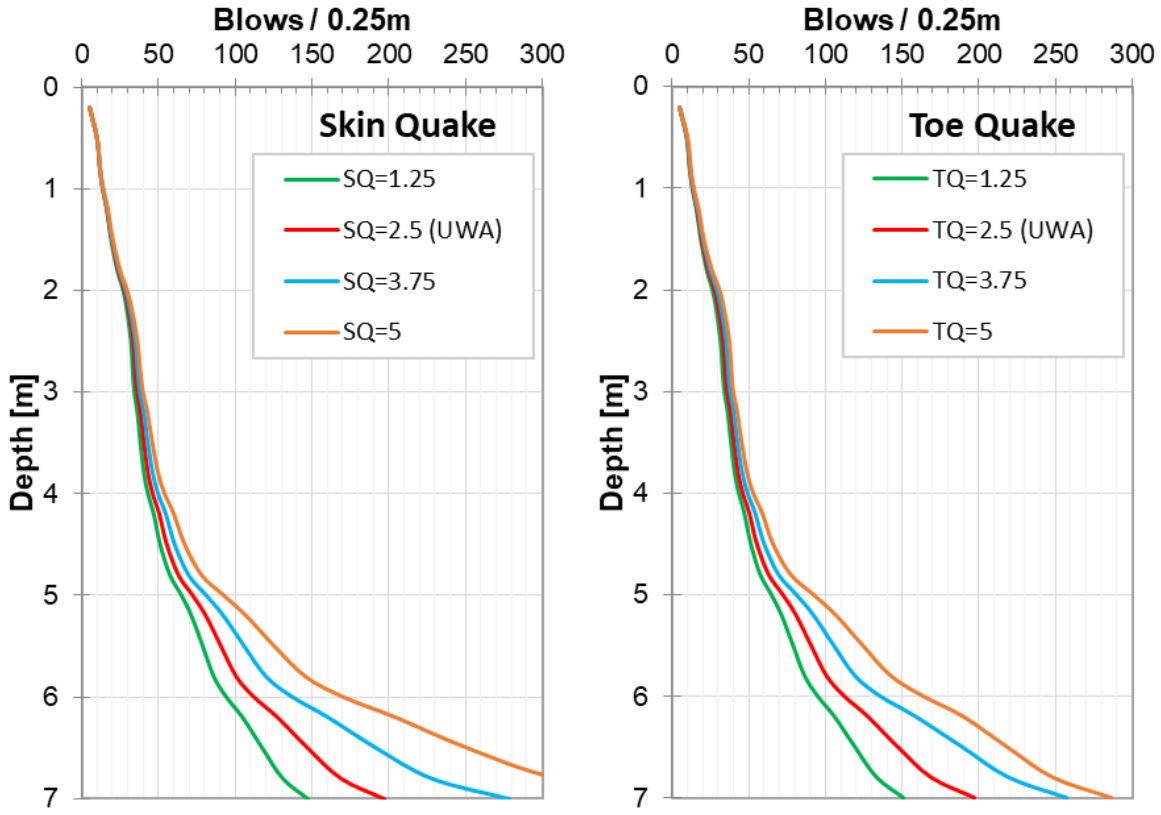

(a) Skin quake (b) Toe quake

Figure 5.3 Effect of quake

5.3. Stroke Height

The height of hammer stroke influences the energy applied to drive a pile. Figure 5.4a shows the blow count/0.25m resulting from varying the hammer stroke height. The blow count and stroke height have a non-linear negative relationship. The blow count at the pile tip decreases by a factor of 0.38 when the hammer stroke height increases from 0.3m to 0.45m, as shown in the red line and the light blue line respectively. This non-linear relationship is shown in the graph when increasing the stroke height with the same increment of 0.15m, from 0.45m to 0.6m, the blow count at the pile base decrease by a factor of 0.65. Increase in the stroke height causes higher energy to drive a pile or decrease blow count required to install the pile.

The hammer stroke height must be carefully assessed. Installing pile with excessive energy prone to cause pile damage. In another hand, pile driving using low stroke lead to premature refusal. Therefore, as an addition to blow count prediction, the stress along the pile must be considered when adjusting the hammer stroke height.

5.4. Hammer Efficiency

Hammer efficiency accounts for the energy losses that cannot be calculated during the pile driving process. The standard value of the hammer efficiency depends on the type of hammer. The pile S2 installation process at Blessington site uses a hydraulic impact hammer. This type of hammer has hammer efficiency value of 0.8 following the GRLWEAP recommendation. Figure 5.4b shows that hammer efficiency gives a negative correlation with the blow count result. The blow count is increasing as the hammer efficiency decrease. The change in the blow count increase toward the pile base. The blow count at the pile base increases by a factor of 1.72 while the hammer efficiency decrease from 0.8 to 0.7. More efficient hammer provides higher energy cause lower blow count required to install the pile. The effect of changing hammer efficiency gives the highest change in the blow count result compare to other parameters in this study. Therefore, it is crucial to ensure the hammer efficiency design match to actual hammer efficiency, so that the blow count prediction can represent the actual driving process.

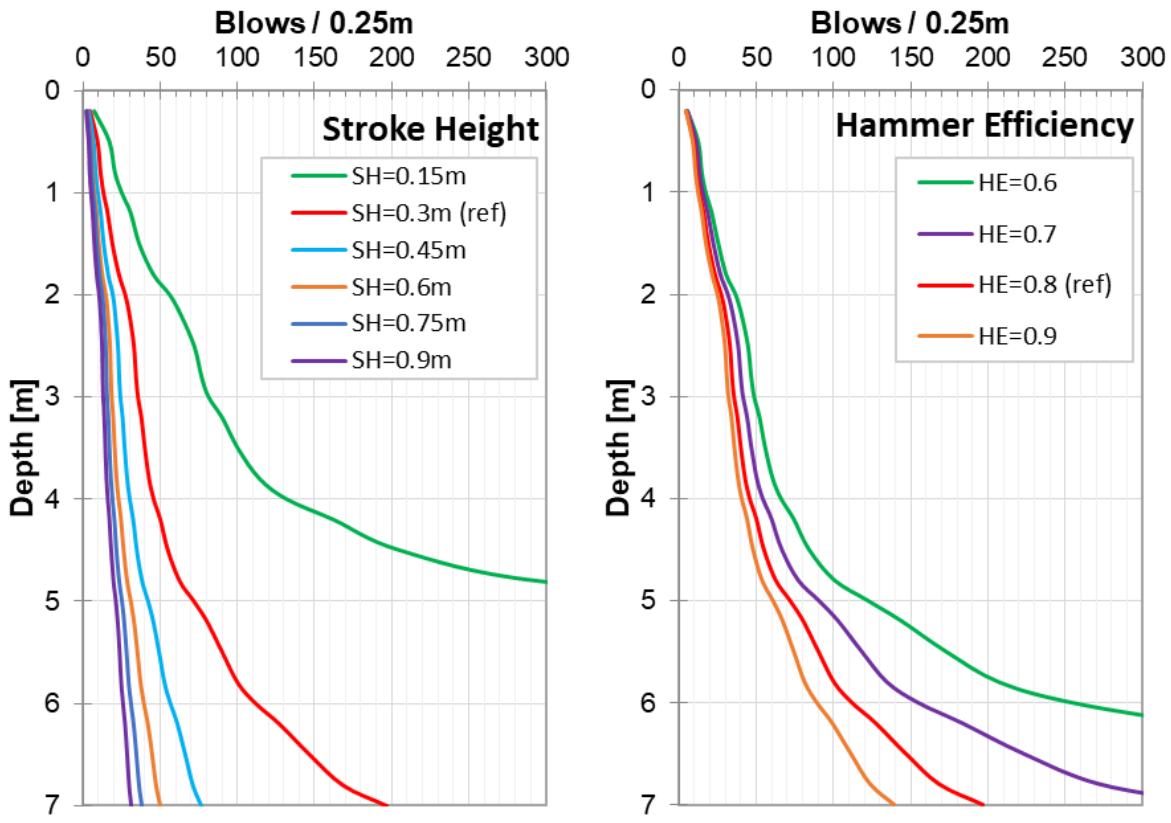

Figure 5.4 Effect of (a) stroke height (b) hammer efficiency

6 Case Study – Rotterdam Harbour

This chapter presents a case study of pile installation in Rotterdam Harbour. The input data from the Rotterdam site will be presented. The driveability models that have been developed for Blessington site is applied at Rotterdam site. The primary input for the SRD calculation will incorporate several aspects such as the ageing effect, the degree of displacement and residual base stresses. The result of various models CPT-based axial static capacity approaches are discussed.

6.1. Database at Rotterdam

The project undertakes 4 full-scale test piles at Rotterdam Harbour, the Netherlands. The test location is comprised of clay with organic soil, and medium dense sand. A total of 10 CPTs were conducted at Rotterdam site. Figure 6.1a describes the cone tip resistance (q_c) profiles indicate that low q_c (< 2MPa) in the clay layer from 4m to 21m. The soil shear modulus (G_o) profiles were derived from the $6q_c$ values since the shear wave velocity (V_s) are unknown (Prendergast *et al.*, 2013). These G_o profiles are derived from the q_c value are shown in Figure 6.1b. Poisson's ratio (v) at a very small strain of 0.1 is used as an assumption in this project.

Piles P1-P4 have the identical properties, square close-ended concrete piles with 0.45m width. The total pile length of 36m is driven until 35m below ground level. Blow count records at Rotterdam for all piles are plotted in Figure 6.1c. The incremental blow counts are recorded over the last 5m of pile driving, from 30 to 35m depth. Freefall occurs only over a minor length, but in the principal, the hammer is worked over the entire length of the pile. All the blow counts record has a similar profile which ranges around 10 blows/0.25m and increases at the last 1m near the pile tip.

The blow counts record at Rotterdam are directly comparable since the piles had the same hammers and stroke heights. Pile is driven using 6200kg Delmag D62-22 as a piling hammer. The hammer blow energy ranges between 107 and 224 kNm. The stroke height of 1.7m is determined from the minimum hammer blow energy of 107 kNm. Pile cushion consists of three layers of spruce. There is no available data about the thickness of the pile cushion, thus this study will assumes cushion thickness is 0.1m according to the minimum required pile cushion thickness for the concrete pile (PDCA, 2007).

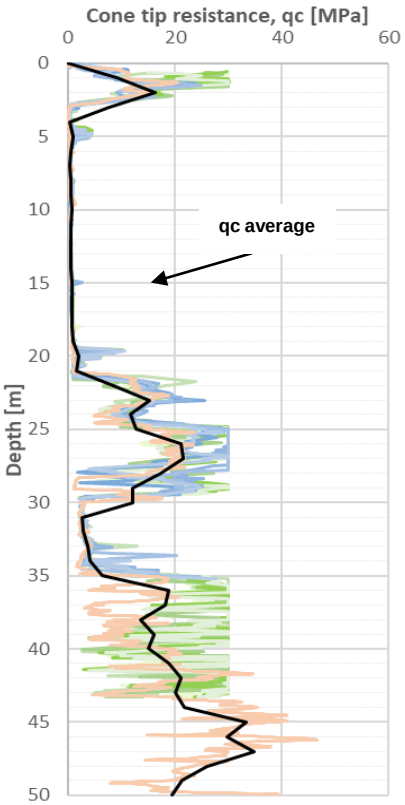

(a) Cone tip resistance, q_c

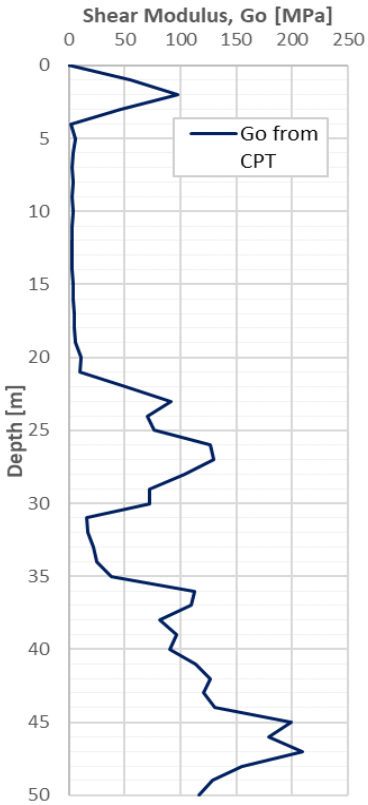

(b) Shear modulus, G_o

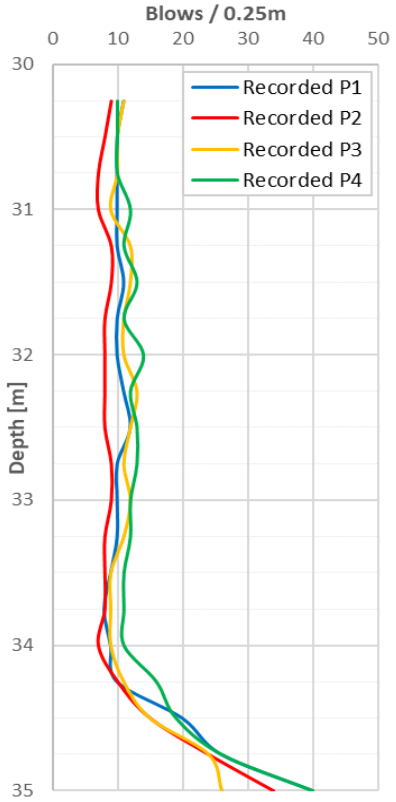

(c) Incremental blow counts

Figure 6.1 Soil database at Rotterdam

6.2. Static capacity in clay

In cohesion soil, the static axial capacity is related to the undrained shear strength (S_u). The most broadly used for shaft friction calculation in clay is the total stress approach. Average shaft friction (τ_{av}) is determined by a non-linear relationship with undrained strength (S_u) and back-figured adhesion factor (α) values (Tomlinson, 1957). The total stress approach is developed from the static load test by using un-instrumented driven piles with variable soil layers which resulted in uncertainty concerning the alpha coefficient (Chow and Jardine, 1996). The α values were the lowest when mobilised in over-consolidated soil and close to one in deep deposits of normally consolidated clay or stiff clay with large overburden pressure (McClelland, 1974). The correlation of α values with S_u was developed from the load tests as shown in Figure 6.2.

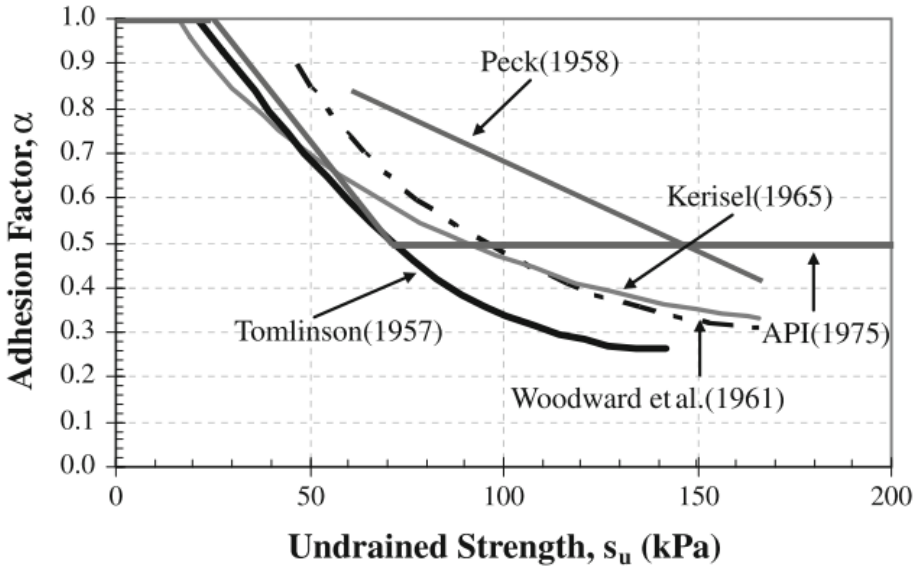

Figure 6.2 The correlation of α values developed from the load test (after Doherty and Gavin, 2011)

The friction fatigue effect in the clay is shown by measuring the radial total stress during driving and the radial effective stress after stress equalisation. The friction fatigue measurement being highest close to the pile tip and reducing as *h/D* increases (Gavin *et al.*, 2010). Partial dissipation of excess pore-water pressure occurs as a specific location in the soil experience unloading as the distance from the pile tip increases, thus causing friction fatigue effect in clay. The shaft resistance reduction due to the friction fatigue effect in the clay is lower than in the sand. The distribution of the shaft resistance on the displacement pile in the clay is affected by the q_c value, a constant volume interface friction angle and the friction fatigue. The total stress approach gives a reliable estimation of the static axial capacity in the clay layer. However, the total stress approach ignores the friction fatigue effect when calculating shaft friction capacity which results to overestimate calculation prediction.

A direct CPT-based method for the shaft friction calculation is proposed by the Fugro-10 method (Dijk and Kolk, 2010). The Fugro-10 is a function of the net cone resistance (q_n) and mathematical expression. This mathematical expression is determined by using regression

analysis to explore the lowest coefficient of variation to measure the pile capacity. Before using Fugro-10, the cone tip resistance (q_c) needed to be converted to the total cone resistance (q_t) by using a simplified correlation which is suggested in Lehane *et al.* (2017) as shown in Table 6.1. The Fugro-10 shaft friction calculation is influenced by over-consolidation and pile length, instead of by load direction, soil plasticity, pile diameter, and pile tip displacement. The Fugro-10 method incorporates the friction fatigue effect in the shaft resistance calculation as represented by the relative depth to the pile tip normalised by the unit length (*h/uL)*. This incorporation gives closer and less conservative representation of the actual condition.

The Fugro-10 unit base resistance is calculated average q_n of 1.5 diameters above and below the penetration. This approach is derived according to the principles of the CPT-based methods that is proposed by API-00 for the sand layer. The API-00 proposed calculating the unit base resistance in weak clay layer with an assumption of the pile tip penetrate more into the layer in question approximately 3 diameters above the bottom of the layer to preclude punch through (API, 2007). The axial shaft capacity calculation approaches for the driven pile in the clay which are used in this study are shown in Table 6.1.

6.3. Blow Count Prediction

The database of full-scale test piles at Rotterdam is used as the input for the driveability analysis. In this section, the pile P1 is taken as a representative pile since all piles have identical pile and hammer properties. The other Rotterdam piles result analysis are summaries in the Appendix C. The soil properties in this project consist of clay, organic soil and sand layer. Therefore, the SRD profile is determined by a combination of several approaches. The first combination is the UWA model by using the UWA-05 in sand, total stress approach and API-00 in clay. The second combination is the ICP model by using the ICP-05 in sand with total stress and API-00 in clay. The last combination is Fugro model using the Fugro-05 in sand and Fugro-10 in clay.

Like Blessington site, the base resistance–displacement modification is applied to the combination with UWA as mentioned in Section 3.3. The residual base stresses in this modification assume to be zero. The actual displacements (w_b) for each blow are back-calculated from the blow count recorded at Rotterdam pile. Later, the actual displacement is normalised by the pile diameter (D). The base resistance-displacement curve first stage is linear until it reaches a yield strain of 0.015D. At this point, the second linear stage is formed until 0.1D.

At Rotterdam project, the blow counts are recorded only the last 5m at the final driving. Therefore, only the actual displacement at 30-35m can be determined by back-calculated the record blow count. Soil at this depth consists of clay layer with q_c between 2 and 6 MPa. Since the recorded blow count is located in the clay layer, the unit base resistance is applied using the API-00 approach while the shaft friction is applied using the total stress approach.

Figure 6.3 shows the base resistance-displacement curve when applying a simplified three-stage base resistance-displacement as suggested by Gavin and Lehane (2007). In the first

linear stage where w_b/D < 0.015, the curves increase as the soil elastic stiffness (*Eo*) increases. In the second stage, when w_b/D equals to 0.1, the base resistance value from API-00 is used as a limit. At a displacement of 0.1*D*, the unit base resistance calculation using the API-00 gives result range between 1.4 and 3.7 MPa. This figure depicts that the actual displacement during driving less than the failure criteria of 0.1*D* as shown in the red dot. The unit base resistance is derived from the actual displacement which results in the range between 1 and 2 MPa.

Table 6.1 CPT-based design method calculation of driven piles in clay

Methods		**Design Equations**
Shaft Friction	**Fugro-10**	$\tau_f = min\left(0.16 \left(\frac{h}{uL}\right)^{-0.3} \left(\frac{q_n}{\sigma'_{v0}}\right)^{-0.4} , 0.08 \right) q_n$ $q_n = q_c + (1-a)\, u_2 - \sigma_{v0}$ $q_n = q_t - \sigma_{v0}$ in the absence of u_2 (pore pressure) Simplified correlation between q_t and q_c $q_t = 1.14 q_c \quad for \left(\frac{q_c}{\sigma'_{v0}}\right) < 6$ $q_t = q_c \quad for \left(\frac{q_c}{\sigma'_{v0}}\right) > 6$ h (relative depth to pile tip) = pile tip elevation – specific depth *z* uL (unit length to render the expression dimensionless) = 1.0m or 3.3 feet a (the cone-dependent net ratio of the cross-section steel area at the gap between the cone and the friction sleeve to the cone base area) = 0.75 in the absence of any additional information
	Total Stress	$\tau_f = \alpha\, S_u$ α (adhesion factor) = range 0.5 (OC-clay) ~ 1 (NC-clay)
Base Resistance	**API-00**	$q_b = 9\, S_u$
	Fugro-10	$q_b = 0.7 q_{n,avg}$ $q_{n,avg} = q_n$ average ± 1.5*D* over the pile tip *D* is the pile outer diameter
Notes		τ_f is the local ultimate shaft friction σ'_{v0} is the effective vertical soil stress at specific depth *z* q_c is the cone tip resistance S_u (undrained shear strength) = $\left(\frac{q_c - \sigma'_{v0}}{N_k}\right)$ N_k = 15 (in the absence of any additional information), range 12 ~ 25 depending on soil type and depth

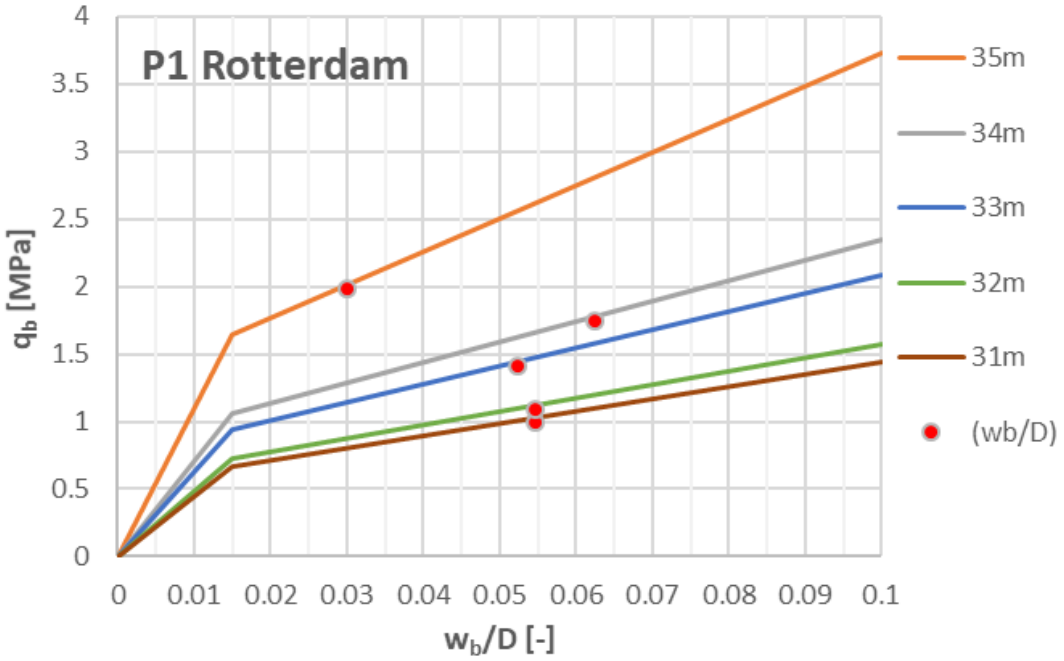

Figure 6.3 Base resistance-displacement curves at various driving depth

Figure 6.4 shows the recorded and the predicted blow count using the combination of CPT-based approaches for soil profile in sand and clay. In the clay layer, at 4m until 21m where q_c profiles are less than 2 MPa, all the models give similar blow count prediction. In the sand layer at 21m – 30m depth, Fugro unmodified gives the highest blow count prediction follow by UWA and ICP method. However, at 26m-27m where the maximum q_c of 21 MPa occurs, the UWA unmodified provide a similar prediction to the ICP unmodified which exceed the Fugro unmodified blow count prediction. In the clay layer at 31-35m, the blow count prediction are compared and modified using recorded blow count. At this last 5m, all the unmodified models over-predict actual blow count recorded by the Coefficient of Variation (CoV) of 2.4, 2.1 and 1.92 accordingly using the combination of Fugro, UWA and ICP approach.

All the modified models integrate the ageing effects in the shaft friction SRD calculation. Moreover, the combined UWA model incorporates the base resistance - displacement as the base resistance modification factor. The result from modified models is shown in Figure 6.4. Similar to the unmodified model, the Fugro modified provides the highest blow count estimation along the pile except at 26-27m depth compare to the UWA modified and ICP modified. In the clay layer at 31-34m, the modification provides all modified models better prediction than the unmodified model. At this depth, the Fugro, UWA, and ICP give estimation by the CoV of 1.55, 1.17, and 1.18 respectively. At the last penetration or 34-35m depth, the Fugro combination gives the best prediction while UWA and ICP give underestimate the recorded blow count. The last penetration located in transition between clay and sand layer with q_c value of 6 MPa and 19 MPa respectively, as shown in Figure 6.4. Fugro-10 is calculated average q_n before and after the last penetration which is considered the sand underneath the clay layer.

The base resistance for combined UWA by using UWA-05 in the sand, the total stress approach and API-00 in clay are modified further to account for the residual base stresses. The residual base stresses occur after each hammer blow during pile installation. In this modification, the model has integrated not only the base resistance-displacement but also the residual base stresses. The residual base stress is cooperated with adding {1, 2,5,8,10}% of the cone tip resistance (q_c) to the unit base stress as mentioned in Section 3.4. The additional base residual must less than the negative shaft resistance available at the specific pile depth penetration. Like Blessington model, the Rotterdam model takes the time factor of 0.69 due to the ageing effect and a tension factor of 0.75 as a recommended by the UWA-05. The time factor and tension capacity are used when calculating the negative shaft resistance. After ensuring that base resistance load less than the negative shaft resistance, the SRD profile for the UWA modified including base resistance residual are derived.

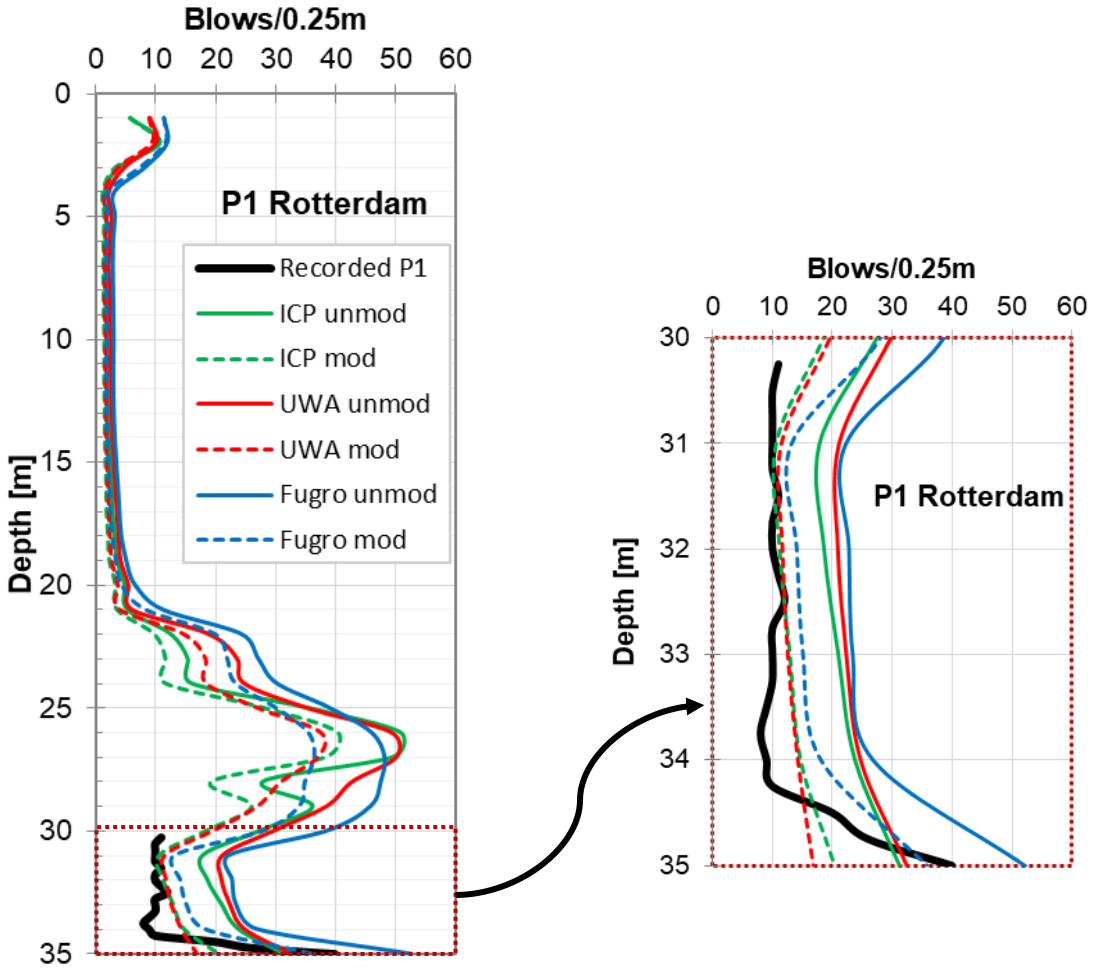

Figure 6.4 Predicted blow counts comparison using CPT-based approaches at pile P1

Figure 6.5 presents the result of modified UWA base resistance with varying residual stresses at Rotterdam. Whether the residual stress is added in the base resistance is depends on the magnitude of q_c at each layer. The small q_c values in the clay layer at 4 until 21m depth and 31 until 35m lead to an insignificant addition to the base resistance SRD. In the sand layer, for instance at 26m when the maximum cone tip resistance equals to 21 MPa, noticeable change in the base resistance SRD result is observed due to adding base residual stresses. The base resistance SRD profile is updated after adding the residual base stress value. Then,

the wave equation analysis is performed using GRLWEAP. Figure 6.5b shows the blow count prediction by adding the residual stresses. There is no momentous change in the clay layer causing the blow count result in almost the same prediction. Distinct alteration in the blow count results is presented in the sand layer at 21m until 31m. At 27m depth, the blow count increases 1 blow/0.25m when the additional base residual to the base resistance SRD increases from 1% q_c to 2% q_c.

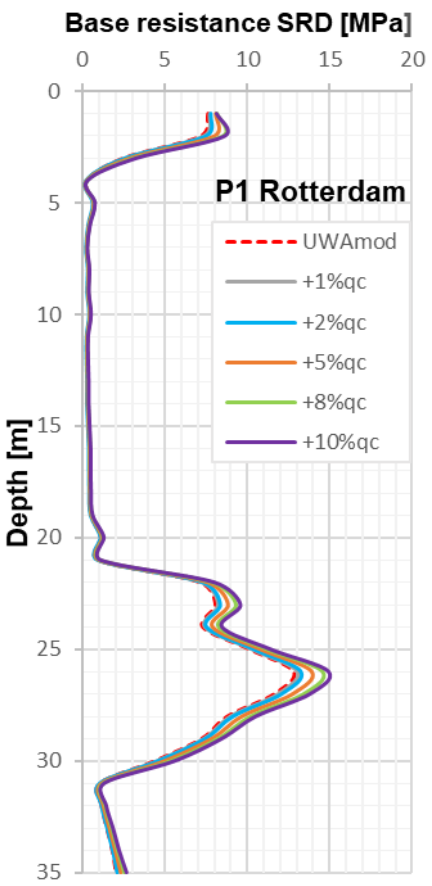

(a) Residual stresses SRD

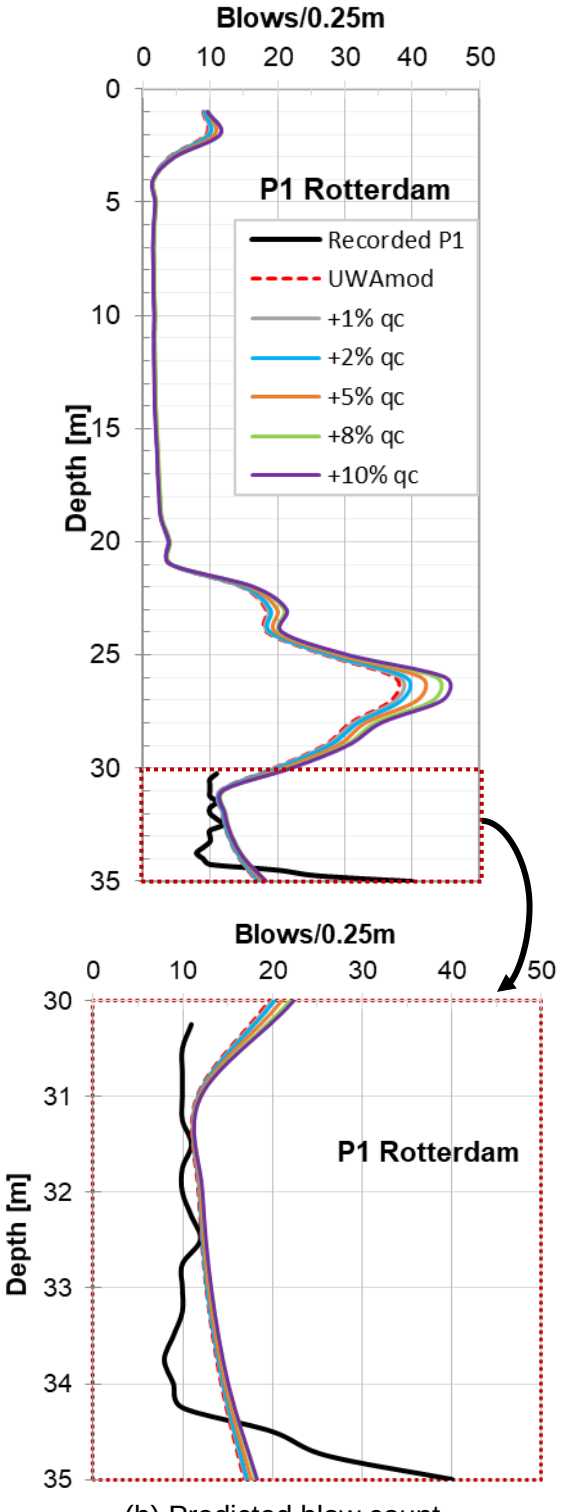

(b) Predicted blow count

Figure 6.5 The UWA modified model with residual base stresses added analysis results

Driveability analysis performance by using the CPT-based axial static capacity approaches in combine sand-clay layer with modification model provide a better prediction than the unmodified model. All modified models are addressing the ageing and the friction fatigue effect in the shaft friction SRD profile. The combine UWA model (UWA-05 in sand, total stress approach and API-00 in clay) is modified further by addressing the degree of mobilisation and the residual base stresses. The combine UWA without additional base resistance is provided the closest blow count prediction to the actual blow count except in the last depth penetration. The upper prediction cannot be verified due to record blow count is only available at the last 5m.

7 Conclusions and Recommendation

The primary focus of the research is to gain knowledge on the performance of the CPT-based axial static capacity approaches to evaluate pile driveability in sand. A literature study to determine the pile driveability from the axial static capacity is conducted. Then, the site database including the site condition, hammer and pile properties will be compiled as the inputs to perform the wave equation analysis. Several factors concerning driveability analysis are addressed to develop an efficient model. Finally, the blow count results from every model are assessed. To be able to achieve the primary focus of this research, the answer to sub-question is listed as follows:

1. How to calculate the axial static capacity using available CPT-based methods?
This study uses several approaches to calculate the CPT-based axial static capacity (i.e. the UWA-05, ICP-05, and Fugro-05). These axial static approaches address the friction fatigue effect when computing the shaft resistance capacity in a pile which is represented in the ICP-05 and Fugro-05 by h/R^* and in the UWA-05 method by h/D. The friction fatigue effect causes a reduction in the shaft resistance as the distance from the pile tip to the specific soil horizon increases. All the approaches consider plugging condition in the unit base resistance calculation. However, only the UWA-05 method considers partial plugging conditions in the calculation approach, which is accounted for in the shaft friction and the unit base resistance by IFR and FFR respectively. The ICP-05 and Fugro-05 take conservatively the fully plugged or unplugged condition in the unit base resistance calculation.

2. How to develop an efficient model for the driveability analysis using the CPT-based axial capacity methods?
Soil resistance during driving is a combination of static and dynamic components of the soil. The static resistance to driving (SRD) is analogous with the static axial capacity but incorporates base resistance for each driving increment (as opposed to static capacity which has only one base resistance). The axial static capacity methods are derived from the axial static piles load test database. Therefore, in developing a driveability analysis, several factors must be carefully evaluated. The dynamic components which affect the soil resistance during driving are the soil damping and quake. Driveability analysis integrates both the static and dynamic components in the wave equation analysis. Inputs needed to perform the wave equation analysis are the SRD and dynamic soil components, the pile and hammer properties. The driveability analysis is applied to calculate the blow count for each depth increment.

The first factor that affects the driveability analysis is the friction fatigue effect that occurs for each driving increment. Thus, the pseudo average shaft friction calculation is implemented in the shaft resistance SRD to calculate the change in the shaft resistance distribution between two successive depth increments. The second factor that needs to be considered is the pile

ageing effect in a pile. The CPT-based axial static capacity approaches are derived 10-30 days after the pile installation. A time-dependent increase in the static axial capacity is observed for the driven piles in sand. Therefore, a time factor of 0.69 is applied to quantify the magnitude of shaft resistance reduction when performing the driveability study with the axial static capacity approaches.

The base resistance-displacement curves are determined by back-calculating the actual blow counts record to establish the degree of soil displacement during driving. The actual displacement from the base-displacement curves are applied to the unit base resistance using the UWA-05 approach. These curves indicated soil displacement during driving less than the assumption of the pile tip displacement suggested by the UWA-05 methods of 0.1 of the pile diameter. As a consequence, the unit base resistance SRD inputs less than the unit base resistance calculation using the UWA-05 approach.

During pile driving, the pile will experience compression when the driving force from the hammer is applied and tension when the pile is unloaded. At zero pile loading, the residual base stress occurs at the pile base. The sensitivity study analysis to account for the residual base stresses are conducted with an additional {1; 2; 5; 8; 10} % of the cone tip resistance. This sensitivity analysis with additional base resistance load must not exceed the negative shaft resistance available at that specific pile depth penetration. The negative shaft resistance calculation incorporates the pile ageing effect and tension factor of 0.75 as recommended by the UWA-05 approach. The minimum value between the base resistance load and the negative shaft resistance is the value of residual stresses which is added to base resistance SRD profile as input for wave equation analysis.

3. What parameters primarily affect pile driveability analysis?

The parameter study is conducted using sensitivity analysis for the dynamic soil component and hammer properties. The dynamic soil components are used in this study based on the UWA-05 recommendation value for steel pile driven in the sand. Therefore, to aim efficient model for analysis, the influence of these dynamic soil parameters must be assessed. The result of the hammer properties sensitivity analysis must be considered when selecting equipment for driving a pile. From all the sensitivity analysis of parameters result can be concluded that the most influential factor that determines blow count is the hammer efficiency. Influence parameters followed by the stroke height, quake, and damping value. Blow count will increase related to lower hammer efficiency, lower stroke height, higher quake and higher damping.

Finally, the aim of this research can be concluded. Performing unmodified axial static capacity approaches give an unreasonable prediction. The raw model of the ICP-05 and Fugro-05 are taken conservative plugging condition. These two approaches give over-predict blow count estimation in the fully plugging pile base condition. In another hand, the ICP-05 and Fugro-05 unmodified in the unplugged pile base condition provide under estimate blow count prediction. Under-predict blow count result is highly avoided in the driveability analysis. The UWA-05 unmodified also give unreasonable over-prediction despite including the partially plugging effect in the base resistance calculation.

Performing driveability analysis using the CPT-based axial static capacity approaches (i.e., UWA-05, ICP-05, Fugro-05) with modification model provide a better prediction. However, integrating the friction fatigue effect and the pile ageing effect into the Fugro-05 approach still produces over-predictions in blow counts along the pile. The ICP-05 modified give reasonable prediction with slight under-predictions in several locations along the pile length. Model using the UWA-05 modified further addressing the degree of mobilisation and base residual stresses provide reasonable blow count prediction. This UWA-05 modified model can be recognised as an exemplary model to estimate the blow counts from the CPT-based axial static capacity approach.

Conducting driveability analysis study with a complete record blow count along the pile is complimentary. The recorded blow counts not only for actual displacement calculation and model modification but also as the model validation. The model validation will make the analysis result become more reliable. Beside recorded blow count, the completeness of hammer driving equipment data is favourable. As the hammer properties profoundly affect the driveability analysis, using complete hammer properties make more confident blow count prediction which represent the actual blow count during pile installation.

Driveability analysis is essential to consider the driving stresses and installation time as an addition to blow count prediction. Considering maximum driving force during pile installation can prevent the pile material damage. Knowing the pile installation time give an advantage in project scheduling, especially when a large number of piles need to be installed. The driveability analysis considering these aspects will ensure the pile quality, time-frame and budget according to the plan. More research to perform driveability analysis that considers these aspects will be beneficial for driveability analysis.

Bibliography

Alawneh, A. S. and Husein Malkawi, A. I. (2000) 'Estimation of Post-Driving Residual Stresses Along Driven Piles in Sand', *Geotechnical Testing Journal*, 23(3), pp. 313–326. doi: 10.1520/GTJ11053J.

Alm, T. and Hamre, L. (2001) 'Soil model for pile driveability predictions based on CPT interpretations', *International Conference on Soil Mechanics and Geotechnical Engineering*, pp. 1297–1302. Available at: http://scholar.google.com/scholar?hl=en&btnG=Search&q=intitle:Soil+model+for+pile+driveability+predictions+based+on+CPT+interpretations#0.

API (2007) 'Recommended Practice for Planning, Designing and Constructing Fixed Offshore Platforms — Working Stress Design', *Api Recommended Practice*, 24–WSD(December 2000), p. 242. doi: 10.1007/s13398-014-0173-7.2.

Byrne, T. *et al.* (2012) 'Comparison of Pile Driveability Methods In North Sea Sand', *Offshore Site Investigation and Geotechnics: Integrated Technologies - Present and Future*. doi: SUT-OSIG-12-52.

Byrne, T. *et al.* (2018) *Performance of CPT-based methods to assess monopile driveability in North Sea sands*. Ocean Engineering (In Review).

Chauhan, S. (2008) *Pile Design Using Wave Equation Analysis Program Application in Offshore Wind Farm*. Massachusetts Institute of Technology.

Chow, F. C. and Jardine, R. J. (1996) *Investigations into the behaviour of displacement piles for offshore foundations*, *Ground Engineering*. Imperial College London.

Das, B. M. (2011) *Principles of Foundation Engineering*. Seventh Ed. Cengage Learning, USA. Available at: https://tudelft.on.worldcat.org/oclc/840451377.

Dijk, B. F. J. Van and Kolk, H. J. (2010) 'CPT-Based design method for axial capacity of offshore piles in clays', *Frontiers in Offshore Geotechnics II, ISFOG 2010 - Proceedings*, (1990), pp. 555–560. doi: doi:10.1201/b10132-73 10.1201/b10132-73.

Doherty, P. and Gavin, K. G. (2011) 'The Shaft Capacity of Displacement Piles in Clay: A State of the Art Review', *Geotechnical and Geological Engineering*, 29(4), pp. 389–410. doi: 10.1007/s10706-010-9389-2.

Fang, H.-Y. (1991) 'Foundation Engineering Handbook', pp. 890–902. doi: 10.1007/978-1-4615-3928-5.

Gavin, K. G. *et al.* (2010) 'Field investigation of the effect of installation method on the shaft resistance of piles in clay', *Canadian Geotechnical Journal*, 47(7), pp. 730–741. doi: 10.1139/T09-146.

Gavin, K. G., Igoe, D. J. P. and Kirwan, L. (2013) 'The effect of ageing on the axial capacity of piles in sand', *Proceedings of the Institution of Civil Engineers - Geotechnical Engineering*, 166(2), pp. 122–130. doi: 10.1680/geng.12.00064.

Gavin, K. G. *et al.* (2015) 'The effects of pile ageing on the shaft capacity of offshore piles in sand', *Frontiers in Offshore Geotechnics III*, 0(1), pp. 129–151. doi: 10.1201/b18442-8.

Gavin, K. G. and Lehane, B. M. (2007) 'Base load – displacement response of piles in sand', *Canadian Geotechnical Journal*, 44(9), pp. 1053–1063. doi: 10.1139/T07-048.

Gavin, K. G. and O'Kelly, B. C. (2007) 'Effect of Friction Fatigue on Pile Capacity in Dense Sand', *Journal of Geotechnical and Geoenvironmental Engineering*, 133(January), pp. 63–71. doi: 10.1061/(ASCE)1090-0241(2007)133:1(63).

Jardine, R. J. and Chow, F. C. (2007) 'Some recent developments in offshore pile design', *Proceedings of the 6th International Offshore Site Investigation and Geotechnics Conference: Confronting New Challenges and Sharing Knowledge, London*, (September), pp. 11–13.

Jardine, R. J. *et al.* (2005) 'ICP design methods for driven piles in sands and clays', *ICP design methods for driven piles in sands and clays*, 106, pp. 1–14. doi: 10.1680/idmfdpisac.32729.

Jardine, R. J., Standing, J. R. and Chow, F. C. (2006) 'Some observations of the effects of time on the capacity of piles driven in sand', *Géotechnique*, 56(4), pp. 227–244. doi: 10.1680/geot.2006.56.4.227.

Karlsrud, K. *et al.* (2014) 'Significant ageing effects for axially loaded piles in sand and clay verified by new field load tests', *Offshore Technology Conference*, (May). doi: 10.4043/25197-MS.

Kirwan, L. (2014) *Investigation into Ageing Mechanisms for Axially Loaded Piles in Sand*. University College Dublin.

Kolk, H. J., Baaijens, A. E. and Senders, M. (2005) 'Design criteria for pipe piles in silica sands', *Frontiers in Offshore Geotechnics, ISFOG 2005 - Proceedings of the 1st International Symposium on Frontiers in Offshore Geotechnics*, 1, pp. 711–716. doi: 10.1201/NOE0415390637.ch80.

Lehane, B. M. (1992) *Experimental investigations of pile behaviour using instrumented field piles*. Imperial College London. Available at: http://ethos.bl.uk/OrderDetails.do?uin=uk.bl.ethos.283868.

Lehane, B. M. *et al.* (2017) 'Characteristics of Unified Databases for Driven piles', *Proceedings of the 8th International Conference of Offshore Site Investigation and Geotechnics OSIG*, (September).

Lehane, B. M., Schneider, J. A. and Xu, X. (2007) 'Development of the UWA-05 Design Method for Open and Closed Ended Driven Piles in Siliceous Sand', *Contemporary Issues In Deep Foundations*, pp. 1–10. doi: 10.1061/40902(221)12.

Lehane, B. M., Schneider, J. A. and Xu, X. (2005) *A Review of Design Methods for Offshore Driven Piles in Siliceous Sand*.

Lowery, L. L., Edwards, T. C. and Hirsch, T. J. (1968) *Use of the wave equation to predict soil*. Texas.

McClelland, B. (1974) 'Design of deep penetration piles for ocean structures', *ASCE J.Geotech. Eng*, Div. 100(G, pp. 705–747.

Overy, R. and Sayer, P. (2007) 'The Use Of ICP Design Methods As A Predictor Of Conductor Drill-Drive Installation', *Offshore Site Investigation and Geotechnics, Confronting New Challenges and Sharing Knowledge*, (OSIG-07-333). doi: 10.1146/annurev.soc.30.012703.110603.

Paik, K. *et al.* (2003) 'Behavior of Open- and Closed-Ended Piles Driven Into Sands', *Journal of Geotechnical and Geoenvironmental Engineering*, 129(4), pp. 296–306. doi: 10.1061/(ASCE)1090-0241(2003)129:4(296).

PDCA (2007) *Installation specification for driven piles*. Available at: http://www.piledrivers.org/files/uploads/243653FF-DB89-4FAF-BE2B-1EEBA2B1FAF8.pdf.

Pile Dynamics Inc. (2010) 'GRLWEAP 2010 Background Report'.

Pile Dynamics Inc. (2010) 'GRLWEAP Software'.

Poulos, H. G. and Davis, E. H. (1984) *Pile Foundation Analysis and Design*, *Engineering Geology*. doi: 10.1016/0013-7952(84)90010-3.
Prendergast, L. J. *et al.* (2013) 'An investigation of the changes in the natural frequency of a pile affected by scour', *Journal of Sound and Vibration*. Elsevier, 332(25), pp. 6685–6702. doi: 10.1016/j.jsv.2013.08.020.
Santamarina, J. and Cho, G. (2004) 'Soil behaviour: The role of particle shape', *Advances in Geotechnical Engineering. Proceedings of the Skempton Conference*, pp. 1–14. doi: http://pmrl.ce.gatech.edu/tools/santamarina_cho_2004.pdf.
Schneider, J. A. and Harmon, I. A. (2010) 'Analyzing Drivability of Open Ended Piles in Very Dense Sands', *DFI Journal - The Journal of the Deep Foundations Institute*, 4(1), pp. 32–44. doi: 10.1179/dfi.2010.003.
Smith, E. A. (1960) 'Pile-driving analysis by the Wave Equation', *Journal of the Soil Mechanics and Foundation Divisions - ASCE*, 86(SM4), pp. 35–61.
Stevens, R., Wiltsie, E. and Turton, T. (1982) 'Evaluating Drivability for Hard Clay Very Dense Sand and Rock', *Offshore Technology Conference*. Offshore Technology Conference, pp. 465–482. doi: http://dx.doi.org/10.4043/4205-MS.
Taylan, Z. N. and Senol, A. (2007) 'Effects of Soil Dynamic Parameters', *OttawaGeo2007*, pp. 1631–1636.
Tomlinson, M. J. (1957) 'The adhesion of piles driven in clay soils', *Proceedings of the 4th international conference on soil mechanics and foundation engineering*. Available at: https://tudelft.on.worldcat.org/oclc/841420612.
Toolan, F. E. and Fox, D. A. (1977) *Geotechnical planning of piled foundation for offshore platforms*.
Wang, J. (1992) *Prediction of pile drivability from CPT and WEAP analysis*. The University of British Columbia. Available at: https://circle.ubc.ca/handle/2429/4597.
White, D. J. and Bolton, M. D. (2001) 'Displacement and strain paths during plane-strain model pile installation in sand', *Geotechnique*, 54(6), pp. 375–397. doi: 10.1680/geot.54.6.375.45427.
White, D. J. and Bolton, M. D. (2005) 'Comparing CPT and pile base resistance in sand', *Proceedings of the Institution of Civil Engineers-Geotechnical Engineering*, 158(1), pp. 3–14. doi: 10.1680/geng.2005.158.1.3.
White, D. J. and Lehane, B. M. (2004) 'Friction fatigue on displacement piles in sand', *Géotechnique*, 54(10), pp. 645–658. doi: 10.1680/geot.2004.54.10.645.
Xu, X. (2007) *Investigation of the end bearing performance of displacement piles in sand*. The University of Western Australia.
Xu, X., Schneider, J. A. and Lehane, B. M. (2008) 'Cone penetration test (CPT) methods for end-bearing assessment of open- and closed-ended driven piles in siliceous sand', *Canadian Geotechnical Journal*, 45(8), pp. 1130–1141. doi: 10.1139/T08-035.
Yang, J. (2006) 'Influence zone for end bearing of piles in sand', *Journal of geotechnical and geoenvironmental …*, 132(September), pp. 1229–1237. doi: 10.1061/(ASCE)1090-0241(2006)132:9(1229).
Yang, Z. X. *et al.* (2014) 'Field Behavior of Driven Prestressed High-Strength Concrete Piles in Sandy Soils', *Journal of Geotechnical and Geoenvironmental Engineering*, 141(2), pp. 1–10. doi: 10.1061/(ASCE)GT.1943-5606.0001303.

A Shaft Friction SRD

The friction fatigue effect cause shear resistance reduction as a vertical distance from the tip to specific soil horizon increases. The shaft resistance reduction due to the friction fatigue effect in the clay is lower than in the sand. In this study, the shaft friction is calculated using the UWA-05, ICP-05, and Fugro-05 for the sand layer, the Fugro-10 and total stress approach for the clay layer. All these shaft friction calculation approaches as mentioned in Table 2.1 and Table 6.1, incorporate the friction fatigue effect except the total stress approach. The shaft resistance SRD distribution is altered for each pile penetration. Shaft resistance distribution is calculated using pseudo average shaft friction following Equation 2.1.

In this appendix, the change in the shaft friction for each method is elaborated. In the UWA-05 shaft friction calculation method (Table 2.1), the friction fatigue effect represents by relative depth to pile tip normalise by diameter (*h/D)*. Figure A.1a illustrates the friction fatigue effect using the UWA-05 approach. The below-left figure shows the result from the shaft resistance calculation using the axial static capacity method for each penetration depth. It shows that the shaft resistance (Q_s) reduces as the pile penetration increases. In the right figure, the shaft friction ($\Delta\tau_{f,avg}$) result between the static axial capacity and the SRD pseudo average is compared. The SRD by using the UWA-05 shows in the blue line, provide relative constant value along the pile length. This means the change in the shaft resistance between two successive depth are fluctuated in similar value. Initially, the SRD profile give higher shaft friction compare to the static capacity profile. It is reasonable since the friction fatigue effect are accumulated as the pile driving into the ground.

The friction fatigue effect represents in the ICP-05 and Fugro-05 shaft friction equation by relative depth to pile tip normalise by equivalent radius (*h/R**). Figure A.1b and Figure A.1c illustrate the friction fatigue effect in the shaft friction SRD calculation using the ICP-05 and Fugro-05 respectively. The Q_s by using ICP-05 method give similar trend to the Q_s using UWA-05. However, the Q_s value from the ICP-05 calculation is generally lower than the UWA-05 as shown in the left figure. The Fugro-05 shaft friction equation did not have minimum *h* value, unlike the UWA-05 and the ICP-05. Therefore, on the last penetration depth when *h* equals to zero, shaft friction (τ_f) at this increment depth give zero result and Q_s result equals to shaft resistance in the previous depth.

The shaft friction SRD at Rotterdam are shown in Figure A.2. The right figure shows that the shaft friction SRD has negative values. It indicates shaft resistance at the pile tip at the specific depth is less than shaft resistance in previous depth increment. This condition is possible if pile driving from dense sand to loosen sand or from sand to weak clay. The shaft friction SRD calculation method which gives most to less sensitive due to change in soil layer is Fugro, UWA and ICP as shown in the right figure of Figure A.2c, Figure A.2a, Figure A.2b respectively.

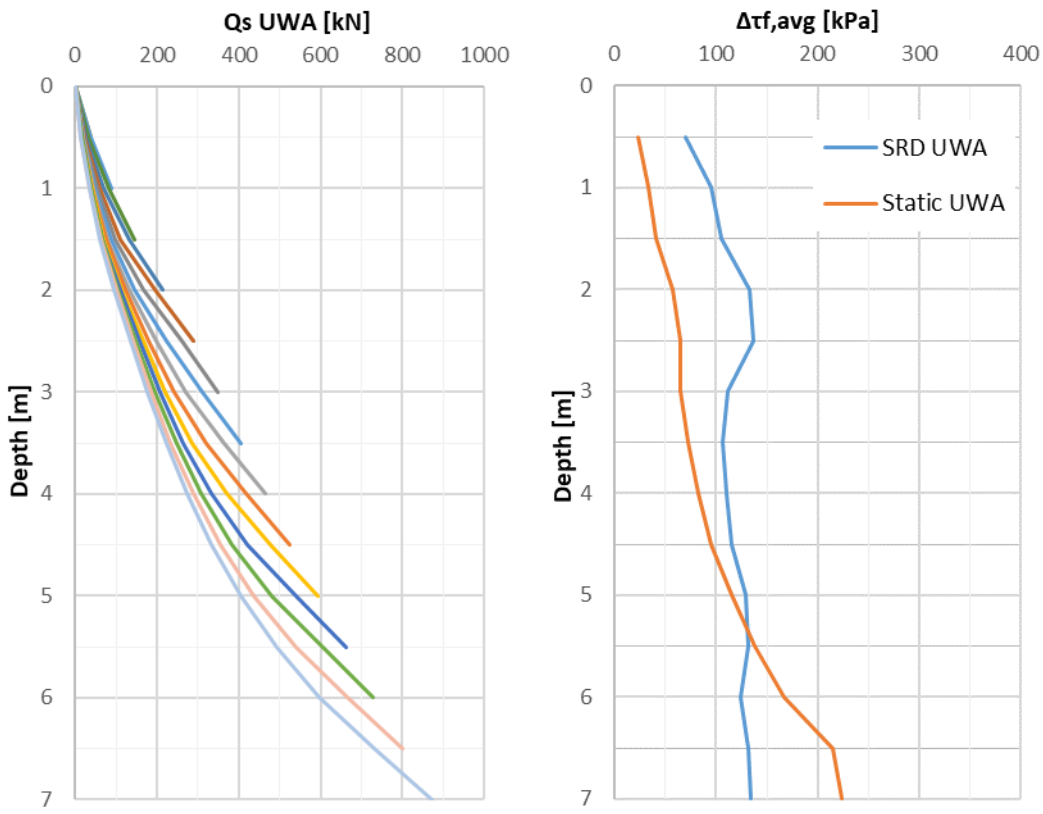

(a) The UWA-05 approach

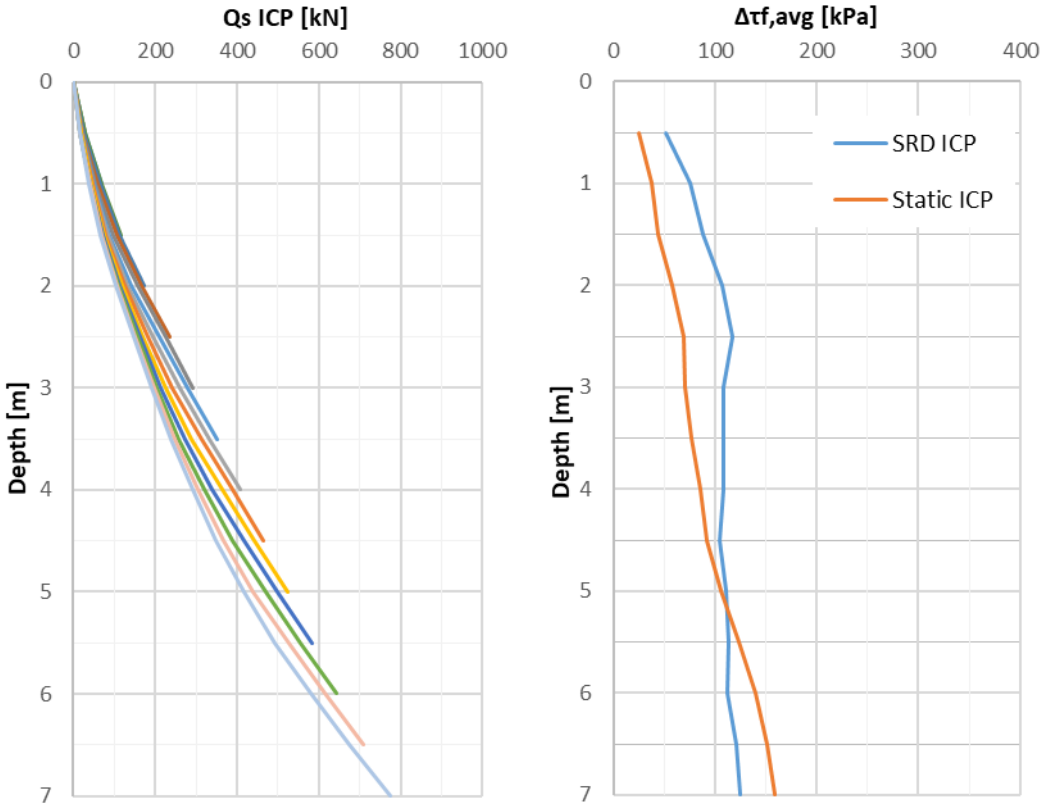

(b) The ICP-05 approach

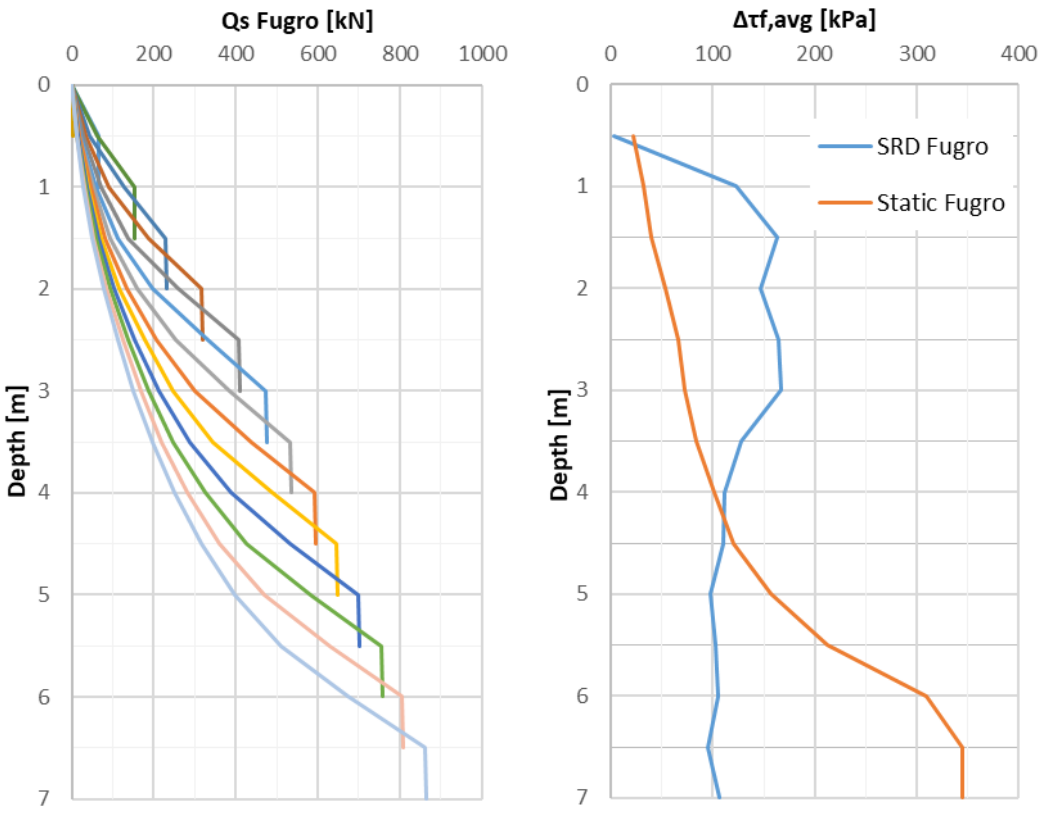

(c) The Fugro-05 approach

Figure A.1 The friction fatigue effect in the shaft friction SRD at Blessington

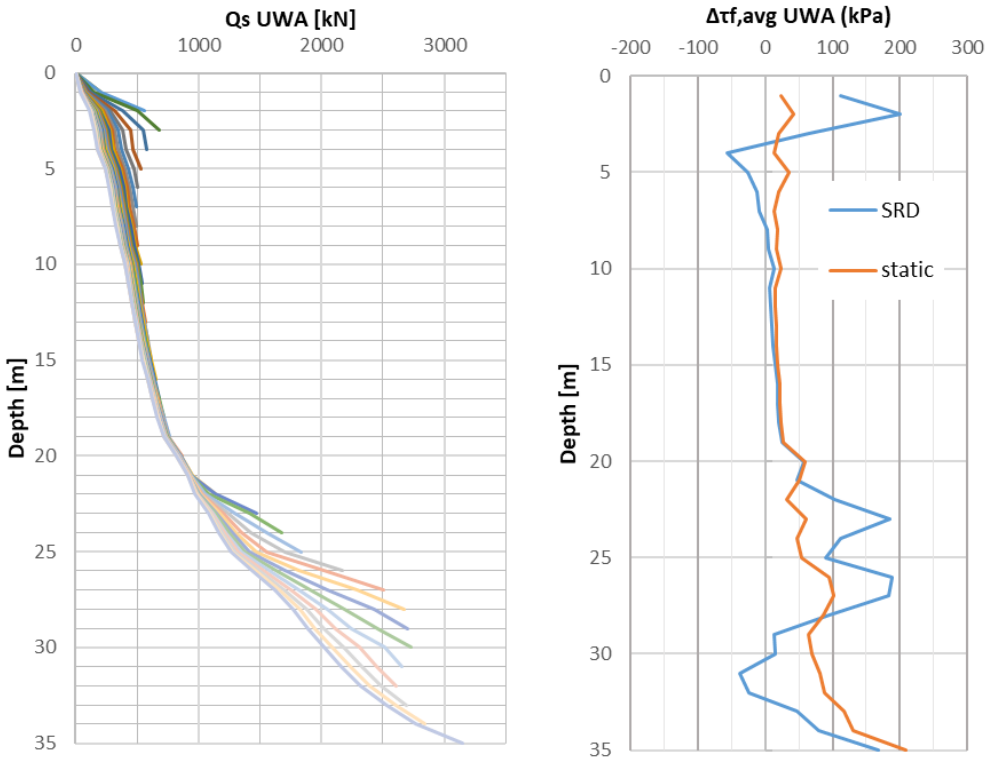

(a) The UWA-05 in sand and the total stress approach in clay

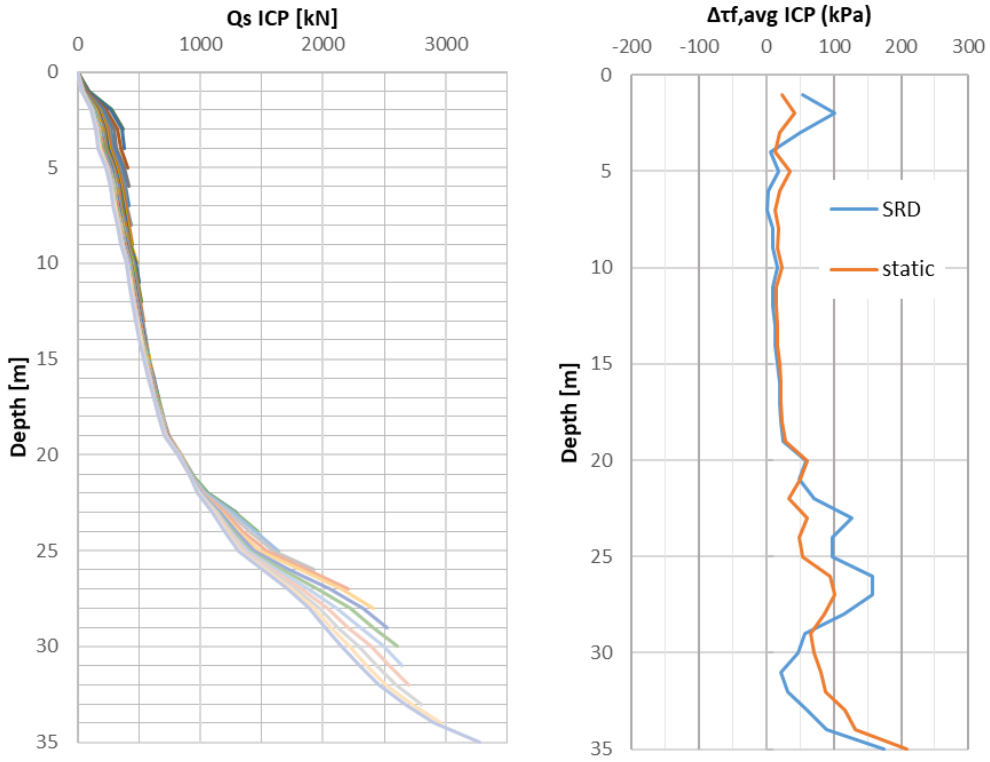

(b) The ICP-05 in sand and the total stress approach in clay

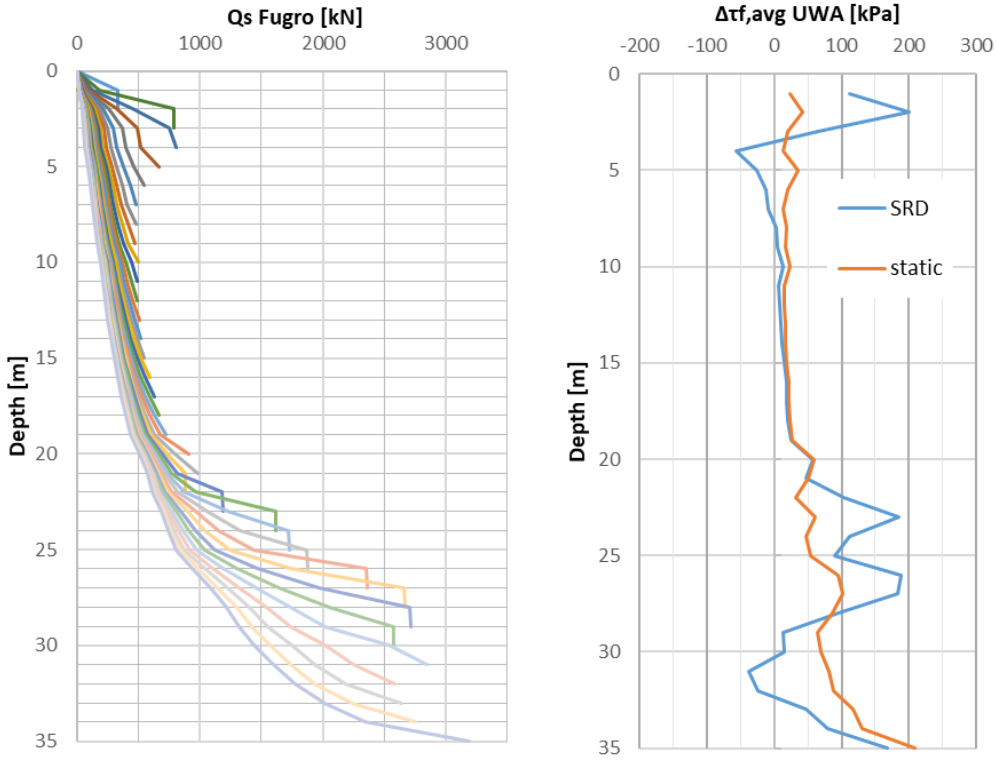

(c) The Fugro-05 in sand and Fugro-10 in clay

Figure A.2 The friction fatigue effect in the shaft friction SRD at Rotterdam

B Blessington site Result

B.1 Base Resistance-Displacement

This appendix section shows the base resistance-displacement curves for piles S2-S7 at Blessington (Figure B.1). As mentioned in Section 3.3, the base resistance-displacement curve based on the data blow count record at the site. From the blow count/0.25m data record, the actual pile tip displacement (w_b) normalised by a number of the blow is calculated. Then, each w_b is normalised by the pile diameter. On this stage, the unit base resistance in modified model assumes no residual base stress ($q_{b,res}$) occurs in a pile. The base resistance results from the q_b - w_b/D curves are implemented by using the UWA-05 approach which accommodates partial plugging condition at pile tip.

The base resistance-displacement curves for all piles except pile S6 at Blessington which is shown in Figure B.1 have a similar result to pile S2 which is shown in Figure 4.1. At w_b/D < 0.015 in the Figure B.1, the q_b - w_b/D curves are increased along the pile depth. The base resistance value from the UWA-05 approach ($q_{b01,UWA}$) is used as a limit at w_b/D equals to 0.1. Almost all w_b/D which are shown in red dot, occur at the second linear stage between 0.015 and 0.1. The w_b/D are decreased as the blow counts increased at deeper pile penetration. The w_b during driving is less than failure criteria of 0.1D except for the first meter when the pile is fully coring (IFR=1).

Figure B.1d shows the base resistance - displacement curves for pile S6. This figure shows the actual pile tip displacement (w_b) at pile S6 is smaller than other piles. As a consequence, the pile S6 base resistance SRD value is small, in the range between 2 and 4.3 MPa. This is unlike other piles which have the base resistance maximum average of 5.3 MPa as shown in Table B.1. This small w_b due to pile S6 has the highest blow counts record data as shown in Figure 3.3a.

Table B.1 The base resistance – displacement average along the pile at Blessington

Pile	w_b/D		q_b [MPa]		$q_{b0,1UWA}$ [MPa]	
	Min	Max*	Min	Max	Min	Max
S1	0.00	0.31	0.00	5.89	2.06	8.55
S2	0.01	0.37	1.92	5.17	2.06	8.55
S3	0.01	0.37	2.00	5.19	2.06	8.55
S4	0.02	0.37	2.00	5.57	2.06	8.55
S5	0.02	0.37	2.18	5.54	2.06	8.55
S6	0.01	0.12	2.07	4.30	2.06	8.55
S7	0.02	0.21	2.11	5.45	2.06	8.19
Average	0.01	0.30	1.76	5.30	2.06	8.50

*) Maximum w_b/D value in the base resistance-displacement modification is taken equal to failure criteria 0.1.

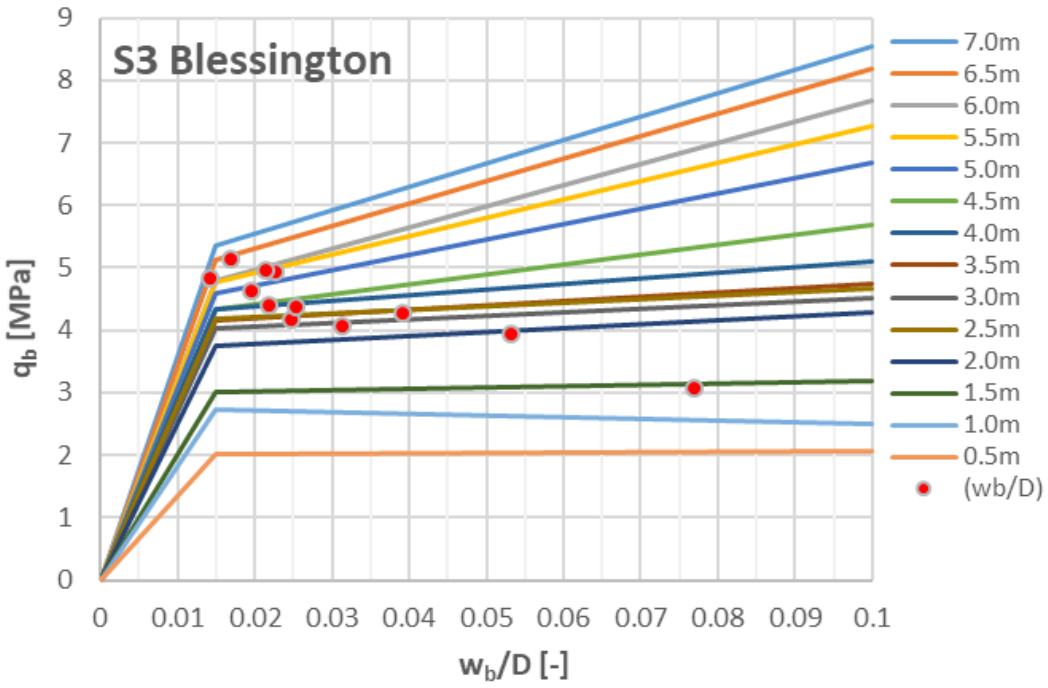

(a) Pile S3 Blessington

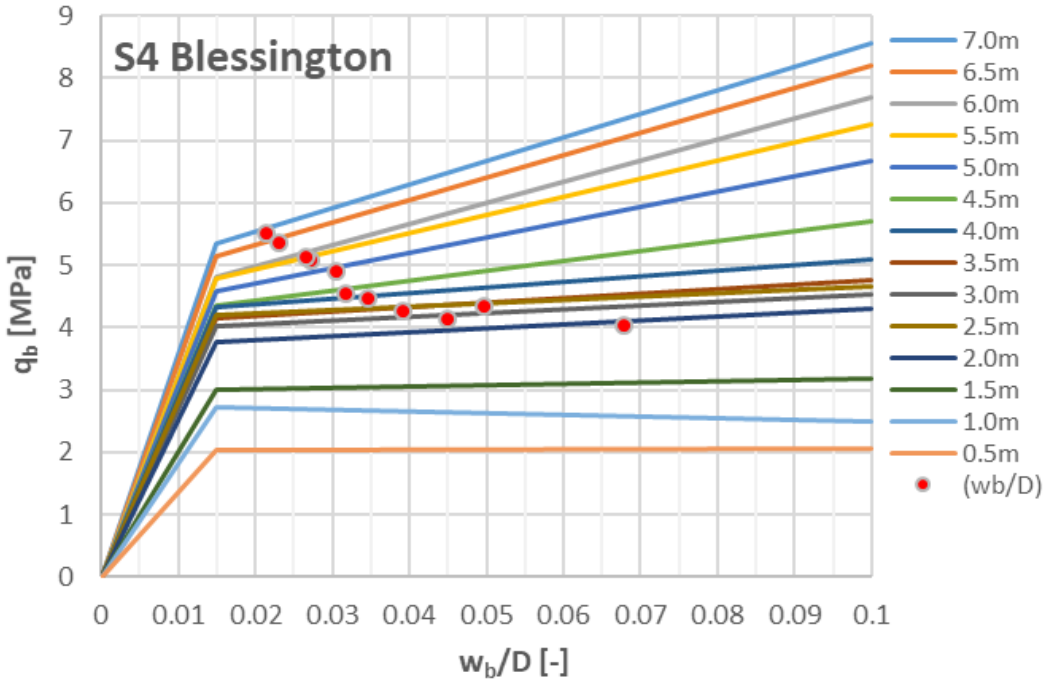

(b) Pile S4 Blessington

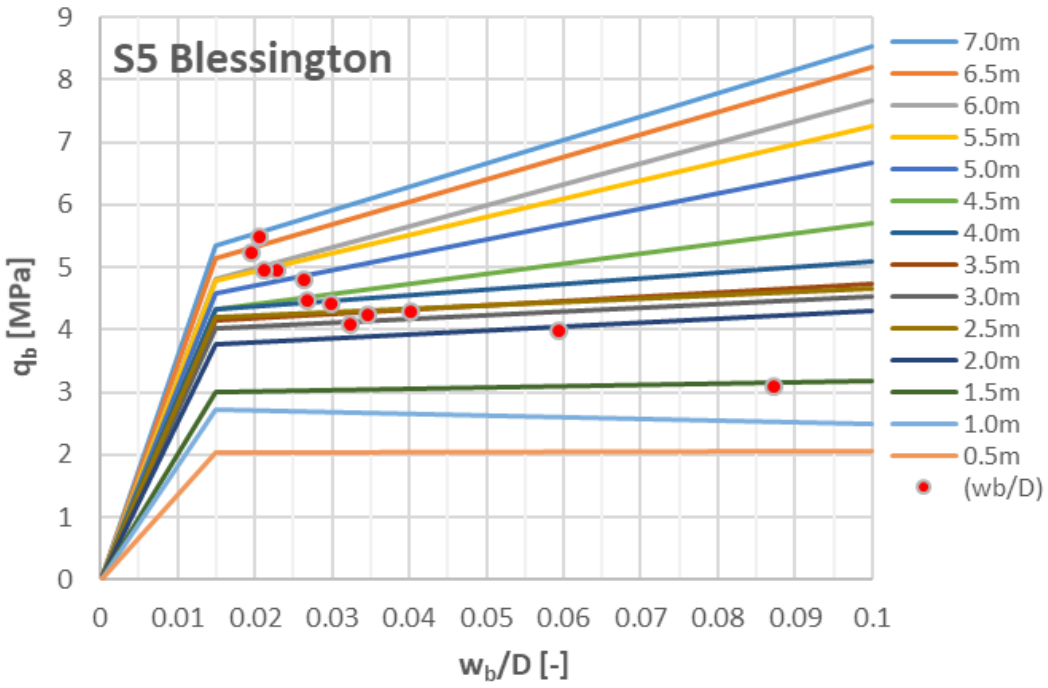

(c) Pile S5 Blessington

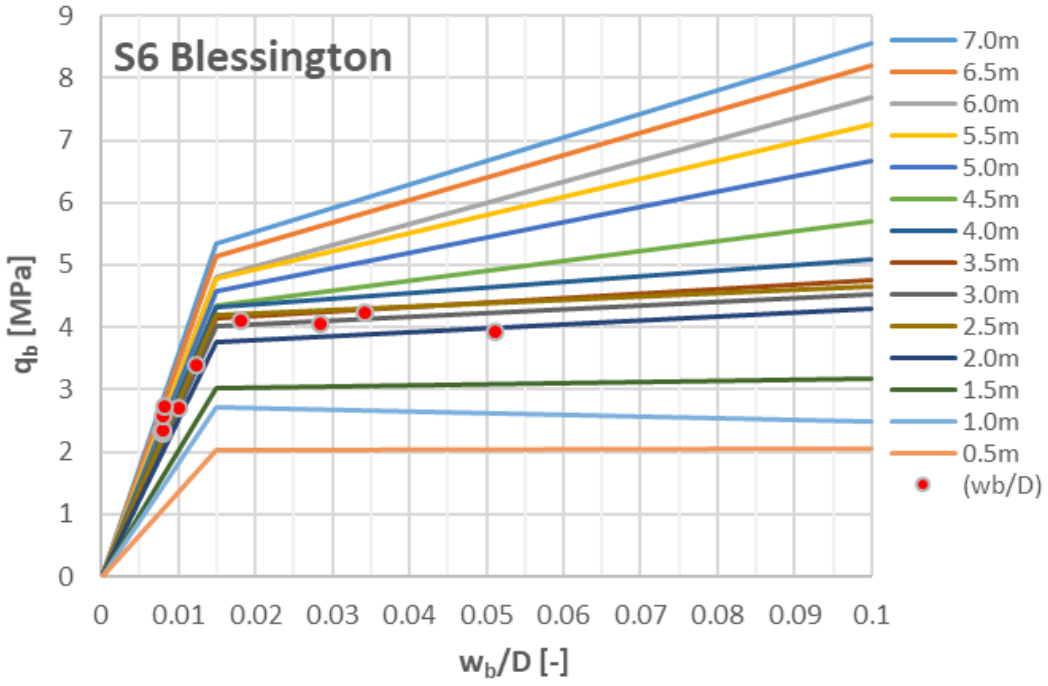

(d) Pile S6 Blessington

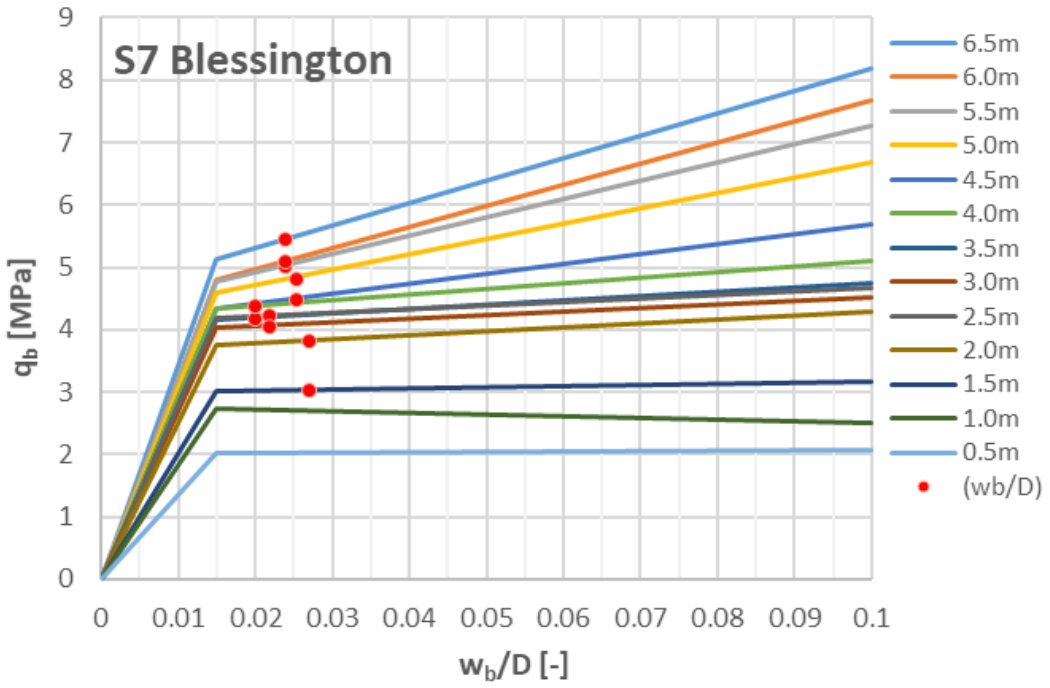

(e) Pile S7 Blessington

Figure B.1 Base resistance-displacement curves at various depth in Blessington site

B.2 Blow Count Comparison

This appendix presents the recorded and predicted blow count at Blessington piles. The prediction result from piles S1 and S2 Blessington have been explained in Section 4.2, piles S3-S7 are shown in Figure B.2. The estimation with a slight of underprediction and overprediction are given when applying the unmodified model to Fugro-05 in unplugged and ICP-05 in plugged respectively. Both unmodified model of UWA-05 and Fugro-05 in plugged condition give poor prediction with overestimate increase along the pile depth. The unmodified model is derived from the ICP-05 approach in unplugged condition provide under-estimate blow counts prediction. All the unmodified models describe the soil layer along the pile.

The modified models have integrated pile ageing effects and the base-displacement model to estimate driveability. The pile ageing applied with a time factor following Equation 3.1 is applied to skin friction from all unmodified model along the shaft area. The unit base resistance of UWA-05 modified further based on base-displacement as mentioned in Section 3.3. The result of the base-displacement modification is presented in Figure B.1. The presence of residual base stresses is ignored or assumed equals zero. The modified ICP-05 and Fugro-05 only consider ageing effect with reducing shaft friction during driving while unit base resistance remains the same as the unmodified model.

Generally, the prediction trend for every method is similar for every pile in Blessington except for pile S6 and S7 as shown in Table B.2. The Coefficient of Variation (CoV) is adopted to represent the ratio of average blow count prediction compared to the average actual blow count record along the pile. The UWA unmodified at pile S6 give the best average CoV value

of 1.1. However, Figure B.2d shows that no methods can closely predict actual blow count along the pile at S6 Blessington. The UWA unmodified give the best prediction compare to another method at pile S7. As shown in Figure B.2e, the UWA unmodified give pile S7 a reasonable prediction until 4m depth. After this depth, the UWA unmodified overestimate the actual blow count record. The best CoV for all pile in Blessington provide by using the ICP modified in plugging condition with CoV of 1.1. Although, Figure B.2 shows that ICP modified give slightly underpredict result between 4 and 6.5m. The performance of blow count prediction must closely evaluated from blow count prediction along the pile length due to CoV calculation only calculate the average value without considering the underestimation result. Based on Table B.2 and Figure B.2, the best blow count without under-predict is provides by using the UWA modified model.

Table B.2 The CoV from the average blow count along the pile depth at Blessington

Method	**CoV**							
	S1	**S2**	**S3**	**S4**	**S5**	**S6**	**S7**	**Average**
ICP unmodified in plugged	1.7	1.6	1.4	1.9	1.6	0.9	0.5	**1.4**
ICP modified in plugged	1.4	1.3	1.2	1.6	1.3	0.8	0.3	**1.1**
ICP unmodified in unplugged	0.7	0.6	0.6	0.8	0.7	0.3	1.0	**0.7**
ICP modified in unplugged	0.5	0.5	0.4	0.6	0.5	0.3	0.9	**0.5**
UWA unmodified	2.2	2.3	2.1	2.9	2.5	1.1	1.4	**2.1**
UWA modified	1.6	1.4	1.2	1.8	1.5	0.8	0.9	**1.3**
Fugro unmodified in plugged	2.4	2.3	2.1	2.9	2.4	1.4	1.5	**2.1**
Fugro modified in plugged	2.0	1.9	1.7	2.3	1.9	1.2	1.2	**1.8**
Fugro unmodified in unplugged	0.9	0.8	0.8	1.1	0.9	0.5	0.6	**0.8**
Fugro modified in unplugged	0.7	0.6	0.6	0.8	0.7	0.3	0.4	**0.6**

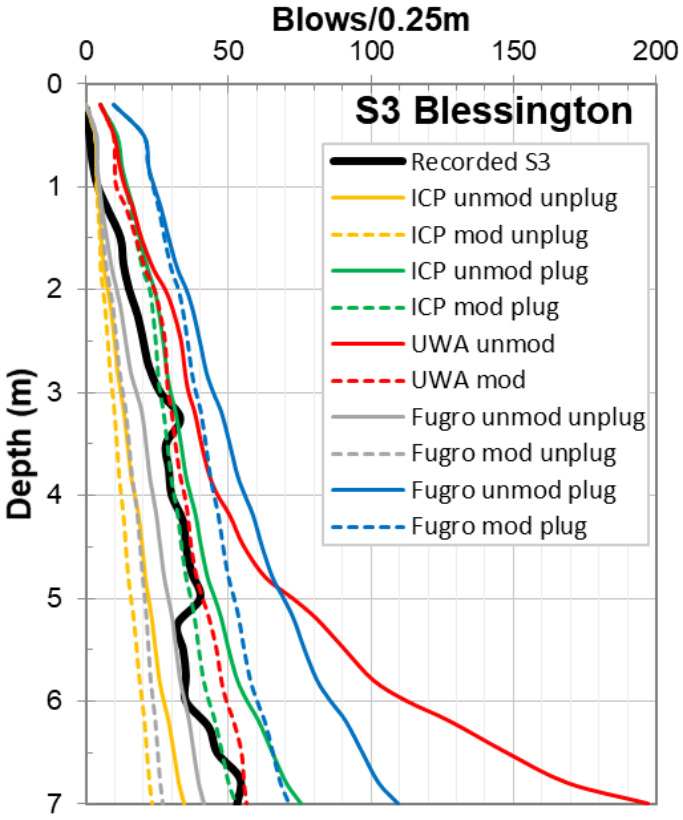

(a) Pile S3 Blessington

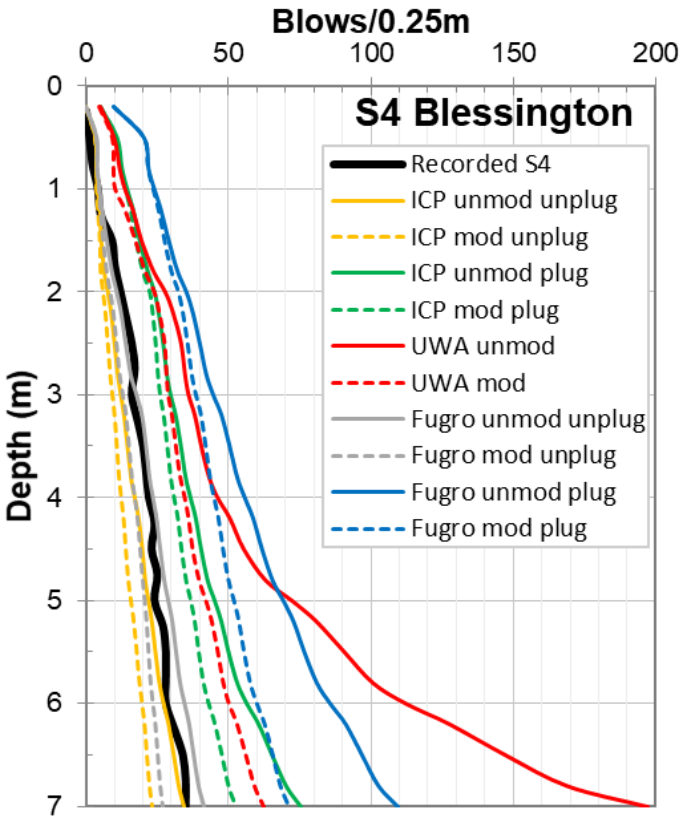

(b) Pile S4 Blessington

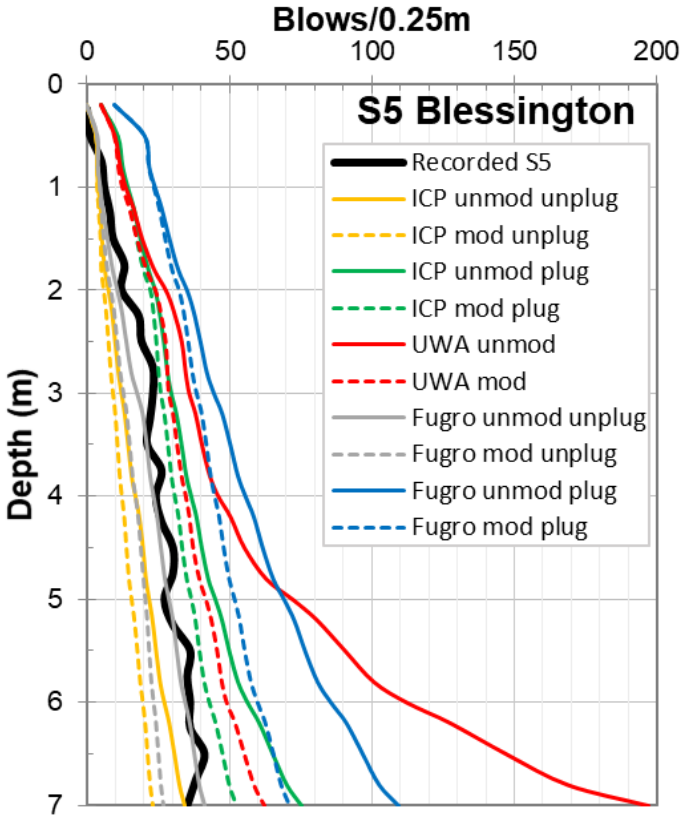

(c) Pile S5 Blessington

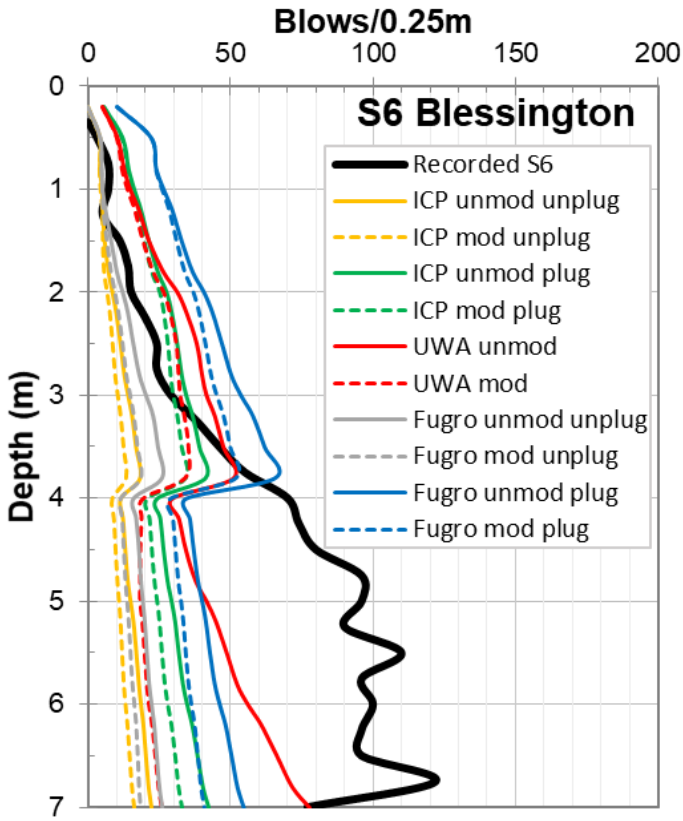

(d) Pile S6 Blessington

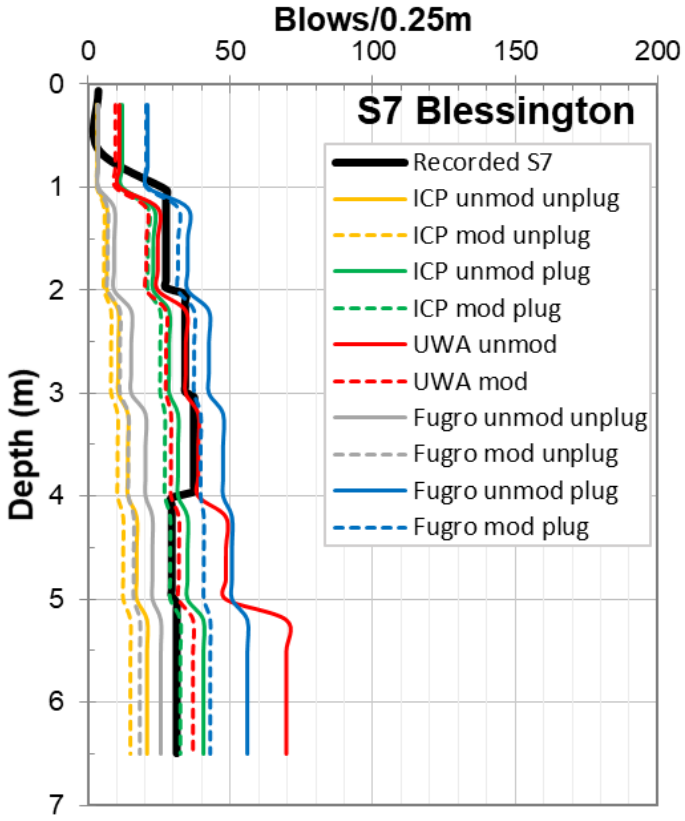

(e) Pile S7 Blessington

Figure B.2 Recorded and predicted blow count comparison at Blessington site

B.3 Residual Base Stresses

The base resistance by using the UWA-05 are modified further to account for the residual base stresses. The residual base stresses occur after each hammer blow during pile installation. In this modification, the model has integrated not only the base resistance-displacement but also the residual base stresses. The residual base stress is cooperated with adding {1,2,5,8,10}% of the cone tip resistance (q_c) to the unit base stress as mentioned in Section 3.4. The additional base residual must less than the negative shaft resistance available at the specific pile depth penetration. The model takes the time factor due to the ageing effect and a tension factor as a recommended by the UWA-05. The time factor and tension capacity are used when calculating the negative shaft resistance. The SRD profile for the UWA-05 modified including base resistance residual are derived after ensuring that base resistance load less than the negative shaft resistance.

Figure B.3 shows the recorded and modified additional base residual stresses at Blessington. This figure shows that residual base stresses developed along the pile length with the highest value of 4 MPa at the pile base. There is no modified additional base residual stress that matches entirely along the pile length. The close base residual stresses model is given by using 8% q_c between 3 and 5m depth and 19% q_c at the final depth.

The results of the base resistance SRD with varying residual base stresses for piles S1-S2 and piles S3-S7 at Blessington are shown in Figure 4.3 and Figure B.4 respectively. All piles have a similar trend when adding stepwise residual base stresses. Initially, the base resistance SRD versus depth has an independent curve until exceeding negative skin friction along the pile shaft area. In the case of negative shaft resistance is exceeded, the base residual will follow the previous additional value.

The result of the blow count prediction with residual base stresses for piles S1-S2 and piles S3-S7 at Blessington are shown in Figure 4.4 and Figure B.5 respectively. The blow count data recorded at Blessington also present as a reference for the comparison to blow count prediction. The blow count prediction results mirror the base resistance SRD input after adding base residual for every pile in Blessington as shown in Figure B.4. Adding the residual base stresses lead to reasonable blow count estimation without underprediction for piles S1-S4. However, adding the residual base stresses at piles S4-S5 give over-predict the blow count since the blow count prediction already over estimate without additional residual base stresses. Applying additional base stresses at pile S6 give insignificant improvement for blow count prediction result. It gives over-estimate at upper part and under-predict at the lower part of the pile. At pile S7, predicted blow count with 10%qc as the residual base stresses under estimate blow count prediction at the first 1m.

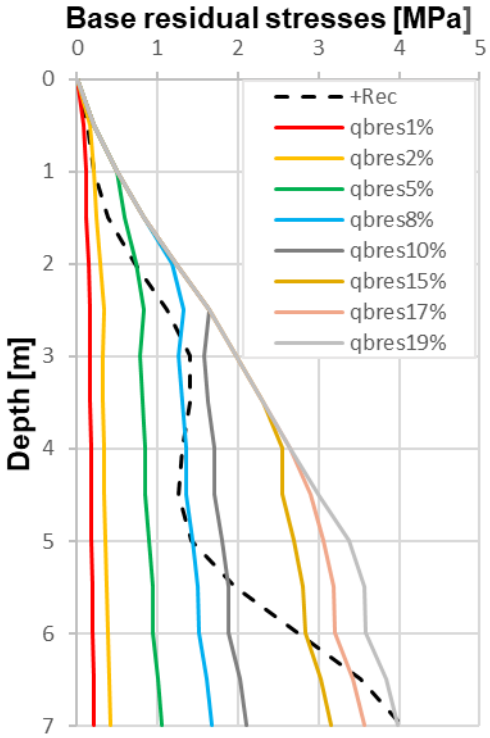

Figure B.3 Recorded and modified additional base residual stresses at Blessington

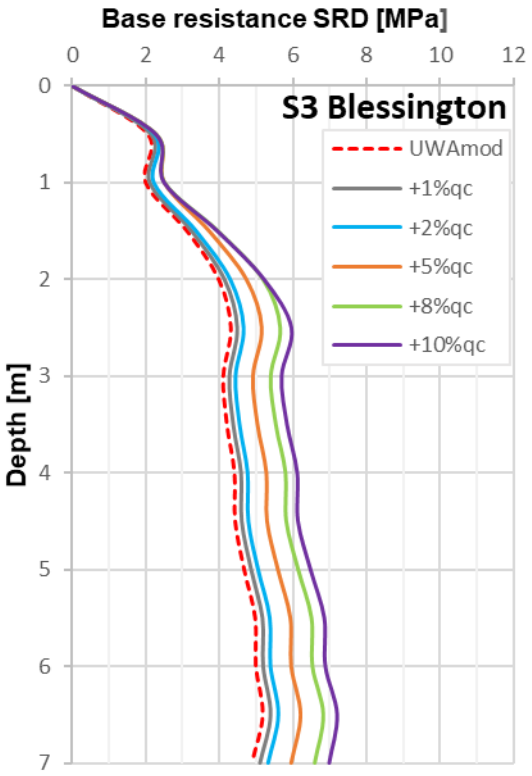

(a) Pile S3 Blessington

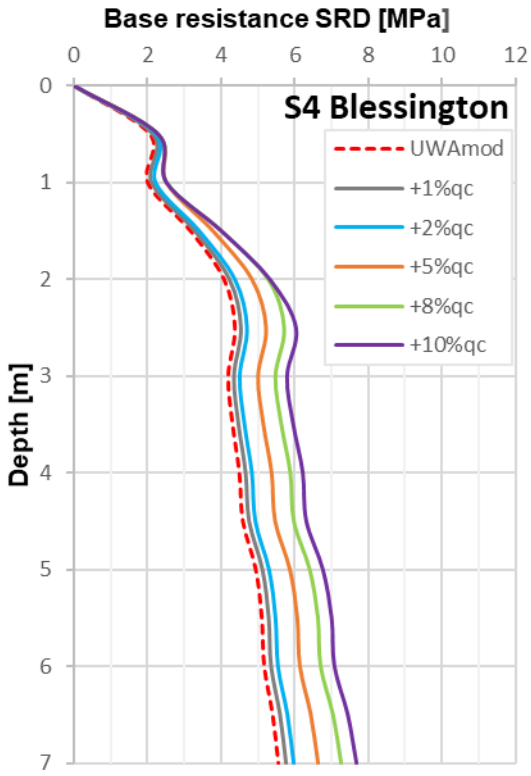

(b) Pile S4 Blessington

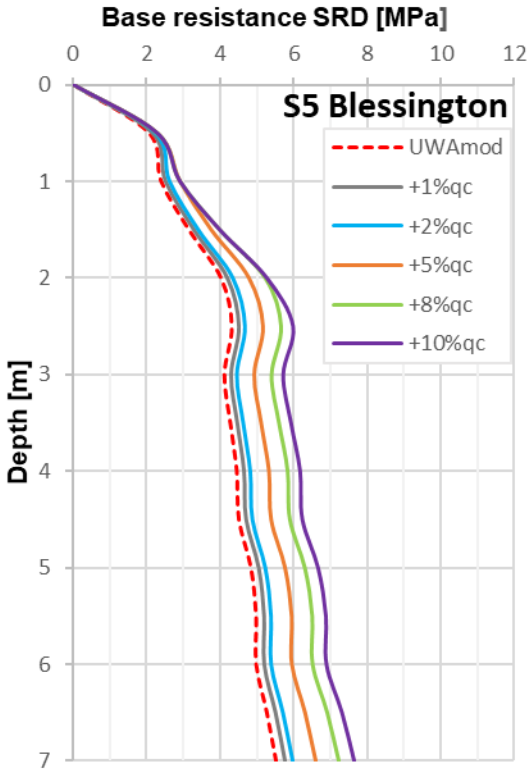

(c) Pile S5 Blessington

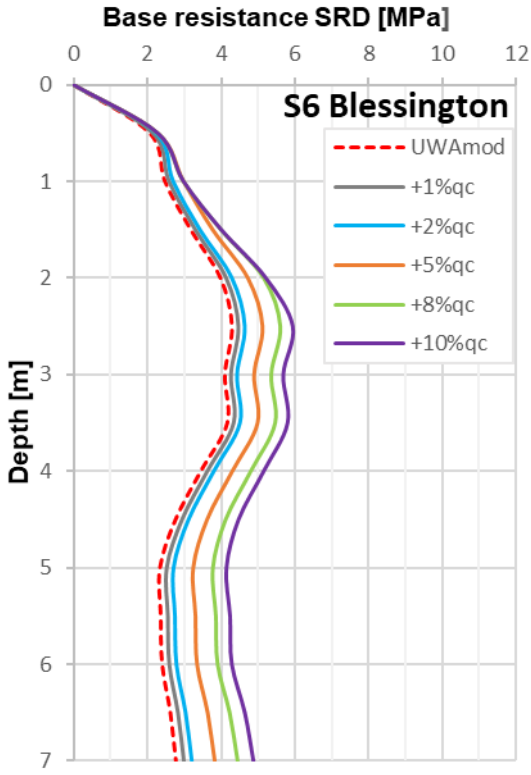

(d) Pile S6 Blessington

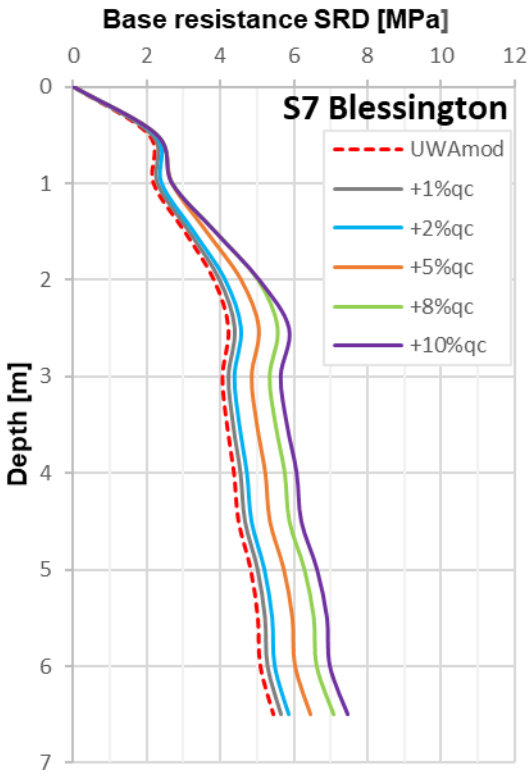

(e) Pile S7 Blessington

Figure B.4 The UWA unit base resistance with varying residual base stresses added at Blessington site

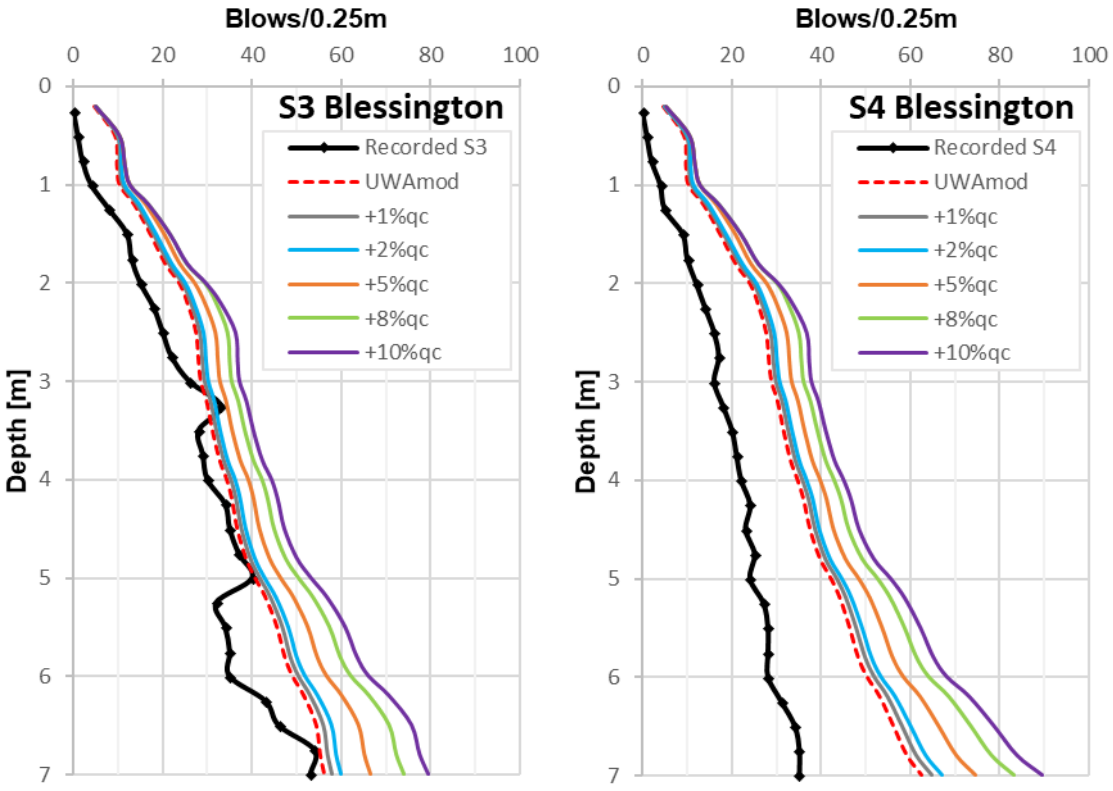

(a) Pile S3 Blessington

(b) Pile S4 Blessington

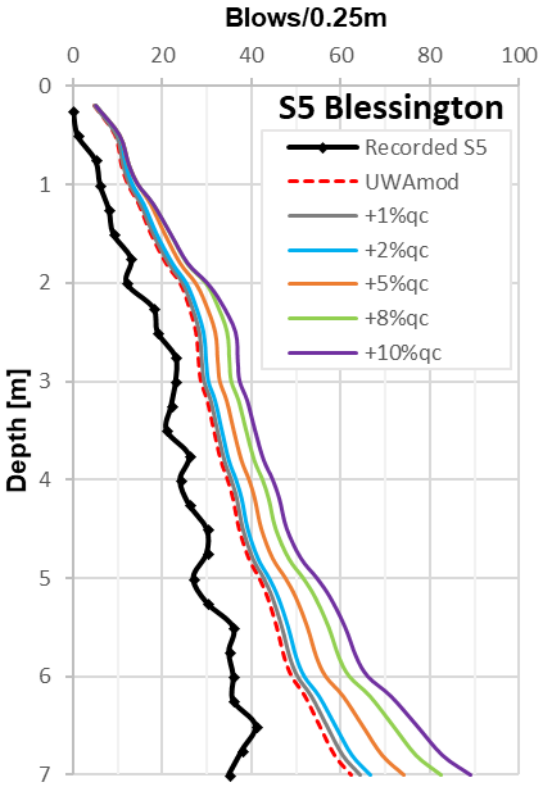

(c) Pile S5 Blessington

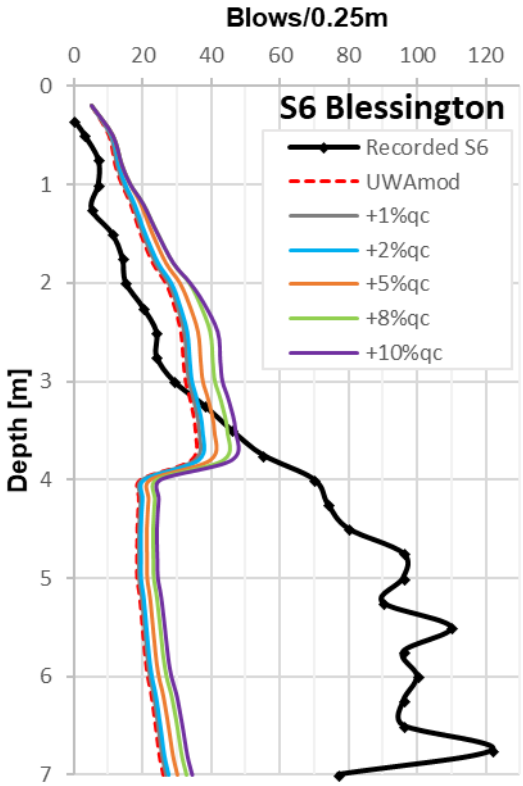

(d) Pile S6 Blessington

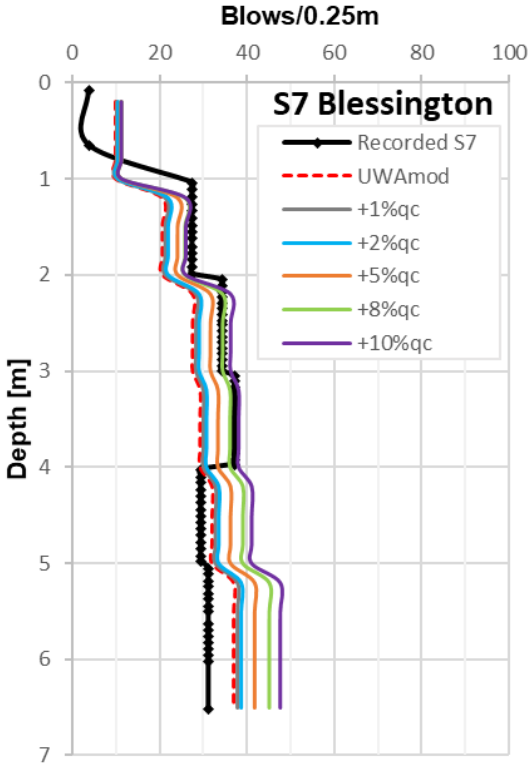

(e) Pile S7 Blessington

Figure B.5 Recorded and predicted blow count with residual base stresses added at Blessington site

C Rotterdam site Result

C.1 Base Resistance-Displacement

Figure C.1 shows the base resistance – displacement curves for piles P2-P4 at Rotterdam. All these curve results from every Rotterdam piles give a similar trend. In the first linear stage where w_b/D < 0.015, the curves increase as the soil elastic stiffness (*Eo*) increases. In the second stage, when w_b/D equals to 0.1, the base resistance value from API-00 for clay is used as a limit. This figure depicts that the actual displacement during driving less than the failure criteria of 0.1*D* as shown in the red dot. The unit base resistance is derived from the actual pile tip displacement which results in the range between 1 and 2 MPa for all piles in Rotterdam as shown in Table C.1.

Table C.1 The base resistance – displacement average at 30-35m pile depth in Rotterdam

Pile	w_b/D		q_b [MPa]		$q_{b0,1API}$ [MPa]	
	Min	Max	Min	Max	Min	Max
P1	0.03	0.06	1.02	2.00	1.44	3.73
P2	0.03	0.07	1.19	2.09	1.44	3.73
P3	0.03	0.06	1.04	2.09	1.44	3.73
P4	0.02	0.05	1.01	1.88	1.44	3.73
Average	0.03	0.06	1.07	2.01	1.44	3.73

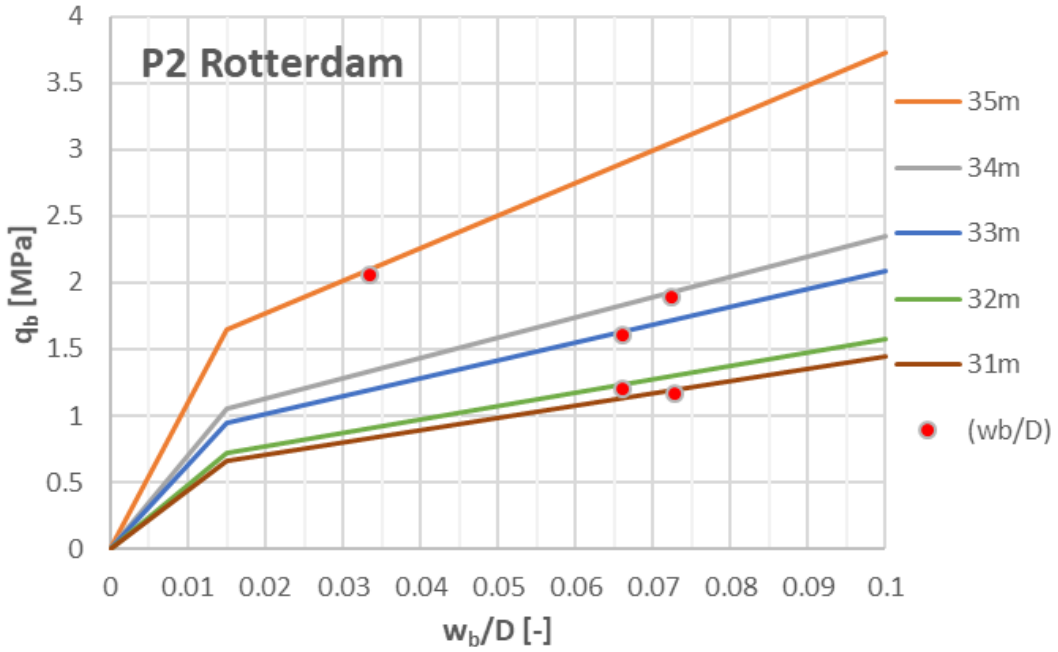

(a) Pile P2 Rotterdam

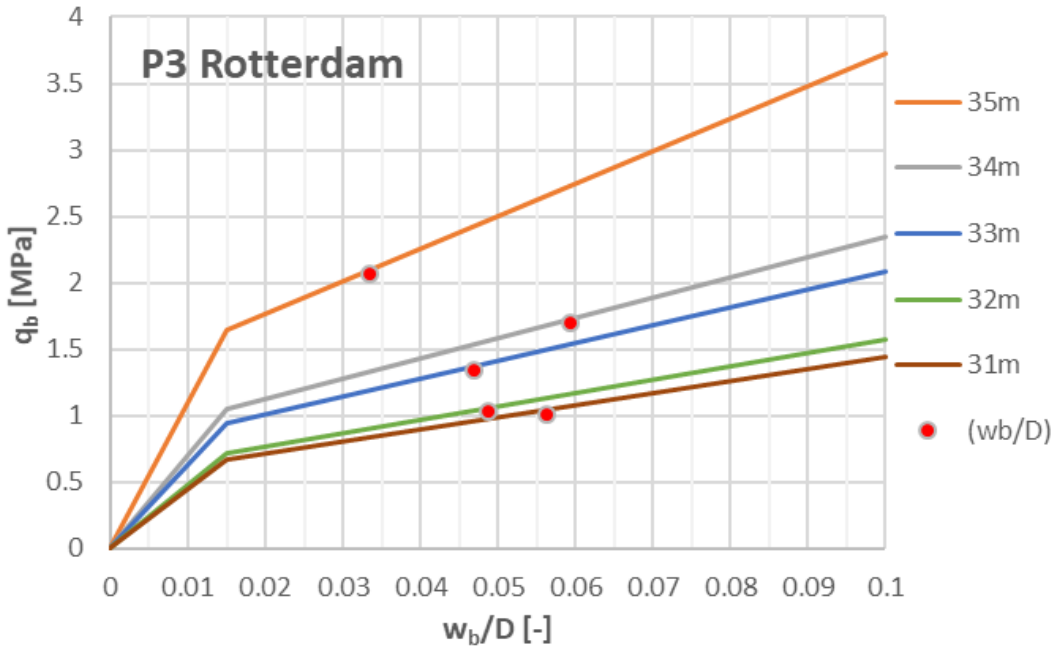

(b) Pile P3 Rotterdam

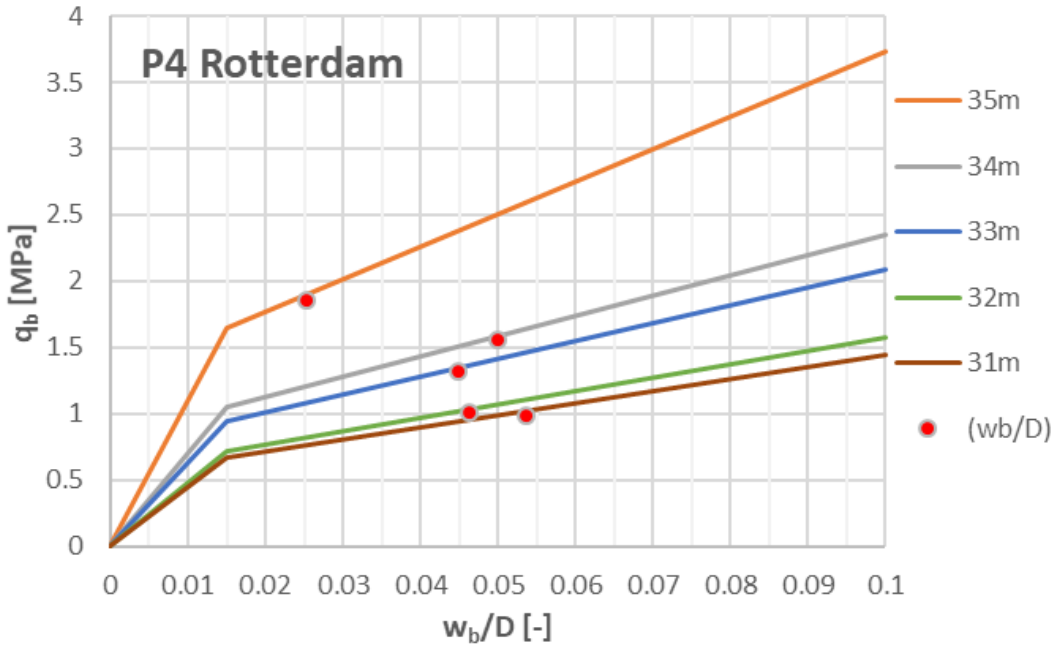

(c) Pile P4 Rotterdam

Figure C.1 Base resistance-displacement curves at various driving depth in Rotterdam site

C.2 Blow Count Comparison

Figure C.2 shows the recorded and the predicted blow count for piles S2-S4 at Rotterdam. All the results are alike for all piles in the Rotterdam. These are results by using the combination of CPT-based approaches for soil profile in sand and clay. In the upper clay layer, at 4m until

21m, all the models give similar blow count prediction. In the sand layer at 21m – 30m depth, Fugro unmodified gives the highest blow count prediction except between 26 and 27m. At 26m-27m, the UWA unmodified provide a similar prediction to the ICP unmodified which exceed the Fugro unmodified blow count prediction. At the last 5m, all the unmodified models over-predict actual blow count recorded.

Like the unmodified model, the Fugro modified gives the highest blow count estimation along the pile except at 26-27m depth. In the clay layer at 31-34m, all modified models provide better blow count prediction than the unmodified model. At the last penetration or 34-35m depth, the Fugro combination gives the best prediction while UWA and ICP give underestimated the recorded blow count. This is due to Fugro-10 calculated average q_n before and after the last penetration which is considered the sand layer underneath the clay layer. The actual blow count record only available at the last 5m, between 30 and 35m. Thus, the CoV is calculated only at this layer. Table C.2 shows the UWA and the ICP combination use the same SRD input by using API-00 and total stress approach provide the best CoV of 1.2.

Table C.2 The CoV from the average blow count at 30-35m at Rotterdam

Method	**CoV**				
	P1	**P2**	**P3**	**P4**	**Average**
ICP unmodified plug (The ICP-05 in sand, API-00 and total stress approach in clay)	1.9	2.3	1.9	1.6	**1.9**
ICP modified plug (The ICP-05 in sand, API-00 and total stress approach in clay)	1.2	1.4	1.1	1.0	**1.2**
UWA unmodified (The UWA-05 in sand, API-00 and total stress approach in clay)	2.1	2.5	2.0	1.8	**2.1**
UWA modified (The UWA-05 in sand, API-00 and total stress approach in clay)	1.1	1.4	1.1	1.0	**1.2**
Fugro unmodified (Fugro-05 in sand, Fugro-10 in clay)	2.3	2.9	2.3	2.1	**2.4**
Fugro modified (Fugro-05 in sand, Fugro-10 in clay)	1.5	1.8	1.5	1.3	**1.6**

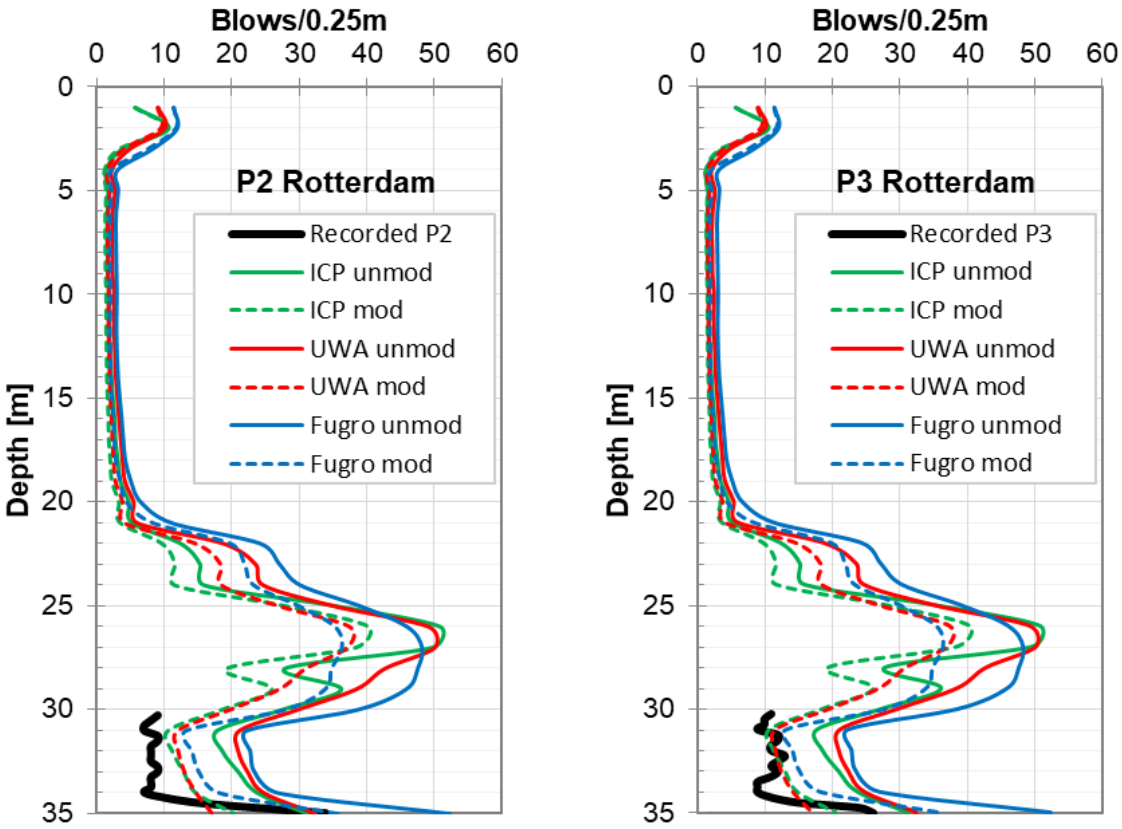

(a) Pile P2 Rotterdam

(b) Pile P3 Rotterdam

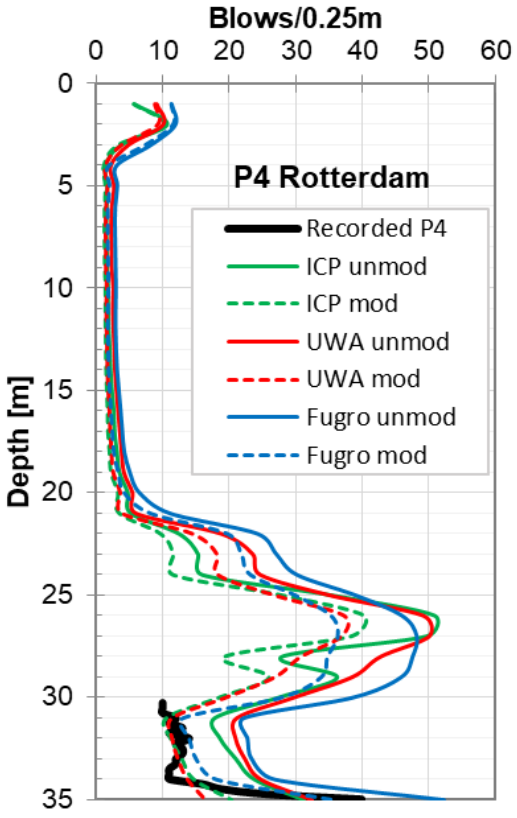

(c) Pile P4 Rotterdam

Figure C.2 Recorded and predicted blow count comparison at Rotterdam

C.3 Residual Base Stresses

At Rotterdam, the base resistance for combine UWA is modified further not only with base resistance-displacement but also by using the residual base stresses which occur after each hammer blow. The combined UWA method is derived by using a combination of the UWA-05 in sand, the total stress approach in clay for skin friction calculation and the API-00 in clay for base resistance calculation. The base residual stress is calculated by sensitivity analysis of stepwise {1%, 2%, 5%, 8%, 10%} of cone tip resistance (q_c) as mentioned in Section 3.4. The base resistance stress is added to the base resistance must less than available negative skin friction at that specific depth.

The results of the base resistance SRD with varying residual base stresses for pile P1 and piles P2-P3 at Rotterdam are shown in Figure 6.5a and Figure C.3 respectively. All piles at Rotterdam have a similar trend when adding stepwise residual base stresses. The clay layer between 4 and 21m depth have small q_c which lead unnoticeable addition to the base resistance SRD. A distinct change in the base resistance SRD result are observed at the sand layer between 22 and 30m.

The result of the blow count prediction with residual base stresses for pile P1 and piles P2-P4 at Rotterdam are shown in Figure 6.5b and Figure C.4 respectively. There is insignificant change in the clay layer causing the blow count result in almost the same prediction. A noticeable alteration in the blow count results is presented in the sand layer at 21m until 30m. At 27m depth, the blow count increases 1 blow/0.25m when the additional base residual to the base resistance SRD increases from 1% q_c to 2% q_c. This increase trend is applied for all piles in the Rotterdam.

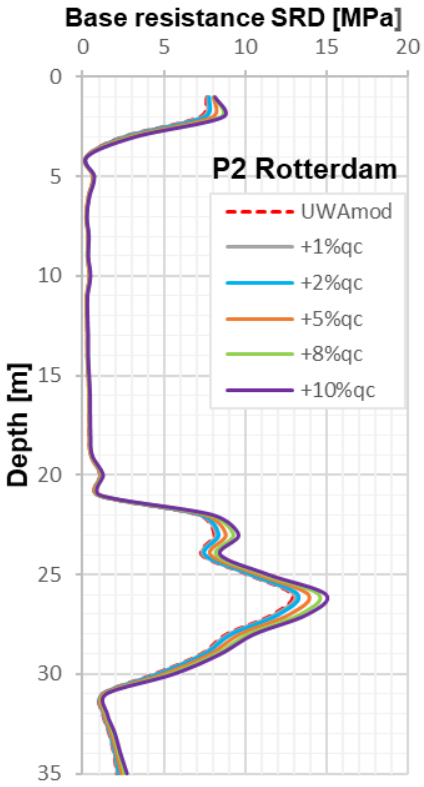

(a) Pile P2 Rotterdam

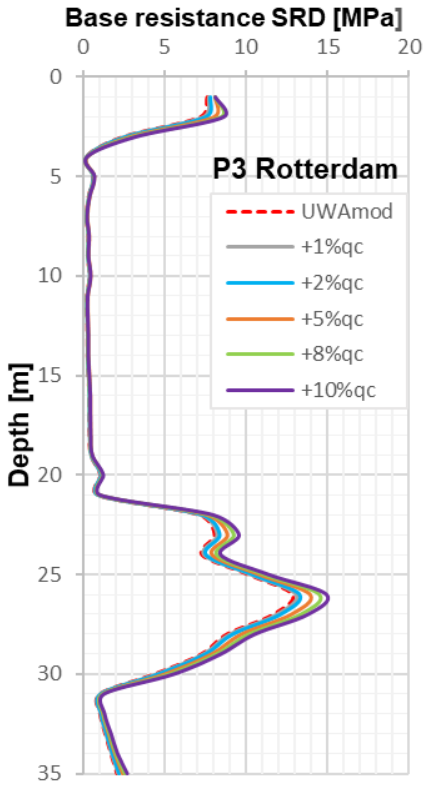

(b) Pile P3 Rotterdam

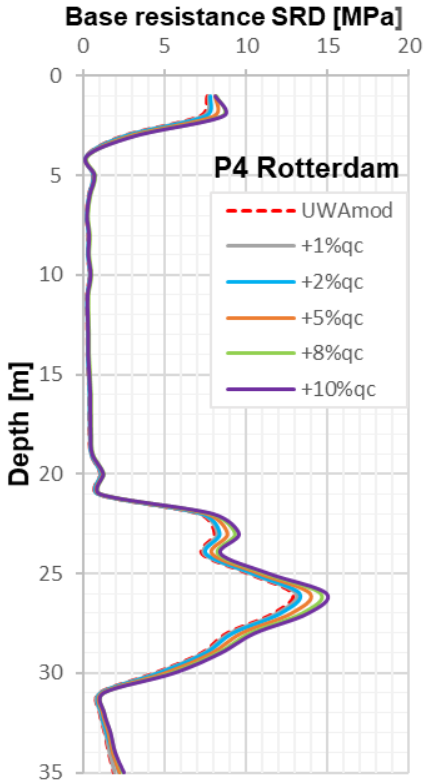

(c) Pile P4 Rotterdam

Figure C.3 The UWA unit base resistance with varying residual base stresses added at Rotterdam site

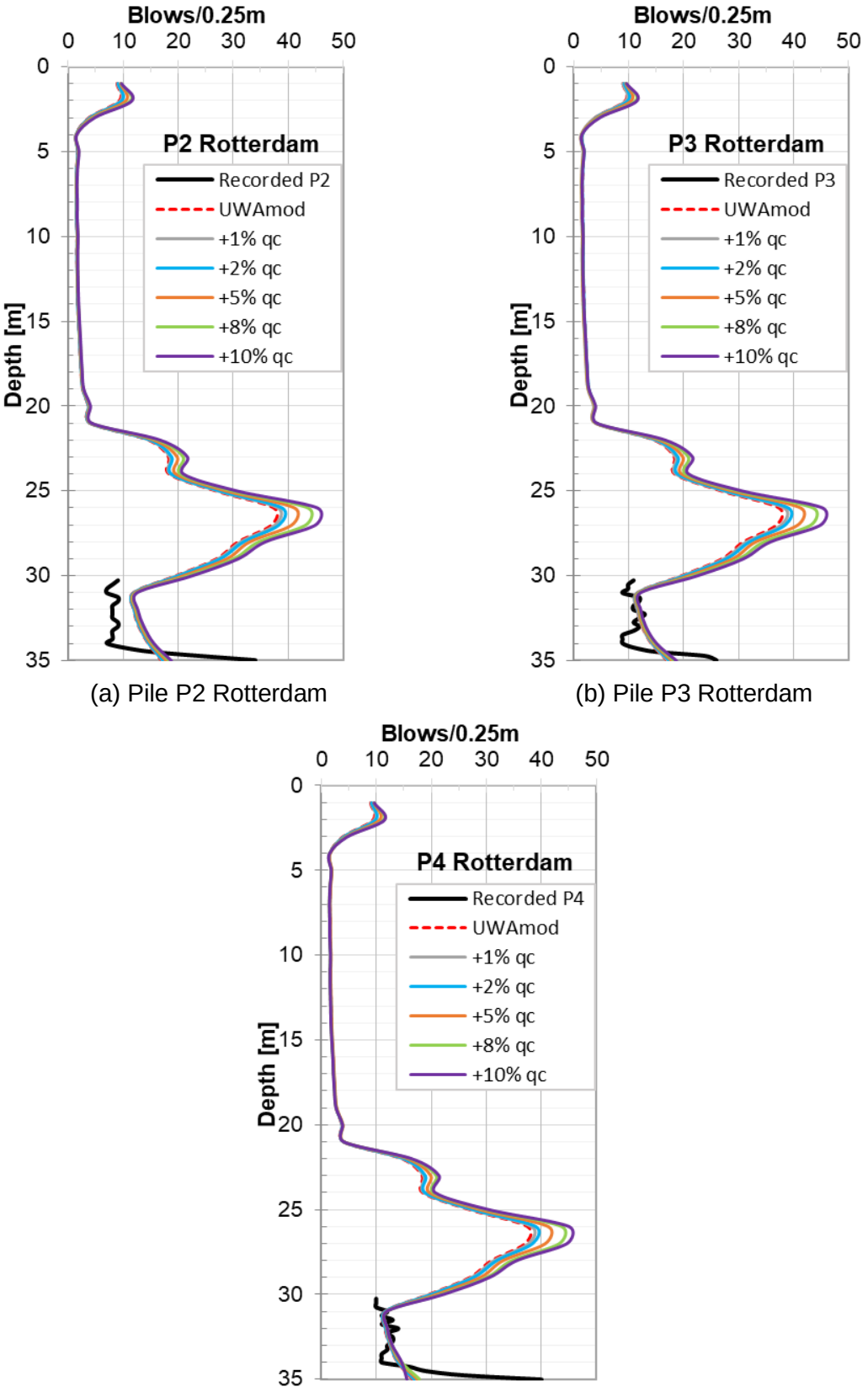

(a) Pile P2 Rotterdam

(b) Pile P3 Rotterdam

(c) Pile P4 Rotterdam

Figure C.4 Recorded and predicted blow count with residual base stresses added at Rotterdam site